School of Chemical and Petroleum Engineering

Department of Chemical Engineering

Inorganic nanocatalysts for chemical decomposition of organic pollutants in contaminated water

Qiaoran Liu

This thesis is presented for Degree of

Master of Philosophy (Chemical Engineering)

Of

Curtin University

April 2016

Declaration

To the best of my knowledge and belief this thesis contains no material previously published by any other person except where due acknowledgment has been made. This thesis contains no material which has been accepted for the award of any other degree or diploma in any university.

Signature: 

Qiaoran Liu

Date: 22/04/2016

Acknowledgment

This research is supervised and supported by Prof. Shaobin Wang. I would have no chance to complete this thesis without his guidance, encouragement and patience during my Master Program at the Department of Chemical Engineering, Curtin University. I also want to show my thanks to my co-supervisor, Dr. Hongqi Sun, who has provided insight and expertise which have greatly advanced the research. My sincere gratitude must go to Dr. Xiaoguang Duan for sharing his pearls of wisdom with me during my research. I also thank Wenjie Tian, Heng Ye, Jian Kang, Ping Liang, Stacy Indrawirawan, Chen Wang, Li Zhou and Huayang Zhang, who are always ready to help me in the experiments. I am also grateful to all laboratory technical staff: Jason Wright, Roshanak Doroushi, Anja Werner, Andrew Chan, and Xiao Hua, for their technical supports. And last, but not the least, I would like to thank my parents for everything they give me. Thanks also go to my beloved boyfriend Dingkun Chen who has taken good care of me and encouraged me during my research study.

Abstract

Emerging and priority organic pollutants are causing intensive scientific and public concerns in recent years due to their widely release from industrial and household wastewaters. Applications of advanced oxidation processes for treatment of the persistent organic pollutants in wastewater have been thoroughly investigated. The sulfate radical-based reaction has been employed as a low-cost, environmentally-friendly and sustainable technique to treat wastewater, and several novel inorganic nanocatalysts have be fabricated. This study focuses on synthesizing manganese oxide nanospheres and mixed valent manganites microspheres ($CaMn_3O_6$ and $CaMn_4O_8$), which present high activity and good magnetic performance in the oxidation of phenol solutions. The particle structure, size distribution and composition of the synthesized magnetic nanocatalysts were examined by XRD, SEM, TGA, ICP, BET, etc. And all of these catalysts were tested in oxidative degradation of phenol. In all the catalysts, porous manganese oxide nanospheres which were synthesized with butyric acid showed the best ability, which could give effective phenol decomposition in 60 minutes.

Content

Chapter 1: Introduction

1.1 Motivation..... 1

1.2 Objectives of thesis..... 2

1.3 Thesis organization..... 3

1.4 References..... 5

Chapter 2: Literature Review

2.1 Introduction..... 8

2.2 The overview of water pollutions..... 10

2.3 Advanced oxidation processes (AOPs)..... 11

2.3.1 Wet air oxidation (WAO)..... 12

2.3.2Catalytic Wet Air Oxidation (CWAO)..... 13

2.3.3 Fenton reaction..... 13

2.3.4 Photocatalytic oxidation..... 15

2.3.5 Ozonation/catalytic ozonation..... 17

2.3.5 Sulfate radical-based advanced oxidation processes..... 20

2.4 Conclusions..... 25

2.5 References..... 27

Chapter 3: The effect of particle size of the porous manganese oxide catalysts on phenol degradation

A B S T R A C T..... 42

3.1 Introduction..... 43

3.2 Experimental..... 44

3.3 Results and discussion..... 45

3.4 Conclusions..... 58

3.5 References..... 59

Chapter 4: Synthesis of highly- stable manganese oxide catalysts

A B S T R A C T..... 63

4.1 Introduction..... 64

4.2. Experimental..... 65

4.3 Results and discussion..... 67

4.4 Conclusions..... 79

4.5 References..... 82

Chapter 5: Synthesis of GO supported calcium-manganese oxide

A B S T R A C T..... 84

5.1 Introduction..... 85

5.2. Experimental..... 85

5.3 Results and discussion..... 87

5.4 Conclusions..... 101

5.5 References..... 102

Chapter 6: Effect of diluted acid treatment on catalysis over calcium-manganese oxide catalysts

A B S T R A C T..... 105

6.1 Introduction..... 106

6.2. Experimental..... 107

6.3 Results and discussion..... 108

6.4 Conclusions..... 122

6.5 References..... 123

Chapter 7: Conclusion and future work

7.1 Concluding comments..... 126

7.2 The effect of particle size of the porous manganese oxide catalysts on phenol degradation..... 127

7.3 The effect of highly- stable manganese oxide catalysts..... 127

7.4 The effect of GO supported calcium-manganese oxide.....128

7.5 Effect of diluted acid treatment on catalysis over calcium-manganese oxide catalysts...128

7.6 Recommendation for future work.....128

1

Chapter 1: Introduction

1. Introduction and Overview

1.1 Motivation

Water ensures the ecosystem services to meet the basic human needs and support economic and social activities. The uses of water by humans are driven by five sectors: agriculture, energy, industry, human settlement and ecosystems[1]. However in recent years, there has been a growing concern regarding water pollution [2 3 4]. As one of the most serious pollutants, phenol comes from the release of by-products in the petrochemical industry [5], coal liquefaction plants [6] and production of plastics, as well as the pulp industry. The released phenol has long life-time that is resistant to natural attenuation[7]. A high level of phenol in water is toxic and cannot be degraded by nature system, therefore, chemical, physical or biological remediation technologies are required [8]. To this end, researchers have shown considerable interests in the treatment techniques[9], and the advanced oxidation processes (AOPs) have been carried out as one of the most effective methods in wastewater treatment[10].

1.2 Objectives of thesis

The main focus of this research is to synthesize inorganic nanocatalysts for degradation of phenol in wastewater via chemical oxidation processes. The following objectives are defined to meet the research goals:

i. To investigate the catalytic capacity of manganese oxide for degrading phenol in aqueous phase via chemical oxidation process.

ii. To investigate the catalytic activities of calcium manganese oxide for degradation of organic compounds.

iii. To synthesize porous manganese oxide catalysts with different sizes and investigate their effect on phenol degradation.

iv. To synthesize highly monodisperse porous manganese oxide spheres as catalysts for degradation of phenol.

v. To synthesize calcium manganese oxide loaded on graphene oxide for phenol oxidation.

vi. To synthesize acid treated calcium manganese oxides, and evaluate the catalytic capacity in aqueous phase.

1.3 Thesis organization

Chapter 1: This chapter presents the technical comments on removing persistent organic pollutants in water system, which have great significance for public health. The aims and objectives are listed and the structure of this thesis is shown.

Chapter 2: The second chapter describes literature review on pollutant removal methods in three aspects: the technology of water pollution control, classification of advanced oxidation processes (AOPs) and categorization of the catalysts. This chapter also provides an overview of the technology to remove toxic substances in aqueous phase, especially by AOPs. It briefly describes the main types of wastewater sources and the harm to human body system caused by organic pollutants

Chapter 3: This chapter introduces the synthesis of porous manganese oxides with different particle sizes, and the effect of size on phenol degradation are discussed.

Chapter 4: The synthesis, characterization and catalytic activity of manganese oxide catalysts with highly monodisperse porous structures are described, and the optimum synthesis conditions are discussed.

Chapter 5: It describes the synthesis of the hybrids of graphene oxide (GO) and calcium manganese oxides ($CaMn_3O_6$, $CaMn_4O_8$), namely GO/$CaMn_3O_6$, and GO/$CaMn_4O_8$. The characterization and catalytic decomposition of phenol are presented in this chapter.

Chapter 6: This chapter investigates the method to synthesize acid treated calcium manganese oxides. Characterization and catalytic activities are examined.

Chapter 7: This chapter summarizes the overall thesis and discusses the performance of all the materials in phenol degradation. The final part of this chapter would be devoted to the suggestions to future work.

1.4 References

1. UN Water Report, the United Nations World Water Development Report 4: Managing Water under Uncertainty and Risk. Volume 1, 2012. p. 60.

2. A. Rivas, N. Olea, F. Olea-Serrano, Trends Anal. Chem. 16 (1997) 613.

3. M. Castillo, D. Barceló, Trends Anal. Chem. 16 (1997) 574.

4. T.M. Crisp, E.D. Clegg, R.L. Cooper, W.P. Wood, D.G. Anderson, K.P. Baetcke, J.L. Hoffmann, M.S. Morrow, D.J. Rodier, J.E. Schaeffer, L.W. Touart, M.G. Zeeman, Y.M. Patel, Env. Health Perspect. 106 (1998) 11.

5. G.E. Bately, J. Chromatogr. 389 (1987) 208.

6. K. Ogan, E. Katz, Anal. Chem. 53 (1981) 160

7. Thangavadivel, K.; Megharaj, M.; Smart, R. S. C.; Lesniewski, P. J.; Naidu, R., Application of high frequency ultrasound in the destruction of DDT in contaminated sand and water. Journal of Hazardous Materials 2009, 168 (2-3), 1380-1386.

8. Patricio J. Espinoza-Montero,a, Ruben Vasquez-Medrano,b,z Jorge G. Ibanez,band Bernardo A. Frontana-Uribea, Efficient Anodic Degradation of Phenol Paired to Improved.Cathodic Production of H2O2 at BDD Electrodes. Journal of the Electrochemical Society, 160 (7) G3171-G3177 (2013)

9. Chen, J.; Wang, X.; Liu, X.; Huang, J.; Xie, Z., Removal of Dye Wastewater COD by Sludge Based Activated Carbon. Journal of Coastal Research 2015, 1-3; (b) Chen, Z.; Zayed, T.; Qasem, A., An Efficiency-Centred Hierarchical Method to Assess Performance of Wastewater Treatment Plants. International Journal of Environmental Research 2015, 9 (1),

10. Wang, Y.; Sun, H.; Ang, H. M.; Tade, M. O.; Wang, S., Magnetic Fe_3O_4/ carbon sphere/ cobalt composites for catalytic oxidation of phenol solutions with sulfate radicals. Chemical Engineering Journal 2014, 245, 1-9.

2

Chapter 2: Literature Review

2.1 Introduction

Our human activities are based on the water. In recent years, environmental protection has become a critical worldwide issue, due to the fast pace of global industrialization and the great development of human civilization[1]. The discharged sewage with persistent organic pollutants (POPs) is contributing to approximately 80% of wastewater. The POPs such as polycyclic aromatic hydrocarbons (PAHs), polychlorinated biphenyls (PCBs), di-(2-ethyhexyl)-phthalate (DEHP), benzene, phenol and dyes in water , have seriously threaten to public health, food system and groundwater quality.

Advanced treatment processes have been developed in order to achieve lasting degradation of persistent organic pollutants (POPs), and the methods include chemical treatment, physical treatment (ultrafiltration[3], nanofiltration[4]) and biological treatment. An appropriate method would be employed according to the classification of pollutants in water. Table 2. 1 gives a summary of selected removal processes and their applicability.

Table 2. 1. Processes for removing organic pollutants from aqueous streams

Organics removal process	Most suitable conditions of organic pollutants	Reference
Incineration	High concentration	2
Wet air oxidation/ catalytic wet air oxidation	Medium—high concentration	28
Hydrogen peroxide	Low concentration	57
Ozonation	Low concentration	74
Activated carbon adsorption	high molecular weight organics	4
Ultrafiltration	high molecular weight organics	3
Biological treatment	toxic or high temperature streams	13

Usually, physical and biological treatments are dependent on the degradation condition and have selectivity, for example, the biological method cannot be employed for some contaminants such as phenol which is not biodegradable. The limitations often bring about high cost, long-cycle and secondary pollution problems in physical methods like incineration and activated carbon adsorption.

Advanced oxidation processes (AOPs), as effective techniques, have been proven to have great efficiencies in degrading aqueous POPs with low concentrations. They can be used for wastewater remediation to remove a variety of organic pollutants to nontoxic inorganics (carbon dioxide, water). AOPs can be classified to be wet air oxidation (WAO), catalytic wet air oxidation (CWAO), Fenton reaction, photocatalytic oxidation, electro-catalytic, ozonation/catalytic ozonation and sulfate radical-based advanced oxidation processes.

However, most of these technologies have shortcomings, and depend on energy input (ozone, UV, ultrasound, electric, supercritical oxidation (SCWO), and heat treatment) and long operating period (bioremediation and photo-remediation). Therefore, a novel method with less demanding condition would be a promising technology for wastewater treatment. In recent years, sulfate radical-based advanced oxidation processes have attracted lots of researchers' attention, due to the moderate energy input, wide-pH condition, high-efficiency and low-cost. Cobalt oxides and ruthenium oxide have been used to produce sulfate radicals (SRs) in Fenton-like system [12]. The SRs can be also produced with adding oxone (peroxymonosulfate, PMS) [14]. However, Co^{2+} and Ru^{3+} can cause even more serious pollution in natural water systems[15-17]. Fe^{2+} can be used as an alternative metal in some studies[18]. However, it was found that the catalytic activity of Fe^{2+} was significantly affected by the pH value, which greatly limits the

application.

Lately, manganese oxides (MnO, MnO_2, Mn_2O_3 and Mn_3O_4) have attracted much attention due to their physical and chemical properties for being used as catalysts[5-11]. Some researchers have shown great interests in degradation of organic compounds in aqueous phase employing manganese oxide. Moreover, a recent study conducted by Watts et al.[17] showed that the catalytic properties of Mn^{2+} was significantly higher than that of Fe^{2+} in H_2O_2 system. Previously, Mn^{2+} has been investigated for the activation of ozone to produce hydroxyl radicals for several organics oxidation and it showed an effective activity[19].

2.2 The overview of water pollution

In the past decades, a large amounts of water has been polluted due to human activities, improper use of chemicals, spills and explosions of industry and oil tankers. Most of the wastewater came from industries (42.4%), while about 36.4% from domestic wastewaters[20]. After the water was polluted, the heavy metals in water and in fish aquatic organisms would bring strong impacts on human's health. According to the World Health Organization (WHO) statistics, about eighty percents of worldwide diseases and more than one-third of deaths are directly caused by unclean drinking water. 18 million people died from polluted drinking water every year, which means about 6000 children and adults died from drinking dirty water every day. To be exact, a 1/6 of the world's population is suffering from unsafe water nowadays, especially in the developing countries[21]. Using unclean water is a long-term potential threat to health, and can result in digestive diseases, infectious diseases, skin diseases, diabetes, cancer, cardiovascular disease and lithiasis, etc. Chemical product is one of the most dangerous pollutants [22]. Among all kind of industrial emissions, persistent organic pollutants (POPs) have

attracted much attention because of the resistance to natural decay. Peng and Song's study was about Yangtze River, which is located in Jiangsu Province of China, with a chemical industry park (CIP) along it. The results showed that chemical leakage from the chemical plants leads to the most serious impact on the surrounding water environment. It has damaged the ecosystem of Yangtze River severely for 3.8 km, and led to a pollution of persistent organic pollutants (POPs) over 73.7 km downstream, due to the long life and toxic of POPs.

Phenol is one of the most toxic organic pollutants in wastewater. It is used as a general disinfectant, and for the manufacture of artificial resins, medicals, dyes, fertilizer, explosives, textiles, paints, pharmaceuticals and as an intermediate in the production of other chemicals. It would cause considerable damage when discharged into natural system even at a low concentration[23].

2.3 Advanced oxidation processes (AOPs)

In order to protect the human's safety, a huge number of researchers have been devoted to achieving a reasonable solution to protect the water environment. Traditional treatments have limits as the characteristics of low-usage and anti-environment [24]. Catalytic process has great potential for industries and human activities by removing POPs to reduce contamination of water system [25]. However, if the catalysts could not be well recycled, there might appear secondary pollution in water system, which could be more serious than the primary one [26].

Recently, AOPs have gained more attention. They are based on various chemical treatments and offer a great potential alternative for removing toxic constrains in wastewater by hydroxyl or sulfate radicals from high oxidizing substance. The radicals could then subsequently oxidize the pollutant into simpler forms and less harmful components. Due to the complete degradation,

the decomposition products are non-toxic and inorganic matters (carbon dioxide, water). AOPs hold several advantages unparalleled in wastewater treatment, such as elimination of wastewater contaminants effectively, wide-spectrum degradation, effective disinfecting action, and no new hazardous substances introduced. There are seven categories of AOPs, namely wet air oxidation (WAO), catalytic wet air oxidation (CWAO), Fenton reaction, photocatalytic oxidation, electro-catalytic, ozonation/catalytic ozonation, and sulfate radical-based advanced oxidation processes [27].

2.3.1 Wet air oxidation (WAO)

Wet air oxidation (WAO) is one of the popular methods for wastewater treatment, and aims at the treatment of toxic and hazardous components in aqueous industrial waste. WAO is a representative of the oxidative techniques to treat organic compounds usually at high temperatures and elevated pressure with pure oxygen gas or air. In the medium-high concentrations of persistent organic pollutants (2% - 20%) in wastewaters, WAO showed the best effect [28]. The solubility of oxygen in the aqueous solution can be increased by enhancing temperatures and pressures, therefore the oxidation rates are increased. The wet air oxidation reactions occurred at a temperature above the normal boiling point of water (100 °C) and below the critical point (374 °C). In this process, the toxic organic compounds are firstly degraded into small molecular compounds, such as formic acid, acetic acid and carboxylic acid. The complete reduction products are H_2O and CO_2. The reaction mechanism are shown in the below equations [29].

Initiation $\quad R - H + O_2 \rightarrow R^{\bullet} + HO_2^{\bullet}$ (2.1)

Propagation $\quad R^{\bullet} + O_2 \rightarrow RO_2^{\bullet}$ (2.2)

$$R{-}H + RO_2^{\bullet} \rightarrow ROOH + R^{\bullet} \quad (2.3)$$

Termination $$RO^{\bullet} + RO_2^{\bullet} \rightarrow ROOR + R^{\bullet} \quad (2.4)$$

2.3.2. Catalytic wet air oxidation (CWAO)

WAO has disadvantages, because it can hardly remove all the organic pollutants in water. Catalytic wet air oxidation (CWAO) technology has been developed for improving WAO process. It can decompose most organic substances to mineralized products such as carbon dioxide and water, and the oxidizable components such as cyanides and ammonia can be also removed. CWAO does not need much power as WAO, and the gas release level is low [36]. In addition, with the technology developed, the operation conditions are lower than before. The temperature and pressure can be around 80-180 ℃ and 1-5 MPa, respectively, which can avoid erosion of the surface and damage of the structure of the material, and also reduce the operating costs. CWAO is also cost-effective for highly concentrated organic pollutants (10,000 to 100,000 mg/L) or the containing pollutants are unable to degradable by biological method.

Recently, CWAO technology has achieved accomplishments in reaction rates, reaction mechanism, reaction kinetics and catalyst improvement. The further studies of CWAO need to develop new catalysts with high activity and stability, which would be important for the more comprehensive degradation of high concentrations of toxic and hazardous wastewater[37].

2.3.3 Fenton reaction

In 1893, a famous chemist H.J. Fenton firstly found that hydrogen peroxide (H_2O_2) had strong oxidation capability when mixed with the solution of divalent iron (Fe^{2+}). It could degrade many kinds of organic compounds, such as carboxylic acids, alcohols and esters[38]. As more and more researchers had enthusiasm in this field, in 1970s, Fenton reaction was found having

great performance in environmental chemistry, reflecting a wide range of applications in removing the refractory organics in wastewater with dyes, kerosene, phenolic compounds, coking, nitrobenzene and diphenylamine[39].

Some researchers have indicated that most AOPs involving hydroxyl radicals (•OH) are generated from Fenton/ Fenton-like reactions to oxidize the organic matters [40 - 45]. The hydroxyl radicals could be originated from the reaction between hydrogen peroxide and ferrous salts at pH 3.0 ± 0.1 [46 47]. It also has high redox potential of 2.7 V and can carry out oxidative degradation of the organic contaminants to inorganic compounds [48]. The details occurred in Fenton reaction are shown in the following chemical reaction equations[49 50].

$$Fe^{2+} + H_2O_2 \rightarrow Fe^{3+} + HO^{\cdot} + HO^{-} \quad (2.5)$$

$$Fe^{2+} + HO^{\cdot} \rightarrow Fe^{3+} + HO^{-} \quad (2.6)$$

$$HO^{\cdot} + H_2O_2 \rightarrow HO^{2\cdot} + H_2O \quad (2.7)$$

$$HO^{2\cdot} + Fe^{2+} \rightarrow Fe^{3+} + HO^{2-} \quad (2.8)$$

$$HO^{2\cdot} + Fe^{3+} \rightarrow Fe^{2+} + O_2 + H^{+} \quad (2.9)$$

The processes of the chain mechanisms of Fe^{2+}regeneration are presented as follwing[51]:

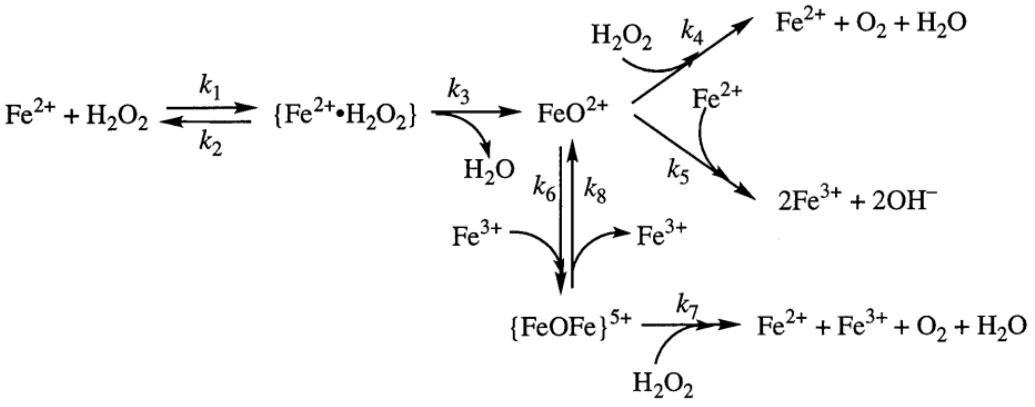

Fig. 2. 1. The chain mechanisms of Fe^{2+}regeneration[51].

Fenton reaction can be used to treat wastewater with the following actions: organic pollutant destruction, toxicity reduction [52], biodegradability improvement [53], BOD/COD removal [54], odor and color removal [55] and destruction of resin in radioactive contaminated sludge [56]. Although Fenton reaction has a lot of advantages in organic pollutant mineralization[57], it still suffers from several drawbacks such as metal leaching problem, production of sludge and difficulties in transportation and storage of hydrogen per-oxide.

2.3.4 Photocatalytic oxidation

Photochemical or photocatalytic oxidation is one of the most popular advanced oxidation technologies, due to its cost-effective and eco-friendly characteristics[58]. The so-called photocatalytic reaction is carried out with the activation of light. The photochemical reaction required specific wavelength of electromagnetic radiation for molecules absorbing, then the molecules can be stimulated to produce excited state, and then generate a new substance, or become intermediate chemical products of the sparking heat reaction. The activation energy of photochemical reaction comes from the photon energy [59].

In photocatalytic oxidation reaction, oxidants (H_2O_2, O_2) are excited via optical, which are mainly ultraviolet light or solar light irradiations [60 - 62]. It can be utilized as an effective treatment of refractory sewage, such as the wastewater containing phenol and chlorobenzene. In addition, there exists a synergistic effect of ultraviolet light and the iron ions in the Fenton system, which could greatly accelerate the rate of generating hydroxyl radical by decomposition of H_2O_2, and promote the oxidative removal of organic pollutants. The following equations described the reactions of photo-Fenton reaction.

$$(OH)_2+ + h\nu \rightarrow Fe^{2+} + HO^{\cdot} + H^{+} \quad (2.10)$$

$$H_2O_2 + hv \rightarrow 2HO^{\cdot} \quad (2.11)$$

In addition, coloured matters, such as organic dyes could also increase the production rate of hydroxyl radicals [63 64]. With exposure in visible light, Fe^{3+} reduce to Fe^{2+} because of the transfer of electron from dyes. The following equation described the participation of light Fenton reaction.

$$dye + visible light \rightarrow dye^{*} \quad (2.12)$$

$$dye^{*} + Fe^{3+} \rightarrow Fe^{2+} + dye^{\cdot +} \quad (2.13)$$

In 1972, Fujishma and Honda discovered the photocatalytic decomposition of water on the semiconductor electrode of TiO_2, thus opening up a new field of semiconductor photocatalysis. In 1977, Yokota et al found that under the light conditions, TiO_2 showed photocatalytic activity to benzenepropanoic epoxidation, which broadening the scope of application of oxidation reaction. During the past forty years, the semiconductor photocatalysis has become one of the most active areas of research. The mechanism of oxidation chains on the photosensitive surface of titania catalyst are described below [65]. $Photoexciation: TiO_2 + hv \rightarrow e^{-} + h^{+}$ (2.14)

$$Charge\text{-}carrier\ trapping\ of\ e^{-}: eCB^{-} \rightarrow eTR^{-} \quad (2.15)$$

$$Charge\text{-}carrier\ trapping\ of\ h^{+}: hVB^{+} \rightarrow hTR^{+} \quad (2.16)$$

$$Electron\text{-}hole\ recombination: eTR^{-} + hTR^{+}\ (hVB^{+}) \rightarrow eCB^{-} + heat \quad (2.17)$$

$$Photoexcited\ e\text{-}\ scavenging: (O_2)\ ads + e^{-} \rightarrow O_2{\cdot}^{-} \quad (2.18)$$

$$Protonation\ of\ O_2{\cdot}^{-}: O_2{\cdot}^{-} + HO{\cdot}^{-} \rightarrow HOO{\cdot} \quad (2.19)$$

$$Co\text{-}scavenging\ of\ e^{-}: HOO{\cdot} + e^{-} \rightarrow HO_2^{-} \quad (2.20)$$

$$Formation\ of\ H_2O_2: HO_2^{-} + H^{+} \rightarrow H_2O_2 \quad (2.21)$$

$Photodegradation\ by\ HO\cdot$: $HO\cdot + organic\ pollutants \rightarrow intermediates \rightarrow Final\ products\ (CO_2 + H_2O)$ (2.22)

$Photodegradation\ by\ photoholes$: $h^+ + organic\ pollutants \rightarrow intermediates \rightarrow Final\ products\ (CO_2 + H_2O)$ (2.23)

The following table summarizes the catalysts, light source and degradation products of different organic matter in photocatalytic degradation [66 - 70].

Table 2. 2. The catalysts, light source and degradation products of different organic matter in photocatalytic degradation

Organic matter	Catalyst	light	Degradation products	Ref
Hydrocarbon (aliphatic hydrocarbons, aromatic hydrocarbons)	TiO_2	UV	CO_2,H_2	70
carboxylic acid (halogenated alkanes, alkenes)	TiO_2	UV	HCl,CO_2	66
Carboxylic acid (acetic acid, propionic acid, butyric acid, lactic acid)	TiO_2	UV	CO,H_2, Dioxane, hydrocarbon, alcohol	67
Surfactant (DBS, SDS,BS, 4-Chlorophenol)	Fe_2O_3, ZO,TiO_2	Solar	CO_2,HCl,SO_3^{2-}	68
Dyes (methylene blue, methyl orange)	TiO_2	UV	CO_2,H_2O, Inorganic ions	68
Oxygenated organic compounds (tetrabutyl ammonium phosphate, phenylalanine)	TiO_2	UV	CO_3^{2-},NO_3^-,NH_4^+	69
Organophosphorus insecticides (DDVP, DEP)	TiO_2	UV	Cl-,PO_4^{3-},CO_2	70

2.3.5 Ozonation/catalytic ozonation

During the 1950s, people began to utilize the ozonation technology for the treatment of urban

sewage and industrial wastewater. In 1970s, combined with activated carbon, oxidation technology became one of the main method to remove pollutants from wastewater and drinking water. Ozone as a powerful oxidizing substance (standard oxidation potential is 2.07 V), could be used to process organic substances in liquid and solid phases [71]. In recent years, as an efficient and economical processing method, ozonation has been regarded as a popular approach for dealing with industrial and environmental issues [72]. It has revealed a high capacity for degrading organic pollutants, lowering the negative effect in natural system [73]. The details of ozonation process are presented in the following equations [74].

$$O_3 + H_2O \rightarrow 2HO^{\cdot} + O_2 \quad (2.24)$$

$$O_3 + HO^- \rightarrow O_2^{\cdot -} + HO_2^{\cdot} \quad (2.25)$$

$$O_3 + HO^{\cdot} \rightarrow O_2 + HO_2^{\cdot} \leftrightarrow O_2^{\cdot -} + H^+ \quad (2.26)$$

$$O_3 + HO_2^{\cdot} \leftrightarrow O_2 + HO^{\cdot} \quad (2.27)$$

$$2HO_2^{\cdot} \rightarrow O_2 + H_2O_2 \quad (2.28)$$

Ozone could effectively degrade organic contaminants with multiple bonds, however, the products of macromolecules cannot be further degraded. Ozone and some organic compounds (inactivated aromatics) are selective and slow. In addition, low solubility and poor stability as well as its high cost have limited the application for wastewater treatment. Therefore, researchers put forward on the production of hydroxyl radicals to enhance the oxidizability [75]. Recently, according to some researches, catalytic ozonation has proven to be useful to remove water-based organic pollutants, and the efficiency is better than ozonation. Moreover, it is non-selective for degradation [76 77]. Typically, the catalytic ozonation process can be divided into two categories, homogeneous and heterogeneous catalytic ozonation.

Two mechanisms are involving in homogeneous ozone catalysis. One is that the ozone is decomposed into free radicals, and the other one is a complex coordination between the catalyst and organic matter or O_3, thereby promoting the reaction between ozone and organics. Radical reaction of ozonation is a Fenton-like reaction under the action of catalysts, while the ozone forms free radicals with strong oxidizing effect. Similar to Fe^{2+} cases, Sauleda et al. proposed that the catalytic decomposition of ozone for formation of $OH\cdot$ [78 79], and the reactions are as follows.

$$Fe^{2+} + O_3 \rightarrow FeO^{2+} + O^2 \quad (2.29)$$

$$FeO^{2+} + H_2O \rightarrow Fe^{3+} + OH\cdot + OH^- \quad (2.30)$$

Another reaction mechanism was raised by Pines et al. when he and his assistants were doing research about Co^{2+} catalyzed oxalate. They found that the catalytic oxidation rate increases with decreasing pH values [80]. Furthermore, the reaction rates would be not affected by radical suppression. Therefore, they supposed that the Co^{2+} oxidation of oxalic acid was carried out through the following reactions.

$$Co^{2+} + C_2O_4{}^2\text{-} + O_3 \rightarrow CoC_2O_4{}^+ + O_3{}^- \quad (2.31)$$

$$CoC_2O_4{}^+ \rightarrow Co^{2+} + C_2O_4{}^{-}\cdot \quad (2.32)$$

$$C_2O_4{}^{-}\cdot + O_3 \rightarrow 2CO_2 + O_3{}^- \quad (2.33)$$

Since homogeneous catalysis, in ionic form, needs to be recycled to avoid secondary pollution of water bodies, it is inconvenient to run the operation in practical applications.

Heterogeneous catalysts had two main categories: metal oxides (such as MnO_2 [81], TiO_2, Al_2O_3, etc.), and supported metals or oxides (such as Cu-Al_2O_3, Cu-TiO_2, Ru-CeO_2, V-O/TiO_2, TiO_2 /Al_2O_3, Fe_2O_3 / Al_2O_3, etc.). The activity of the catalysts are mainly reflected by the catalytic

decomposition of ozone and the production of hydroxyl radicals. It was found that the efficiency of catalytic ozonation is related to the surface properties of the catalyst to a large extent. Table 2.4 summarizes the variable heterogeneous catalysts and the acting organic pollutants.

Table 2.4 The heterogeneous catalysts and the acting organic pollutants

Catalyst	Pollutants	Ref.
MnO_2	Carboxylic acid, phenol	82
Al_2O_3	Carboxylic acid	83
TiO_2	Oxalic acid, naproxen	84
FeOOH	p-Chlorobenzoic acid	85
CeO_2	Aniline, dyes	86
Co_3O_4/Al_2O_3	Pyruvic acid	87
CuO/Al_2O_3	Oxalic acid	88
NiO/Al_2O_3	Oxalic acid	89
$MnOx/Al_2O_3$	Phenazone, ibuprofen, phenytoin, di-phenhydramine	90
Co/CeO, Mn/CeO	Phenolic wastewater	91
Activated carbon	Oxalic acid	92

2.3.5 Sulfate radical-based advanced oxidation processes

With the increasing complexity of environmental pollution, sulfate radical-based processes have been developed as a promising advanced oxidation technology. Compared with other traditional oxidation methods, this technology has attracted extensive attention due to its characteristics of strong oxidation capacity, high efficiency, low cost, low selectivity and mild

reaction conditions. Persulfate salts (E_0 = + 2.01V) include peroxymonosulfate (PMS, HSO_5^-) and persulfate (PS, $S_2O_8^{2-}$) which are stable at room temperature. However, after activation, persulfate salts are decomposed to produce active sulfate radicals ($SO_4^{-}\cdot$), which have a lone pair of electrons with redox potential (E_0) of + 2. 60 V, whose oxidation capacity exceeds persulfate salts (E_0 = + 2. 01V), and closes to the hydroxyl radical (·OH) with E_0 of + 2.80V. Sulfate radical-based advanced oxidation processes have developed in recent years, as the main active substance of pollutants' treatment [93 94].

Persulfate itself has limitations in oxidation of pollutants, but with the activation of light, heat, sound and transition metal ions, $S_2O_8^{2-}$ can be decomposed into $SO_4\cdot^-$ [95].

Peroxymonosulfate (PMS), can generate sulfate radicals, which are substituted derivatives of the sulfo-group of hydrogen peroxide [96]. Oxone as a product of PMS which is available by trade, and the composition is $2KHSO_5\cdot KHSO_4\cdot K_2SO_4$[97]. The decomposition mechanism to catalytically induced activation of PMS follows the following reactions [98 – 100].

$$HSO_5^- + e^- \rightarrow SO_4^{\bullet-} + OH^- \quad (2.34)$$

$$HSO_5^- + e^- \rightarrow SO_4^{2-} + OH^{\bullet} \quad (2.35)$$

$$HSO_5^- \rightarrow SO_5^{\bullet-} + H^+ + e^- \quad (2.36)$$

There are two kinds of generation processes of sulfate radical, namely energy and catalytic activation. In energy activation system, the sulfate radical can be generated by heat, light, ultrasound, radiolysis, etc. Thermal activation is operated mainly through increasing temperature, which provides sufficient activation energy to force the bond cleavage, and produce sulfate radicals. The mechanism is as following:

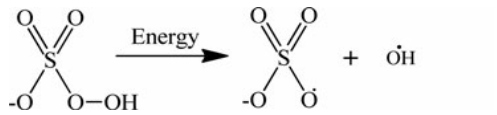

(2.37)

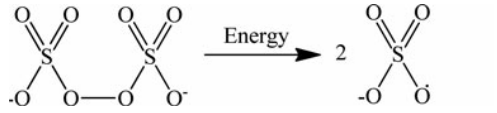

(2.38)

Figure 2. 2. Formation of sulfate radicals under external energy source for PMS (2.37) and PS (2.38) [96].

The thermal technology has been extensively employed in research application, because it is simple and functional in the process of thermal activation. Moreover, it is found that temperature, concentration of persulfate, pH and ionic strength will also affect the degradation rates of organic matters. The rates rise with the increasing of sulfate concentration, while pH value will bring different effects with different organic pollutants. To alkaline persulfate salts, the main active species are $SO_4\cdot^-$ when pH is in the range from 2 to 7, while with pH above 12, the main active species are ·OH. Therefore, to specific reaction system, there is an optimum reaction conditions.

Compared with the high temperature, the technology using transition metal ions can activate persulfate at room temperature. It is a simple reaction system with mild conditions and no external source of energy, and transition metal ion will catalyze the activation. This is a Fenton-like reaction, so transition metal ions are mostly used as homogeneous catalysts (including Fe^{2+}, Cu^{2+}, Mn^{2+}, Ce^{2+}, Co^{2+} etc.) for activating PMS or PS to generate active free radicals. The formula can be seen as follows.

$$HSO_5^- + M^{n+} \rightarrow M^{(n+1)+} + SO_4^{\cdot-} + OH^- \quad (2.39)$$

$$HSO_5^- + M^{n+} \rightarrow M^{(n+1)+} + SO_4^{2-} + OH\cdot \quad (2.40)$$

$HSO_5^- + M^{(n+1)+} \rightarrow M^{n+} + SO_5^{\cdot -} + H^+$ (2.41)

$SO_4^{\cdot -}$ +organics → intermediates → $CO_2 + H_2O + SO_4^{2-}$ (2.42)

The catalytic activities of different transition metals are in the following order: $Ag^+ > Co^{2+} > Cu^{2+} > Fe^{2+}$. Wherein, the energy requirement of Fe^{2+} catalytic activation is about 50.2 kJ /mol, which greatly reduces the energy requirement for the reaction. In the metal ion activation system, addition of chelating or complexing agents can improve the reaction efficiency. Currently, the catalyst activation research main focuses on the exploration of mechanism and the reaction system.

There are various forms of manganese oxides in the nature, such as MnO, MnO_2, Mn_2O_3 and Mn_3O_4. And the toxicity of manganese ions are lower than other metal ions to the environment. Based on these characteristics, the manganese oxides have been reported as promising catalysts to activate PMS to produce active substances [101,102]. In recent studies, manganese oxides have been investigated as a variety of oxidation states[103 - 110], shapes and sizes. When PMS was activated, the pollutants are decomposed into hydroxyl and sulfate radicals [107]. The following figure shows the mechanism of the PMS activated by manganese oxide for phenol degradation.

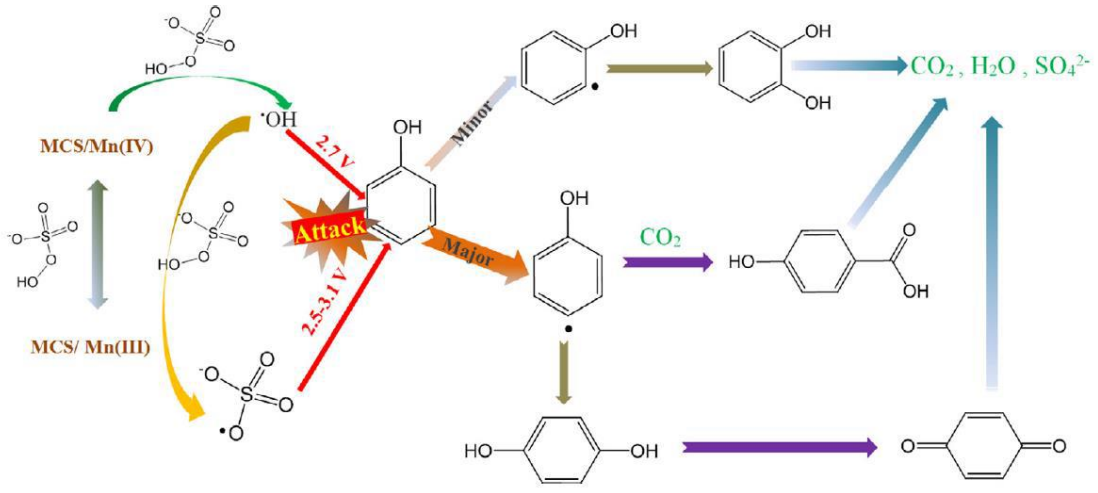

Fig. 2. 3. The mechanism of the PMS activated by manganese oxide in phenol degradation[108].

During the past few years, the mixed valent manganites materials have been receiving increasing attention for their unique physicochemical properties [111,112], and some facile methods have been employed to increase the performance of the mixed valent manganite catalysts. Lee and his group found that a new spinel $LiMn_2O_4$ can be considered as a promising electrode material due to its high thermal stability, low cost, abundance and environmental affinity. Calcium manganites ($CaMn_3O_6$ and $CaMn_4O_8$) microspheres with 3D hierarchical structure were observed as 1D sub-blocks component structure which were synthesized using calcium carbonate, ammonium carbonate and manganese carbonate [115,116]. To our best knowledge, most of the current investigations of mixed valent manganites were applied in energy applications, few researches are related to wastewater treatment, and no further investigation has been reported for using calcium-manganese oxide or calcium-manganese oxide based composite material as catalysts to active PMS for phenol removal.

Apart from manganese catalysts, novel metal-free catalysts such as reduced graphene oxide (rGO) was proven to be effective as a catalyst for decomposing organic pollutions[117]. The activity is higher than graphite powder (GP), activated carbon (AC), carbon nanotube (CNT), and graphene oxide (GO).

To conclude, sulfate radical-based advanced oxidation processes are found to have effective activity for degradation of various organic pollutants. Compared with other catalytic reactions, sulfate radicals-based method has a higher efficiency due to the higher redox potential of the sulfate radicals. Moreover, utilizing sulfate radical to treat wastewater needs less complicated conditions due to the wide pH requirement and no extra power sources. Therefore, utilizing

sulfate radicals for destruction of aqueous organic pollutants has become a promising remediation technology in terms of AOPs.

2.4 Conclusions

As described above, a huge amount of organic compounds in wastewater have been discharged from industrial processes and human activities recently. These synthetic organic compounds are toxic in aqueous phase, and may cause many human diseases like cancer and genic mutation. A variety of techniques have been employed to remove the pollutants in wastewater. Wet air oxidation (WAO) and catalytic wet air oxidation (CWAO) are commonly used technologies in wastewater treatment. However, the commercialization of WAO and CWAO is still a challenge. Advanced oxidation processes (AOPs) are based on the formation of hydroxyl or sulphate radicals, which are used as oxidizing agents to degrade organic pollutants. Chemical oxidation employing reagents to transform organic compounds into harmless components in aqueous phase, although some other substances such as minerals are not the targeted substances. However, these methods do not show great effect, because they need post-treatment. Compared with the traditional technologies, Fenton reaction has better efficiency which could completely mineralize organic contaminants to non-toxic byproducts. Whereas the metal leaching problem is serious, and it required specific pH conditions. While photocatalytic process has low efficiency and presents a great effect with less cost. Compared with the conventional ozone oxidation, catalytic oxidation could effectively degrade organic matters more thoroughly.

Recently, utilizing sulfate radicals has attracted extensive attention. Compared with the

hydroxyl radicals, sulfate radicals have a higher redox potential (2.7V and 3.1V), and can operate under neutral pH conditions. Compared with other metal ion catalysts, manganese oxide catalysts exhibit higher catalytic activity and lower toxicity.

2.5 References:

1. Gupta,V.K.; Ali, I; Saleh, T.A.; Nayak, A; Agarwal, S. Chemical Treatment Technologies for Waste-Water Recycling-An Overview. RSC Adv. 2(2012) pp. 6380-6388.

2. McGraw-Hill. Wastewater solids incineration systems / prepared by the Incineration Task Force of the Water Environment Federation. Water Environment Federation. Incineration Task Force. New York: McGraw-Hill Professional. 2009.

3. Bourge, Robert C.; Tallaj, José A. Ultrafiltration. Journal of the American College of Cardiology. 46(2005) pp.2052-2053.

4. Han, Y.; Xu, Z.; Gao, C. Ultrathin Graphene Nanofiltration Membrane for Water Purification. Advanced Functional Materials, 23(2013) pp.3693-3700.

5. Liang, S.; Teng, F.; Bulgan, R.; Zong, Y.; Zhu, Y. Effect of phase structure of MnO_2 nanorod catalyst on the activity for CO oxidation. Journal of Physical Chemistry C, 112(2008), pp.5307-5315.

6. Zaki M.; Hasan M.; Pasupulety L. Influence of CuOx additives on CO oxidation activity and related surface and bulk behaviours of Mn_2O_3, Cr_2O_3 and WO_3 catalysts. Applied Catalysis A: General. 198 (2000) pp. 247-259.

7. Hasan, M.; Zaki, M.; Pasupulety, L. Oxide-catalyzed conversion of acetic acid into acetone: an FTIR spectroscopic investigation Applied Catalysis A, General, 243(2003), pp.81-92

8. Liu, Z. ; Xing, Y. ; Fang, S. ; Qu, X. ; Wu, D. ; Zhang, A. ; Xu, B. Low temperature self-assembled synthesis of hexagonal plate-shape Mn_3O_4 3D hierarchical architectures and their application in electrochemical capacitors. RSC Advances, 5(2015), pp.54867-54872.

9. Saputra, E. ; Muhammad, S. ; Sun, H. ; Ang, H. ; Tadé, M. ; Wang, S. Shape-controlled activation of peroxymonosulfate by single crystal α-Mn_2O_3 for catalytic phenol degradation in aqueous solution Applied Catalysis B: Environmental, 154-155(2014), pp.246-251.

10. Wang, Y. ; Sun, H. ; Ang, H. ; Tadé, M. ; Wang, S. 3D-hierarchically structured MnO_2 for catalytic oxidation of phenol solutions by activation of peroxymonosulfate: Structure dependence and mechanism. Applied Catalysis B: Environmental, 164(2015), pp.159-167.

11. Nico, P. ; Zasoski, R. Mn(III) center availability as a rate controlling factor in the oxidation of phenol and sulfide on δ-MnO_2. Environmental Science and Technology. 35(2001) pp. 3338-3343.

12. Yao, Y. ; Cai, Y.u ; Wu, G. ; Wei, F. ; Li, X. ; Chen, H. ; Wang, S. Sulfate radicals induced from peroxymonosulfate by cobalt manganese oxides ($CoxMn_3{-}xO_4$) for Fenton-Likereaction in water. Journal of Hazardous Materials. 296(2015) pp.128-137.

13. Bianco, B.; Macolino, P. ; Quattranni, S. ; Veglio', F. Effect of Fenton process on biological treatment of industrial waste waters. Journal of Biotechnology. 150(2010) pp.58-58.

14. Anipsitakis, G. ; Dionysiou, D. Radical generation by the interaction of transition metals with common oxidants. Environmental Science & Technology, 38(2004), pp.3705-3712.

15. Saputra, E. ; Muhammad, S. ; Sun, H. ; Ang, H. ; Tade, M. ; Wang, S. Red mud and fly ash supported Co catalysts for phenol oxidation. Catalysis Today, 190(2012), pp.68-72.

16. Muhammad, S. ; Shukla, P. ; Tade, M. ; Wang, S. Heterogeneous activation of peroxymonosulphate by supported ruthenium catalysts for phenol degradation in water. Journal of Hazardous Materials, 215(2012), pp.183-190.

17. Zhang, B.; Zhang, Y.; Teng, Y.; Fan, M. Sulfate Radical and Its Application in

Decontamination Technologies. Critical Reviews in Environmental Science and Technology. 45(2015), pp.1756-1800.

18. Zazo, J. ; Casas, J. ; Mohedano, A. ; Gilarranz, M. ; Rodríguez, J. Chemical pathway and kinetics of phenol oxidation by Fenton's reagent. Environmental Science and Technology. 39(2005), pp.9295-9302.

19. Watts, R.; Loge, F.; Teel, A.; Sarasa, J. Oxidative and reductive pathways in manganese-catalyzed Fenton's reactions. Journal of Environmental Engineering. 131(2005), pp.158-164.

20. Wastewater engineering: Third Edition. Metcalf & Eddy, Inc. Revised by George Tchobanoglous and Franklin L.Burton. McGraw-Hill, Inc.: New York, NY 1991. pp. 1334. Waste Management. 12(1992), pp.102-102.

21. Diamond, M. ; de Wit, Cynthia A. ; Molander, S. ; Scheringer, M. ; Backhaus, T. ; Lohmann, R. ;Arvidsson, R. ; Bergman, Å. ; Hauschild, M. ; Holoubek, I. ; Persson, L.; Suzuki, N.; Vighi, M.;Zetzsch, C.Exploring the planetary boundary for chemical pollution. Environment International. 78(2015), pp. 8-15.

22. Lu, Y.; Xu, S. ; He, M.; Chen, C.; Zhang, L.; Liu, C.; Chu, F.; Yu, Z.; Zhou, Z.; Zhong, M. Glucose administration attenuates spatial memory deficits induced by chronic low-power-density microwaveexposure. Physiology & Behavior. 106(2012), pp. 631-637.

23. Dohnal, V.; Fenclová, D. Air-water partitioning and aqueous solubility of phenols. Journal of Chemical and Engineering Data. 40(1995), pp. 478-483.

24. Saputra E.; Muhammad S.; Sun H.; Ang H.; Tade M.; Wang S. A comparative study of structured Mn_3O_4, Co_3O_4 and Fe_3O_4 nanoparticles in catalytic oxidation of phenolic contaminants in aqueous. Journal of Colloid and Interface Science. 407(2013) pp. 467-473.

25. Zhang, L. ; Fang, M. Nanomaterials in pollution trace detection and environmental improvement. Nano Today. 5(2010), pp.128-142.

26. Zhang, T. Environmental and Water Resources Institute (U.S.). Nanotechnology Task Committee.Reston, VA: American Society of Civil Engineers (2009).

27. Agustina, T. Comparison of various advanced oxidation processes for the treatment of winery wastewater / Tuty Emilia Agustina.Curtin University of Technology. Dept. of Chemical Engineering. Thesis (Ph. D.)--Curtin University of Technology (2007).

28. Mishra, V. ; Mahajani, V. ; Joshi, J. Wet air oxidation. Industrial and Engineering Chemistry Research. 34(1995), pp.2-48.

29. Luck, F. Wet air oxidation: past, present and future. Catalysis Today. 53(1999), pp.81-91.

30.Imamura, S.Catalytic and noncatalytic wet oxidation.Industrial & Engineering Chemistry Research. 38(1999) pp.1743-1753.

31. Bhargava, S. Wet Oxidation and Catalytic Wet Oxidation. Industrial & Engineering Chemistry Research. 45(2006) pp. 1221-1258.

32. Patterson, D. Wet Air Oxidation of Linear Alkylbenzene Sulfonate 2. Effect of pH. Industrial & Engineering Chemistry Research. 40(2001) pp. 5517-5525.

33. López B. Wet air oxidation of oily wastes generated aboard ships: kinetic modeling. Journal of Hazardous Materials. 67(1999) pp. 61-73.

34. Willms, R. Aqueous-phase oxidation: the intrinsic kinetics of single organic compounds. Industrial & Engineering Chemistry Research. 26(1987) pp. 148-154.

35. Laughlin, R.; T. Gallo; H. Robey. Wet air oxidation for hazardous waste control. Journal of Hazardous Materials. 8(1983): pp. 1-9.

36. Bhargava, S. Catalytic Wet Air Oxidation of Industrial Aqueous Streams. Catalysis Surveys from Asia. 11(2007) pp. 70-86.

37. Zhang Y. Catalytic wet air oxidation of dye pollutants by polyoxomolybdate nanotubes under room condition. Applied Catalysis B: Environmental. 86(2009) pp. 182-189.

38. Henry John Horstman, Fenton - Short biography and brief history of Fenton reagent discovery. Chemia Dydaktyka Ekologia Metrologia 2009, R. 14, NR 1-2, pp. 101-105.

39. Gomes L.; Duarte J.; Pereira N.; Tonholo C.; Zanta C. Development of a system for treatment of coconut industry wastewater using electrochemical processes followed by Fenton reaction. Water Science & Technology 69 (2014) pp. 2258-2264

40. Toda, K. ; Tanaka, T. ; Tsuda, Y. ; Ban, M. ; Koveke, E. ; Koinuma, M. ; Ohira, S. Sulfurized limonite as material for fast decomposition of organic compounds by heterogeneous Fenton reaction. Journal of hazardous materials. 278(2014), pp.426-32. 41. Sekar, R. ; Dichristina, T. Microbially driven Fenton reaction for degradation of the widespread environmental contaminant 1,4-dioxane. Environmental science & technology. 48(2014), pp.12858-67

42. Feng, Y. ; Lu, K. ; Mao, L. ; Guo, X. ; Gao, S. ; Petersen, E. Degradation of (14)C-labeled few layer graphene via Fenton reaction: Reaction rates, characterization of reaction products, and potential ecological effects. Water research. 84(2015), pp.49-57

43. Liang, X. ; He, Z. ; Wei, G. ; Liu, P. ; Zhong, Y. ; Tan, W. ; Du, P. ; Zhu, J. ; He, H. ; Zhang, J. The distinct effects of Mn substitution on the reactivity of magnetite in heterogeneous Fenton reaction and Pb(II) adsorption. Journal of colloid and interface science. 426(2014), pp.181-9.

44. Marković, M. ; Jović, M. ; Stanković, D. ; Kovačević, V. ; Roglić, G. ; Gojgić-Cvijović, G. ; Manojlović, D. Application of non-thermal plasma reactor and Fenton reaction for

degradation of ibuprofen. Science of the Total Environment. 505(2015), pp.1148-1155.

45. Bonfatti, F.; Ferro, S.; Lavezzo, F.; Malacarne, M.; Lodi, G. ; De Battisti, A. Electrochemical incineration of glucose as a model organic substrate. Part I: role of the electrode material. J. Electrochem. 146, 2175–2179.

46. Brillas, E.; Sirés, I.; Oturan, M. A. Electro-Fenton process and related electrochemical technologies based on Fenton's reaction chemistry. Chem. Rev. 109, 6570–6631.

47. Wang, Y.; Sun, H.; Ang, H.; Tade, M.; Wang, S. Facile Synthesis of Hierarchically Structured Magnetic $MnO_2/ZnFe_2O_4$ Hybrid Materials and Their Performance in Heterogeneous Activation of Peroxymonosulfate, ACS. Mater. Interfaces 6 (2014) pp. 19914-19923.

48. Yao, Y.; Cai, Y.; Wu, G.; Wei, F.; Li, X.; Chen, H.; Wang, S. Sulfate radicals induced from peroxymonosulfate by cobalt manganese oxides ($CoxMn_3{-}xO_4$) for Fenton-Like reaction in water. Journal of Hazardous Materials. 296(2015) pp. 128-137.

49. Wang S. A Comparative study of Fenton and Fenton-like reaction kinetics in decolourisation of wastewater. Dyes and Pigments. 76(2008) pp. 714–720.

50. Wang Y. Metal-based Nanocatalysts for Oxidative Degradation of Aqueous Organic Pollutants in Contaminated Water. School of Chemical and Petroleum Engineering Department of Chemical Engineering. 2015

51. Dunford HB. Oxidations of iron (II) (III) by hydrogen peroxide: from aquo to enzyme. Coord. Chem. Rev. 2002; 233–234(0):311-8.

52. Mackuľak, Tomáš; Olejníková, Petra; Prousek, Josef; Švorc, Ľubomír. Toxicity reduction of 2-(5-nitrofuryl) acrylic acid following Fenton reaction treatment. Chemical Papers. 65(2011), pp.835-839.

53. Gong, Y. ; Li, J. ; Zhang, Y. ; Zhang, M. ; Tian, X. ; Wang, A. Partial degradation of levofloxacin for biodegradability improvement by electro-Fenton process using an activated carbon fiber felt cathode. Journal of hazardous materials. 304(2016), pp.320-8.

54. Trujillo, D. ; Font, X. ; Sánchez, A. Use of Fenton reaction for the treatment of leachate from composting of different wastes. Journal of Hazardous Materials. 138(2006), pp.201-204

55. Lee, H. ; Shoda, M. Removal of COD and color from livestock wastewater by the Fenton method. Journal of Hazardous Materials. 153(2008), pp.1314-1319.

56. Sttle T; Khanitchaidecha W. A Nakaruk, Synthesis of iron/GAC catalyst for wastewater treatment using heterogeneous Fenton reaction. Bulletin of Materials Science. 38(2015) pp 1039-1042.

57. Bokare AD.; Choi W. Review of iron-free Fenton-like systems for activating H2O2 in advanced oxidation processes. J. Hazard. Mater. 275(2014):121-35.

58. Li S. ; Li Y. ; Yang F.; Liu Z.; Gao R. Zhao J. Photocatalytic oxidation desulfurization of model diesel over phthalocyanine/$La_{0.8}Ce_{0.2}NiO_3$. Journal of Colloid and Interface Science. 460(2015) pp. 8–17.

59. Southworth B.; Voelker B. Hydroxyl Radical Production via the Photo-Fenton Reaction in the Presence of Fulvic Acid. Environ. Sci. Technol. 37(2003) pp. 1130-6.64.

60. Zepp R.; Faust B.; Hoigne J. Hydroxyl radical formation in aqueous reactions (pH 3-8) of iron (II) with hydrogen peroxide: the photo-Fenton reaction. Environ. Sci. Technol. 26(1992) pp. 313-9.

61. Malato S.; Blanco J.; Alarcón D. Maldonado MI, Fernández-Ibáñez P, Gernjak W. Photocatalytic decontamination and disinfection of water with solar collectors. Catal. Today. 122(2007) pp. 137-49.

62. Oller I.; Malato S.; Sánchez-Pérez J.; Gernjak W.; Maldonado M.; Pérez-Estrada L. A combined solar photocatalytic-biological field system for the mineralization of an industrial pollutant at pilot scale. Catal. Today. 122(2007) pp. 150-9.

63.Cheng M, Song W, Ma W, Chen C, Zhao J, Lin J, et al. Catalytic activity of iron species in layered clays for photodegradation of organic dyes under visible irradiation. Appl. Catal., B. 2008; 77(3–4):355-63.

64.Liu R, Xiao D, Guo Y, Wang Z, Liu J. A novel photosensitized Fenton reaction catalyzed by sandwiched iron in synthetic nontronite. RSC Adv. 2014; 4(25):12958-63.

65. Chong MN, Jin B, Chow CWK, Saint C. Recent developments in photocatalytic water treatment technology: A review. Water Res. 2010; 44(10):2997-3027.

66. Liu, J. ; Liu, R. ; Li, H. ; Kong, W. ; Huang, H. ; Liu, Y. ; Kang, Z.Au nanoparticles in carbon nanotubes with high photocatalytic activity for hydrocarbon selective oxidation. Dalton Transactions, 2014, Vol. 43(34), pp.12982-1298

67. Rodríguez, E. ; Núñez, B. ; Fernández, G. ; Beltrán, F. Effects of some carboxylic acids on the Fe(III)/UVA photocatalytic oxidation of muconic acid in water. Applied Catalysis B, Environmental, 2009, Vol. 89(1), pp.214-222.

68. Eng, Yong Y.; Sharma, V. ; Ray, A. Photocatalytic degradation of nonionic surfactant, Brij 35 in aqueous TiO_2 suspensions. Chemosphere, 2010, Vol. 79(2), pp.205-209.

69. Zhang, D. Photocatalytic oxidation of organic dyes with nanostructured zinc dioxide modified with silver metals. Russian Journal of Physical Chemistry A, 2011, Vol. 85(8), pp.1416-1422

70. Zhao, Y. ; Huang, D. ; Huang, L. ; Chen, Z. Hydrogen peroxide enhances the oxidation of oxygenated volatile organic compounds on mineral dust particles: a case study of methacrolein. Environmental science & technology, 2014, Vol. 48 (18), pp.10614-23

71. Li D.; Qu J. The progress of catalytic technologies in water purification: A review, J. Environ. Sci. 21 (2009), pp. 713–719.

72. Liotta L.; Gruttadauria M.; Carlo G.; Perrini G.; Librando V. Heterogeneous catalytic degradation of phenolic substrates: Catalysts activity, J. Hazard. Mater. 162 (2009), pp. 588–606.

73. Perez C.A.G. Application of heterogeneous catalysts in ozonation of model compounds in water, M.Sc. thesis, University of Saskatchewan, 2010.

74. Kasprzyk-Hordern B.; Ziółek M.; Nawrocki J. Catalytic ozonation and methods of enhancing molecular ozone reactions in water treatment. Appl. Catal., B. 46(2003) pp. 639-69.

75. Andreozzi R.; Canterino M.; Marotta R. Antibiotic removal from wastewaters: The ozonation of amoxicillin J. Hazard. Mater. 122(2005) pp. 243-50.

76. Nawrocki J.; Kasprzyk-Hordern B. The efficiency and mechanisms of catalytic ozonation. Applied Catalysis B: Environmental. 99(2010) pp. 27-42.

77. Legube B.; Karpel Vel Leitner N. Catalytic ozonation: a promising advanced oxidation technology for water treatment. Catal. 53(1999) pp. 61-72.

78. Peixoto, H.J. Izário; Filho, H.J. Izário Brazilian. Statistical evaluation of mature landfill leachate treatment by homogeneous catalytic ozonation. Journal of Chemical Engineering. 27(2010) pp.531-537.

79. Cortés S.; Sarasa J.; Ormad P.; Gracia R.; Ovelleiro J. Comparative Efficiency of the Systems O_3/High pHAnd O_3/catalyst for the Oxidation of Chlorobenzenes in Water. Ozone Sci. Eng. 22(2000) pp. 415-26.

80. Pines D.; Reckhow D. Effect of Dissolved Cobalt (II) on the Ozonation of Oxalic Acid. Environ. Sci. Technol. 36(2002) pp. 4046-51.

81. Koeppe, B. ; Guo, J. ; Tolstoy, P. ; Denisov, G.; Limbach, H. Solvent and H/D isotope effects on the proton transfer pathways in heteroconjugated hydrogen-bonded phenol-carboxylic acid anions observed by combined UV-vis and NMR spectroscopy
Journal of the American Chemical Society. 135(2013), pp.7553-66.

82. Beltrán FJ, Rivas FJ, Montero-de-EspinosaR. Ozone-enhanced oxidation of oxalic acid in water with cobalt catalysts. 1. Homogeneous catalytic ozonation. Ind. Eng. Chem. Res. 42(2003) pp.3210-7.

83. Cooper C.; Burch R. An investigation of catalytic ozonation for the oxidation of halocarbons in drinking water preparation. Water Res. 33(1999) pp.3695-700.

84. Beltran FJ.; Rivas FJ.; Montero-de-Espinosa R. Catalytic ozonation of oxalic acid in an aqueous TiO2slurry reactor. Appl.Catal. B. 39(2002) pp.221-31.

85. Sui M.; Sheng L.; Lu K.; Tian F. FeOOH catalytic ozonation of oxalic acid and the effect of phosphate binding on its catalytic activity. Appl. Catal., B. 2010; 96 (1–2) pp.94-100.

86. Faria P.; Monteiro D.; Órfão J.; Pereira M. Cerium, manganese and cobalt oxides as catalysts for the ozonation of selected organic compounds. Chemosphere. 74(2009) pp. 818-24.

87. Alvarez P.; Beltrán F.; Pocostales J.; Masa F. Preparation and structural characterization of Co/Al2O3catalysts for the ozonation of pyruvic acid. Appl. Catal., B. 72(2007) pp. 322-30.

88. Pi Y.; Ernst M, Schrotter J-C. Effect of Phosphate Buffer upon CuO/Al2O3and Cu (II) Catalyzed Ozonation of Oxalic Acid Solution. Ozone Sci. Eng. 25(2003) pp. 393-7.

89. Avramescu S.; Bradu C.; Udrea I.; Mihalache N.; Ruta F. Degradation of oxalic acid from aqueous solutions byozonation in presence of Ni/Al2O3catalysts. Catal. Commun. 9(2008) pp.2386-91.

90. Yang L.; Hu C.; Nie Y.; Qu J. Catalytic ozonation of selected pharmaceuticals over mesoporous alumina-supported manganese oxide. Environ. Sci. Technol. 43(2009) pp.2525-9.

91. Martins R.; Quinta-Ferreira R. Catalytic ozonation of phenolic acids over a Mn–Ce–O catalyst. Appl. Catal., B. 90(2009) pp.268-77.

92. Cao H.; Xing L.; Wu G.; Xie Y.; Shi S.; Zhang Y. Promoting effect of nitration modification on activated carbon in the catalytic ozonation of oxalic acid. Appl. Catal., B. 146(2014) pp.169-76.

93. Matheswaran M.; Moon I. Influence parameters in the ozonation of phenol wastewater treatment using bubble column reactor under continuous circulation. J. Ind. Eng. Chem. 15(2009) pp.287-92.

94.Bokare A.; Choi W. Review of iron-free Fenton-like systems for activating H_2O_2 in advanced oxidation processes. J. Hazard. Mater. 275(2014) pp.121-35.

95. Chan Y.; Chong M.; Law C.; Hassell D. A review on anaerobic–aerobic treatment of industrial and municipal wastewater. Chem. Eng. J. 155(2009) pp.1-18.

96. Zhang B.; Zhang Y.; Teng Y.; Fan M. Sulfate Radical and its Application in Decontamination Technologies. Crit. Rev. Env. Sci. Technol. 2014.

97. Anipsitakis G.; Dionysiou D. Degradation of Organic Contaminants in Water with Sulfate Radicals Generated by the Conjunction of Peroxymonosulfate with Cobalt. Environ. Sci. Technol. 37(2003) pp. 4790-7.

98. Tsitonaki A.; PetriB, C.; MosbÆK H.; Siegrist R.; Bjerg P. In Situ Chemical Oxidation of Contaminated Soil and Groundwater Using Persulfate: A Review. Crit. Rev. Env. Sci. Technol. 2010; 40 (1) pp. 55-91.

99. Wang S.; Peng Y. Natural zeolites as effective adsorbents in water and wastewater treatment. Chem. Eng. J. 156(2010) pp.11–24.

100. Dias J.; Alvim-Ferraz M.; Almeida M.; Rivera-Utrilla J.; Sánchez-Polo M. Waste materials for activated carbon preparation and its use in aqueous-phase treatment: A review. J. Environ. Manage. 85(2007) pp. 833-46.

101. Saputra E.; Muhammad S.; Sun H.; Ang H.; Tadé M.; Wang S. Different Crystallographic One-dimensional MnO2Nanomaterials and Their Superior Performance in Catalytic Phenol Degradation. Environ. Sci. Technol. 47(2013) pp. 5882-7.

102. Saputra E, Muhammad S, Sun H, Patel A, Shukla P, Zhu ZH, et al. α-MnO2activation of peroxymonosulfate for catalytic phenol degradation in aqueous solutions. Catal. Commun.

26(2012) pp. 144-8.

103. Saputra E.; Muhammad S.; Sun H.; Ang H.; Tadé M.; Wang S. Shape-controlled activation of peroxymonosulfate by single crystal α-Mn2O3for catalytic phenol degradation in aqueous solution. Appl. Catal., B. 154–155(2014) pp.246-51.

104. Saputra E.; Muhammad S.; Sun H.; Ang H.; Tadé M.; Wang S. A comparative study of spinel structured Mn3O4, Co3O4and Fe3O4nanoparticles in catalytic oxidation of phenolic contaminants in aqueous solutions. J. Colloid Interface Sci. 407(2013) pp. 467-73.

105. Saputra E.; Muhammad S.; Sun H.; Ang H.; Tadé M.; Wang S. Manganese oxides at different oxidation states for heterogeneous activation of peroxymonosulfate for phenol degradation in aqueous solutions. Appl. Catal., B. 142–143(2013) pp. 729-35.

106. Saputra E, Muhammad S, Sun H, Ang H, Tadé M, Wang S. Different Crystallographic One-dimensional MnO2Nanomaterials and Their Superior Performance in Catalytic Phenol Degradation. Environ. Sci. Technol. 2013; 47(11) pp. 5882-7.

107. Saputra E, Muhammad S, Sun H, Ang H, Tadé M, Wang S. Shape-controlled activation of peroxymonosulfate by single crystal α-Mn2O3for catalytic phenol degradation in aqueous solution. Appl. Catal., B. 154–155(2014) pp.246-51.

108. Wang Y, Indrawirawan S, Duan X, Sun H, Ang H, Tadé M, Wang S. New insights into heterogeneous generation and evolution processes of sulfate radicals for phenol degradation over one-dimensional α-MnO2nanostructures. Chem. Eng. J. 266(2015) pp.12-20.

109. Wang Y, Sun H, Ang H, Tadé M, Wang S. 3D-hierarchically structured MnO2for catalytic oxidation of phenol solutions by activation of peroxymonosulfate: Structure dependence and mechanism. Appl. Catal., B. 164(2015) pp.159-67.

110. Saputra E.; Muhammad S.; Sun H.; Ang H. Shape-controlled activation of peroxymonosulfate by single crystal α-Mn2O3 for catalytic phenol degradation in aqueous solution. Applied Catalysis B: Environmental 154-155 (2014) pp.245-251.

111. Song M., Cheng S., Chen H., Qin W., Nam K., Xu S., Yang X., Bongiorno A., Lee J., Bai J., Tyson T., Cho J., Liu M., Anomalous pseudocapacitive behavior of a nanostructured, mixed-valent manganese oxide film for electrical energy storage, Nano Lett., 12 (2012) pp.3483-3490.

112. Han X., Zhang T., Du J., Cheng F., Chen J., Porous calcium-manganese oxide microspheres for electrocatalytic oxygen reduction with high activity, Chem. Sci., 4 (2013) pp. 368-376.

113. Si, W.; Wang, Y.; Peng, Y.; Li, J. Selective Dissolution of A-Site Cations in ABO_3 Perovskites: A New Path to High-Performance Catalysts. Angewandte Chemie (International ed. in English), 54 (2015), pp.7954-7

114. Zhang C.; Hua W.; Wang C.; Guo Y.; Guo Y.; Lu G.; Baylet A.; Giroir-Fendler A. The effect of A-site substitution by Sr, Mg and Ce on the catalytic performance of $LaMnO_3$ catalysts for the oxidation of vinyl chloride emission. Applied Catalysis B: Environmental, 2013

115. Mohammad M.; Nayeri S.;Pashaei B. Nano-size amorphous calciummanganese oxide as an efficient and biomimetic water oxidizing catalyst for artificial photosynthesis: back to manganese Najafpour, Dalton Transactions, Dalton Transactions, 40 (2011), pp.9374-9378.

116. Wang Y.; Xie Y.; Sun H.; Xiao J.; Cao H.; Wang S., Hierarchical shape-controlled mixed-valence calcium manganites for catalytic ozonation of aqueous phenolic compounds. Catalysis Science & Technology, 2016

117. Sun H, Wang Y, Liu S, Ge L, Wang L, Zhu Z, et al. Facile synthesis of nitrogen doped

reduced graphene oxide as a superior metal-free catalyst for oxidation. Chemical Communications. 49(2013) pp. 9914-6.

3

Chapter 3: The effect of particle size of the porous manganese oxide catalysts on phenol degradation

A B S T R A C T

The size of the highly porous, monodisperse manganese oxide can be controlled by varying the synthesis conditions, and the performances of the catalysts were assessed by the degradation of phenol with activation of PMS. The prepared samples were characterized by Field Emission Scanning Electron Microscopy (FE-SEM), X-ray Diffraction (XRD), Fourier Transform Infrared Spectroscopy (FTIR) and Thermal Gravimetric Analysis (TGA). The experimental results showed that the sample with a small size exhibited the best efficiency in decomposition of phenol in wastewater, and the organic compounds could be completely decomposed in 60 min.

3.1. Introduction

The preservation of water resources has become one of the most challenging tasks in recent years. With the rapid development of economics and industry, the discharge of wastewater that containing persistent organic pollutant (POPs) have posed a threaten to natural resources [1,2]. Traditional physical or biological methods were difficult to deal with the macromolecular organic pollutants, due to their long life-time[3], toxicity[4] and resistance against natural attenuation[5]. Advanced oxidation processes (AOPs) have demonstrated great prospects of addressing toxic chemicals with complete degradation of organic matters into inorganic substance (CO_2, H_2O)[6]. AOPs include a variety of processes such as wet air oxidation (WAO) [7], catalytic wet air oxidation (CWAO) [8], Fenton reaction[9], photocatalytic oxidation[10], electro-catalytic[12], Ozonation/catalytic ozonation[13] and sulfate radical-based advanced oxidation processes[14]. In recent years, sulfate radical-based AOPs have attracted extensive attention.

The AOPs based on sulfate radical ($SO_4^{\bullet -}$) have been proven as an effective approach for POPs removal, because of the strong oxidizing ability at room temperature, high stability, good water solubility and low price[15 16]. However, as the stability of peroxymonosulfate (PMS) and persulfate (PS) at room temperature, it is difficult to achieve the desired effect without activation, therefore, $SO_4^{\bullet -}$ needs to be produced from PMS or PS by an activation process. The activation methods include thermal excitation, photo activation[17], ultrasonic activation[18], microwave activation[19] and the transition metal activation[20].

Cobalt catalysis had demonstrated to be highly effective in activation of PMS or PS to produce sulfate radicals to completely degrade organic pollutants. However, the problem of cobalt leaching is inevitable, which could bring in serious health problems[21-23]. Manganese, as an

essential element for lives that is widely present in nature, has a low toxicity to the environment. Therefore, Mn has been deemed as promising catalysts in wastewater treatment[24]. The chemical states, morphology, size and crystal phases of manganese oxides were found to be playing critical roles in the catalytic oxidation of phenol[25]. For the first time, this chapter reports the effect of particle size of porous manganese oxide catalysts on phenol degradation.

3. 2. Experimental

3. 2.1 Chemicals

n-Butanol (99%), butyric acid (99%), potassium permanganate (99.9%), methanol (99%), phenol (99%) and Oxone ($2KHSO_5 \cdot 3KHSO_4 \cdot K_2SO_4$) were obtained from Sigma-Aldrich. All the chemicals were used as received without further purification.

3. 2.2. Material synthesis

The porous manganese oxide spheres with different sizes were synthesized via a one-step hydration method. The large-sized one was synthesized via adding 25 mL 40 mM $KMnO_4$ in a 25 mL aqueous mixture of 0.48 M butanol and 1.0 M butyric acid, followed by 0.5 h stirring, and the obtained black suspensions were filtered and washed by ethanol and pure water for three cycles. The precipitate was dried in an oven at 80 ℃, and the obtained sample was labeled as M-l. The medium-sized sample was obtained via a similar procedure, with a variation of the concentration ($KMnO_4$) from 40 mM to 20 mM, while changing to 8 mM for the small one, then labelled them as M-m and M-s, respectively.

3. 3. Results and discussion

3. 3.1 Characterization of the composites

There are several techniques that have been used to characterize the physicochemical properties of the manganese oxides. The crystalline structures and phases of the material were studied with X-ray diffraction (XRD) on a Bruker D8 Advance X-ray instrument (Bruker-AXS, Karlsruhe, Germany), using filtered Cu Kα radiation (λ = 1.5418 Å) operated at voltage of 40 kV and current of 30 mA. The particle morphology, size and texture information were investigated on field emission scanning electron microscopy (FE-SEM, Zeiss Neon 40EsB). The surface area and pore size distribution were obtained using N_2 sorption isotherms by the BET and BJH methods, respectively. The manganese content and thermal stability of the catalysts were carried out by the thermogravimetric analysis and differential temperature gradient (TGA/DTG). TGA was conducted on a Perkin-Elmer Diamond thermal analyzer with a rising temperature of 10 ^{o}C/min under the flow of air. The Fourier transform infrared spectroscopy (FT-IR) analysis was performed on a Perkin-Elmer Model FTIR-100 with a MIR detector.

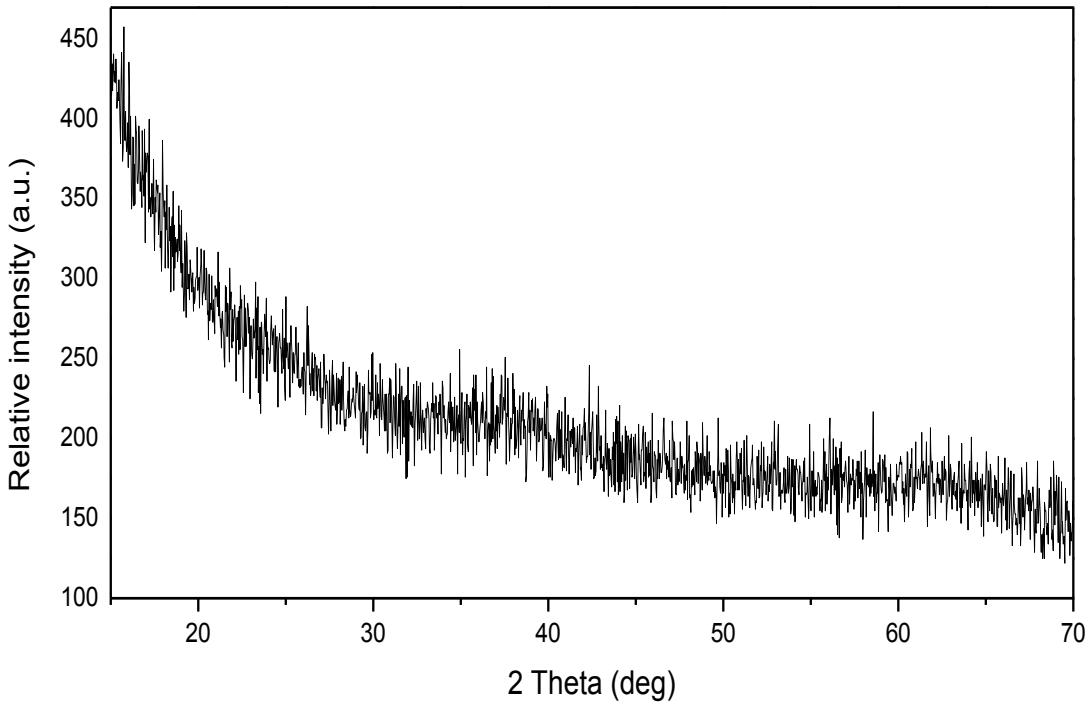

Fig. 3. 1. XRD patterns of M-l

Figure 3.1 is an XRD pattern of the as-prepared M-l. It showed almost none characteristic peaks for phase identification, which revealed the samples were poorly crystalline.

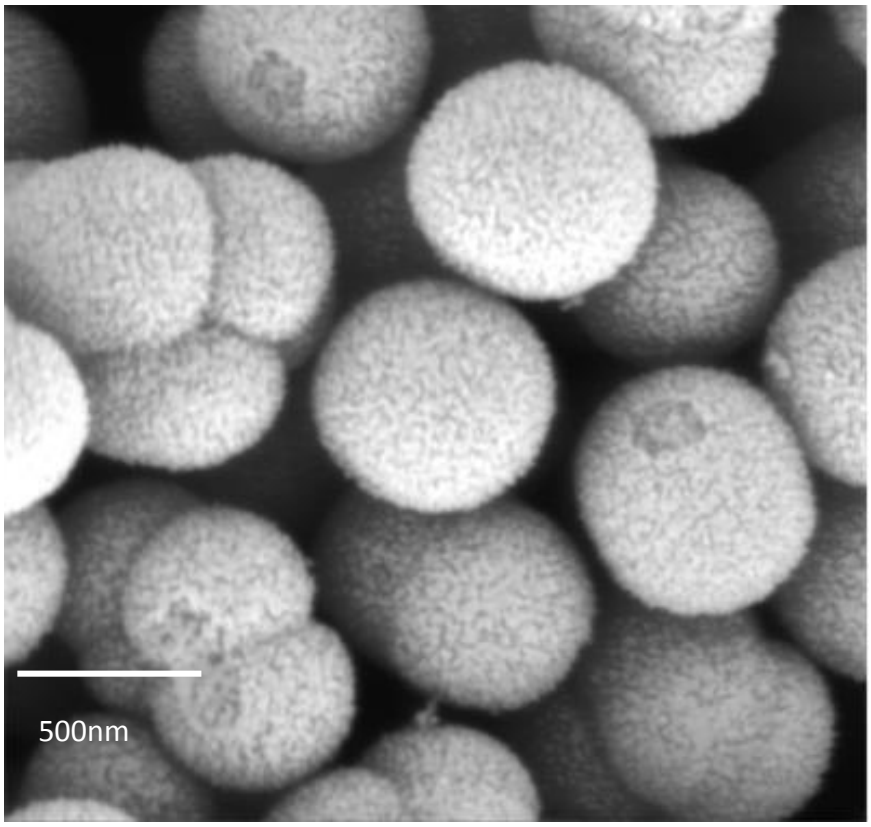

(A)

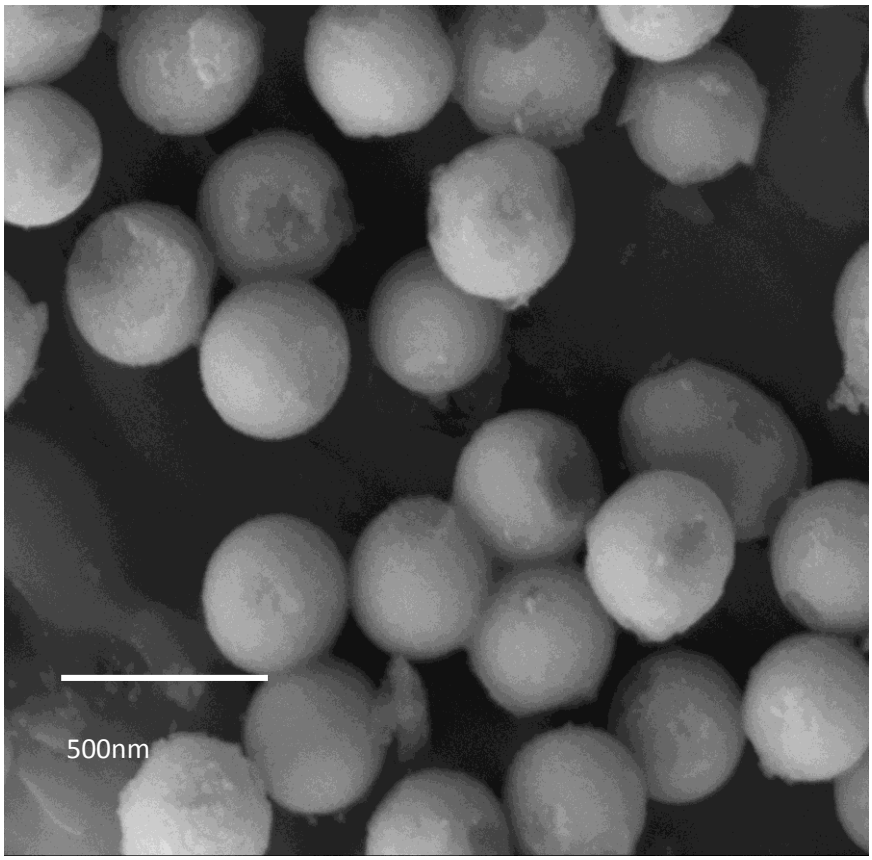

(B)

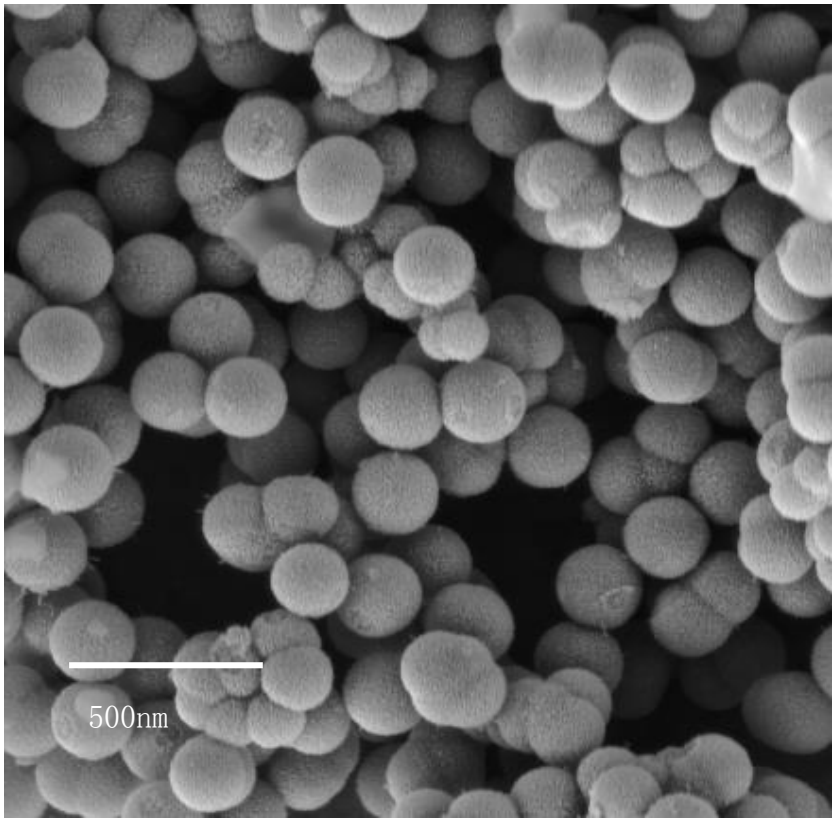

(C)

Fig. 3.2. SEM images of M-l (A), M-m (B) and M-s (C).

Morphologies and sizes of the catalysts are shown in SEM images. It could be observed that M-l, M-m and M-s exhibited mainly a spherical shape with high monodispersion. The average diameters of the spheres were about 500, 350 and 200 nm according to Fig. 3.1A, Fig. 3.1B and Fig. 3.1C, respectively.

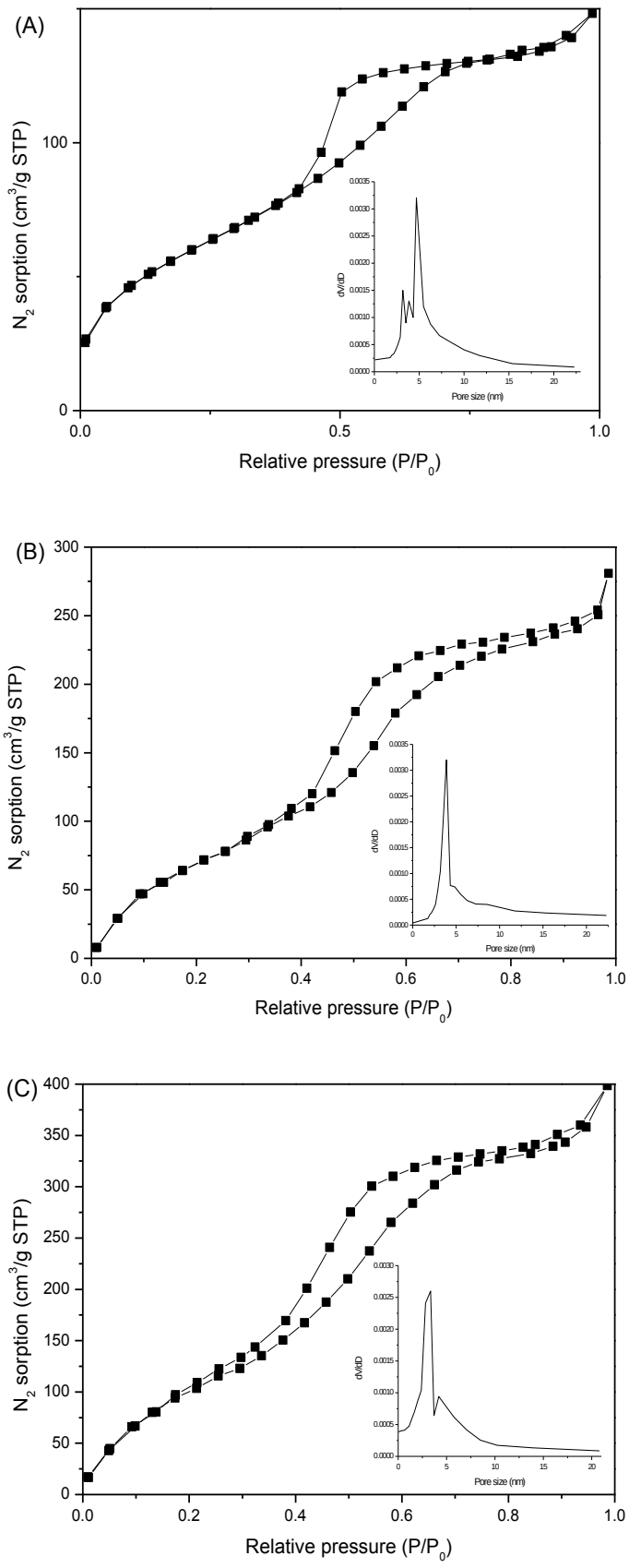

Fig. 3.3. N_2 sorption isotherms and pore size distributions of (A) M-l, (B) M-m and (C) M-s.

Table 3. 1. Textural properties of manganese oxides.

Catalyst	Surface area (S_{BET}, $m^2 g^{-1}$)	Pore volume ($cm^3 g^{-1}$)	Average pore radius (nm)
M-l	115.5	0.155	4.59
M-m	176	0.427	3.88
M-s	217	0.609	3.50

Fig.3.3 shows N_2 adsorption-desorption isotherms and Table 3.1 lists the pore volume and pore size of M-l, M-m and M-s. The hysteresis loops in P/P_0 were 0.40-0.99, 0.33-0.99 and 0.20-0.99, which indicated the mesoporous structure of the sample. Furthermore, the appearance of the H2-type hysteresis loop suggested a porous material with relatively high uniform channel-like pores. The specific surface areas were 116, 176 and 217 m^2/g, respectively. According to the BET analysis, the sample with a smaller size provided a larger surface.

3.3.2 Catalytic oxidation of phenol solutions

Phenol degradation tests were carried out at 25 °C in a 250 mL conical flask containing 20 ppm phenol solution. The conical flask was kept in a water bath with a temperature controller. Firstly, 0.03 g catalyst was put into the phenol solution and constantly stirred at 400 rpm for 5 min until it was dissolved completely. The second step was to start the oxidation reaction with adding 0.3 g Oxone into the reactor, and the reaction was then kept running for 150 min. During the reaction, 1 mL of the solution sample was taken out from the reaction solution at set intervals using a syringe with a filter of 0.45 μm and filtered into a high performance liquid chromatography (HPLC) vial. Then, quenching the reaction with adding 0.5 mL methanol into the vial. The last step was samples analyze, using the HPLC with an UV detector set at wavelength of 270 nm. The mobile phase was 30% acetonitrile and 70% ultrapure water at a flow rate of 1 mL/min passing through a C-18 column. In order to evaluate the catalysts' ability, a regeneration method was employed. The catalyst was filtered and washed after reactions, and then followed with drying overnight in an oven at 60 °C. Finally, the obtained catalyst was used for reuse tests.

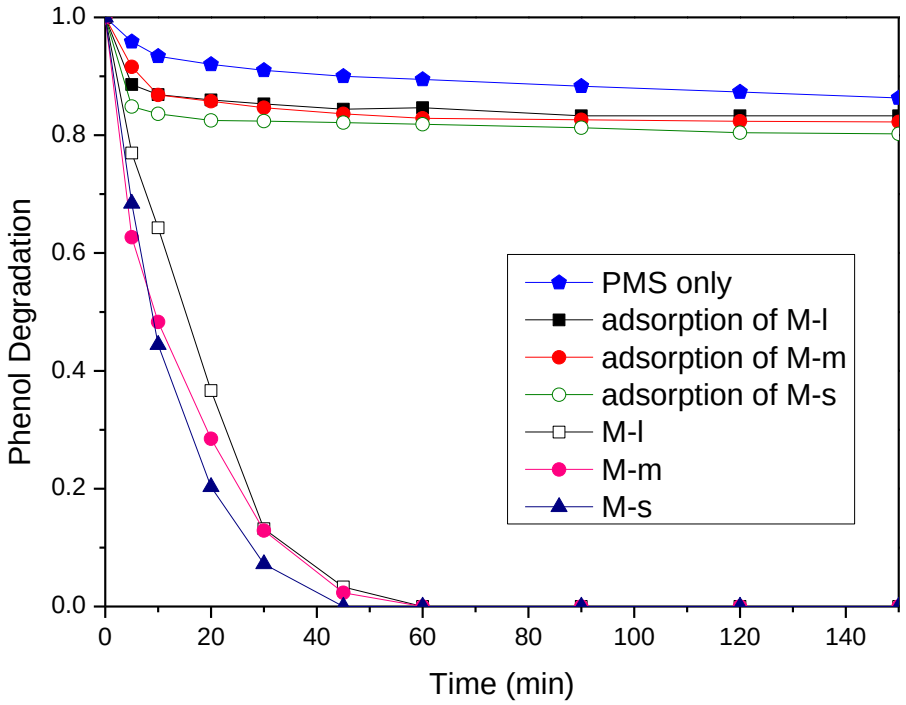

Fig. 3. 4. Phenol removal using M-l, M-m and M-s as the catalysts.

The catalytic oxidation of phenol solutions was carried out in different conditions and the results are shown in Fig.3.4. For the reaction without a catalyst, the final phenol removal rate was about 10% in 150 min. While, within 150 min, 12%, 15% and 18% of phenol could be degraded using catalysts only (M-l, M-m, M-s), which demonstrated that PMS and the catalysts themselves could not induce efficient phenol removal. For the catalytic degradation, M-s showed the best catalytic activity, with 100% removal of phenol in 50 min. In comparison 60 min was required for M-l and M-m to complete phenol degradation.

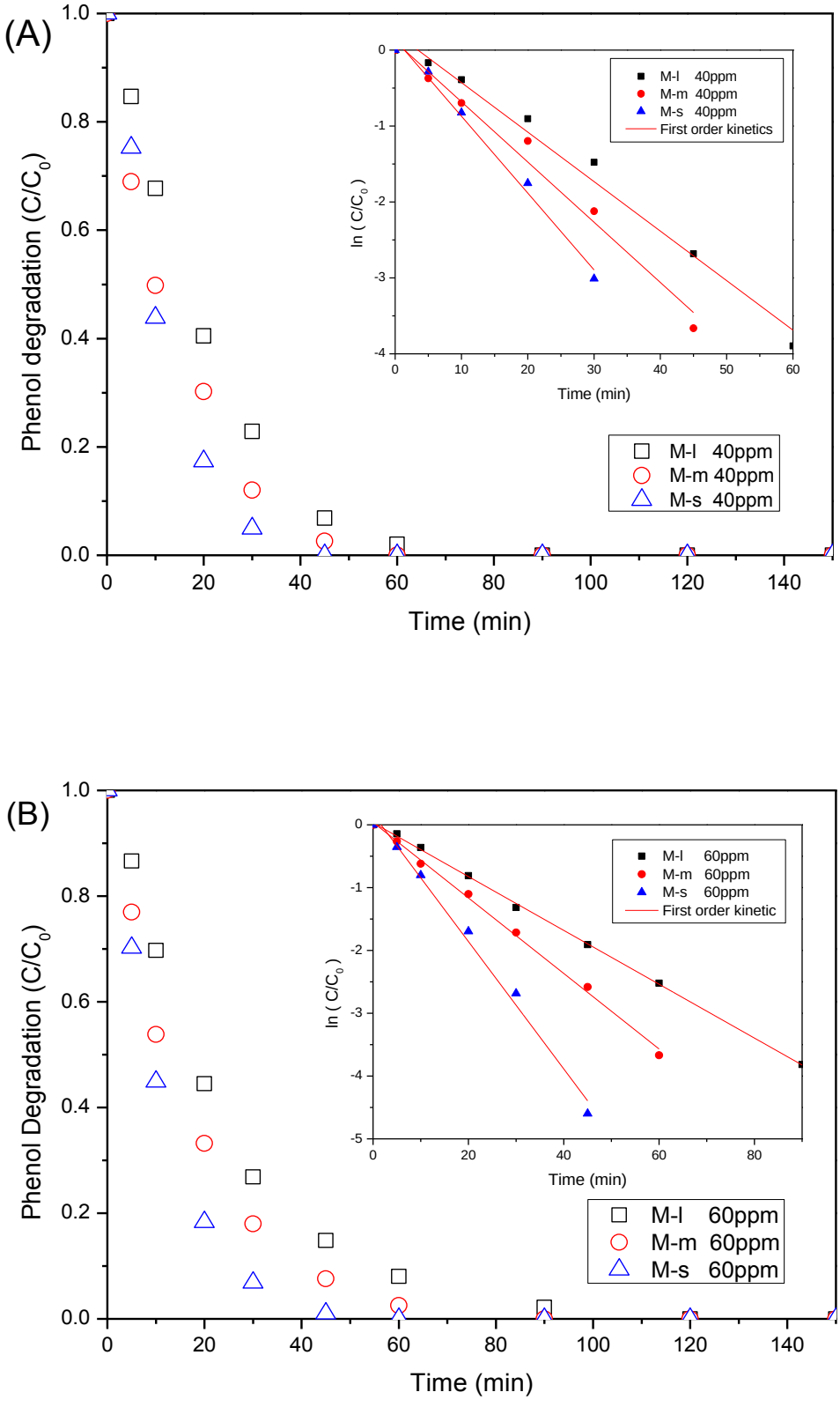

Fig. 3. 5. Effect of different concentration (40 and 60 ppm) on phenol degradation.

To evaluate the effect of phenol condition on the degradation rate, different concentrations of phenol solutions were used for the degradation tests, and the results and kinetic studies are presented in Fig.3.5. A similar trend could be observed in the 40 and 60 ppm of phenol degradation systems that the one employing M-s as a catalyst shows the best results of 45 and 30 min to reach 100% degradations, respectively. M-m showed lower abilities to finish within 60 and 45 min, while M-l needed 60 and 90 min to remove all the organics, suggesting the slowest rate. Comparing with the 20 ppm one in Fig. 3. 4, with the increasing of phenol concentration, the rate of degradation appeared downtrends, which conformed to the catalytic reaction kinetics: $\ln (C/C_0) = -k_t$, where C is the concentration of phenol and C_0 is the initial concentration of pollutants, with the reaction time of t, and k as the first-order reaction rate.

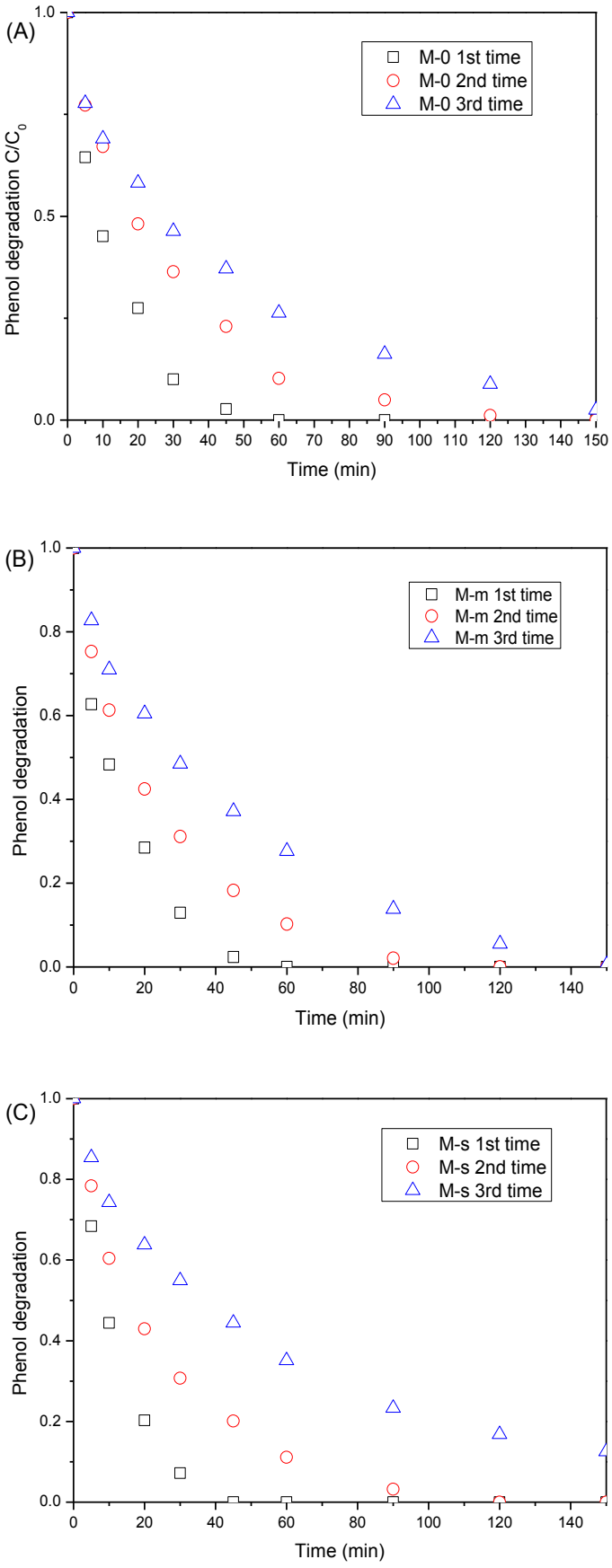

Fig. 3. 6. Stability tests on M-l, M-m and M-s.

Multiple use tests gave direct evidences of the stabilities of M-l, M-m and M-s (Fig.3.6). For M-l, a significant decrease trend of degradation rates was observed in the three runs (finished in 60,120, and 150 min). The trend of M-m was the same as that of M-l, phenol was completely removed in 60, 120 and 150 min, respectively for the three runs. However, the second run of M-s phenol degradation were observed to be finished in 120 min, and the third run only degraded 88% of phenol in 150 min, which were longer than the first run. It suggested that M-s had a poor stability, and the decline of the regeneration might be because of the disabled active sites on the surface of catalysts, which could be hardly removed by simply washed with water, due to the strong van de Waals force of the attachment on reaction intermediate [26].

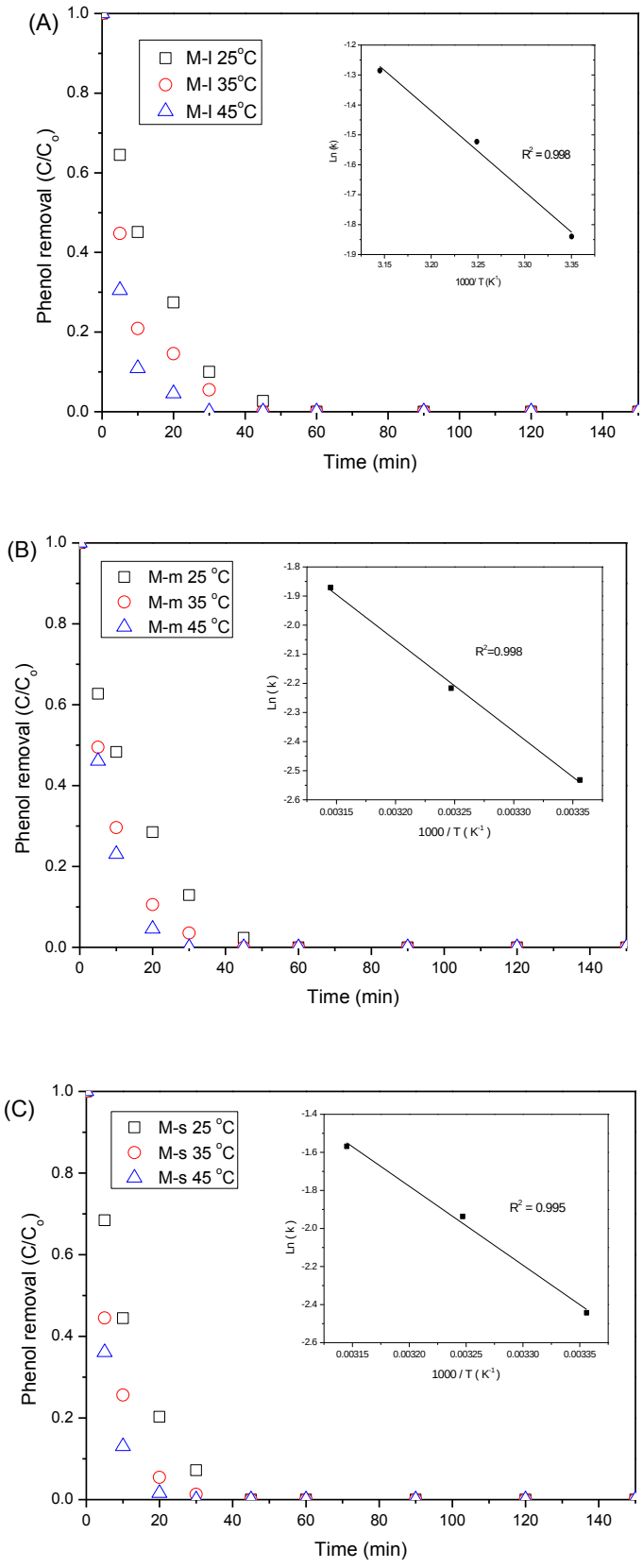

Fig. 3. 7. Effect of reaction temperature on phenol degradation and estimation of activation energy.

Table. 3.2. Kinetic results of the catalysts with PMS for phenol degradation.

Catalysts	T (°C)	K (min^{-1})	R^2 of k	Ea (kJ/mol)	R^2 of Ea
M-l	25	0.0787	0.990	26.5	0.990
	35	0.1188	0.995		
	45	0.1543	0.997		
M-m	25	0.0795	0.976	26.0	0.998
	35	0.109	0.997		
	45	0.154	0.999		
M-s	25	0.0869	0.996	34.5	0.995
	35	0.1442	0.998		
	45	0.2084	0.999		

Fig.3.7. shows the effect of reaction temperature on heterogeneous oxidation of phenol by M-l, M-m and M-s catalysts. Higher reaction temperature can enhance the reaction rate. For M-l, the reactions taking place at 25, 35 and 45 °C led to that phenol removal rate reached 100% in 60, 43 and 20 min, respectively. For M-m, the degradation took 60, 43 and 20 min to finish, and that of M-s took 60, 43 and 20 min, respectively. According to the first order kinetics, the reaction rate constants were fitted. The correlation between reaction rate constant and the temperature was conformed to the Arrhenius equation, which was shown in the insets of Fig.3.7. The activation energies of M-l, M-m and M-s were then calculated as 26.5, 26.0, and 34.5 kJ/mol, respectively.

3.4 Conclusions

Manganese oxide catalysts were synthesized by a one-step method and the size was controlled by varying the concentration of precursors. Their catalytic activities were investigated in activation of PMS for phenol degradation. It was found that the smallest one possessed the highest BET surface area and thus the best catalytic activity.

3.5 References

1. Duan X.; Sun H.; Wang Y.; Kang J.; Wang S. N-Doping Induced Non-Radical Reaction on Single-Walled Carbon Nanotubes for Catalytic Phenol Oxidation, ACS Catalysis,. 5 (2014) pp. 553-559.

2. Shukla P.; Sun H.; Wang S.; Ang H.; Tadé M. Nanosized Co_3O_4/SiO_2 for heterogeneous oxidation of phenolic contaminants in waste water Sep. Purif. Technol., 77 (2011), pp. 230–236

3. Balmer, B. C.; Ylitalo, G. M.; McGeorge, L. E.; Baugh, K. A.; Boyd, D.; Mullin, K. D.; Rosel, P. E.; Sinclair, C.; Wells, R. S.; Zolman, E. S.; Schwacke, L. H., Persistent organic pollutants (POPs) in blubber of common bottlenose dolphins (Tursiops truncatus) along the northern Gulf of Mexico coast, USA. *Science of the Total Environment* **2015,** *527*, 306-312.

4. Elliott, J. E.; Brogan, J.; Lee, S. L.; Drouillard, K. G.; Elliott, K. H., PBDEs and other POPs in urban birds of prey partly explained by trophic level and carbon source. *Science of the Total Environment* **2015,** *524*, 157-165.

5. Zhang, H.; Bayen, S.; Kelly, B. C., Multi-residue analysis of legacy POPs and emerging organic contaminants in Singapore's coastal waters using gas chromatographytriple quadrupole tandem mass spectrometry. *Science of the Total Environment* **2015,** *523*, 219-232.

6. Sandau, Court. Environmental forensics for persistent organic. Amsterdam: Elsevier 2014

7. Tuty Emilia. Comparison of various advanced oxidation processes for the treatment of winery wastewater / Tuty Emilia Agustina. Curtin University of Technology. Dept. of Chemical Engineering. Thesis (Ph. D.)--Curtin University of Technology. 2007

8. Luck, F. Wet air oxidation: past, present and future. Catalysis Today, 1999, Vol. 53(1), pp.81-91

9. Bhargava, S. Catalytic Wet Air Oxidation of Industrial Aqueous Streams. Catalysis Surveys from Asia, 2007. 11(1-2): pp. 70-86.

10. Wang, S. A comparative study of Fenton and Fenton-like reaction kinetics in decolourisation of wastewater. Dyes and Pigments. 76 (2008) pp. 714-720.

11. Ullah, R. Photocatalytic oxidation of air toxics via visible light irradiation and nano-photocatalysts, Curtin University, School of Chemical and Petroleum Engineering, Department of Chemical Engineering. Thesis (Ph.D.)--Curtin University. 2012

12. Zhao, J. ; Zhu, C. ; Lu, J. ; Hu, C. ; Peng, S. ; Chen, T. Electro-catalytic degradation of bisphenol A with modified Co3O4/β-PbO2/Ti electrode, Electrochimica Acta, 2014, Vol.118, pp.169-175

13. Li D; Qu J; Environ J. The progress of catalytic technologies in water purification, Sci. 21 (2009), pp. 713–719.

14. Yang, Y. ; Pignatello, J. ; Ma, J. ; Mitch, W., Comparison of halide impacts on the efficiency of contaminant degradation by sulfate and hydroxyl radical-based advanced oxidation processes (AOPs), Environmental science & technology, 18 February 2014, Vol.48(4), pp.2344-51

15. Yang, Y. ; Jiang, J. ; Lu, X. ; Ma, J. ; Liu, Y. Production of sulfate radical and hydroxyl radical by reaction of ozone with peroxymonosulfate: a novel advanced oxidation process. Environmental science & technology, 49(2015), pp.7330-9

16. Yao, Y. ; Cai, Y.; Wu, G. ; Wei, F. ; Li, X. ; Chen, H. ; Wang, S. Sulfate radicals induced from peroxymonosulfate by cobalt manganese oxides (CoxMn3−xO4) for Fenton-Like reaction in water.. Journal of Hazardous Materials, 296 (2015), pp.128-137

17. Ji, F; Li, C; Liu, Y; Liu, P. Heterogeneous activation of peroxymonosulfate by Cu/ZSM5 for decolorization of Rhodamine B. Separation And Purification Technology, 135 (2014), pp.1-6

18. Cai, C.; Zhang, H.; Zhong, X.; Hou, L. Fe–Co/SBA-15 catalyst for the degradation of Orange II in water. Journal of Hazardous Materials, 283 (2015), pp.70-79.

19. Hajipour, A. R. ; Mallakpour, S. E. ; Baltork, I. M. ; Adibi, H. Oxidative deprotection of trimethylsilyl ethers, tetrahydropyranyl ethers, and ethylene acetals with benzyltriphenylphosphonium peroxymonosulfate under microwave irradiation. Synthetic Communications, 31(2001), pp.1625-1631.

20. Tang, D. ; Zhang, G. ; Guo, S. Efficient activation of peroxymonosulfate by manganese oxide for the degradation of azo dye at ambient condition. Journal of Colloid And Interface Science, 454 (2015), pp.44-51.

21. Sun H.; Liu S.; Zhou G.; Ang H.; Tade M.; Wang S. Reduced Graphene Oxide for Catalytic Oxidation of Aqueous Organic Pollutants. ACS Appl. Mater. Interfaces. 103 2012; 4(10):5466-71.

22.Sun H.; Zhou G.; Liu S.; Ang H.; Tade M.; Wang S. Nano-Fe^0 Encapsulated in Microcarbon Spheres: Synthesis, Characterization, and Environmental Applications. ACS Appl. Mater. Interfaces. 2012; 4(11):6235-41.

23.Sun H.; Liang H.; Zhou G.; Wang S. Supported cobalt catalysts by one-pot aqueous

combustion synthesis for catalytic phenol degradation. J. Colloid Interface Sci. 2013; 394: 394-400.

24. Saputra E.; Muhammad S.; Sun H.; Ang H.; Tade M.; Wang S. A comparative study of spinel structured Mn3O4, Co3O4 and Fe3O4 nanoparticles in catalytic oxidation of phenolic contaminants in aqueous solutions. Journal of Colloid and Interface Science, 407 (2013) 467-473.

25. Saputra E.; Muhammad S.; Sun H.; Ang H.; Tade M.; Wang S. Shape-controlled activation of peroxymonosulfate by single crystal α-Mn_2O_3 for catalytic phenol degradation in aqueous solution. Applied Catlysis B: Environmental. 154-155(2014) 246-251.

26. Wang, Y.; Indrawirawan, S.; Duan, X.; Sun, H., Ang, H.; Tade, M.; Wang, S. New sights into heterogeneous generation and evolution process of sulfate for phenol degradation over one-dimensional α -MnO_2 nanoatructures, Chemical Engineering Journal 266(2015) 12-20.

4

Chapter 4: Synthesis of highly- stable manganese oxide catalysts

A B S T R A C T

Better stability of catalysts means better practical application, especially for wastewater treatment, on account of less leaching problems. In this chapter, spherical manganese oxide catalysts were synthesized via one-step processes, followed by calcination at different temperatures of 200, 400, 600 and 800 ^{o}C. The catalytic performances of the catalysts were assessed by the degradation of phenol with activation of PMS. The samples were characterized by field emission scanning electron microscopy (FE-SEM), X-ray diffraction (XRD), Fourier transform infrared spectroscopy (FTIR), thermogravimetric analysis (TGA) and inductively coupled plasma (ICP). The experimental results showed that M-400 exhibited the best stability in decomposition of phenol, in which the organic compounds could be effectively decomposed in 60 min.

4.1. Introduction

Due to the global industrialization and the lack of public awareness of environmental protection, water and soil pollution has become a worldwide issue [1,2]. Persistent organic pollutant (POP) is one of the most serious pollutants discharged from industrial processes, due to their long life-time, toxicity and resistance against natural attenuation[3]. To degrade the POPs, advanced oxidation processes (AOPs) are the most effective methods with many advantages[4]: (1) the reaction can produce large amounts of reactive radicals (•OH and other radicals), which have strong oxidizing ability to induce the chain reactions; (2) •OH often reacts with the organic matters directly, with no secondary pollution; (3) the methods are easy to operate; and (4) the degradation can be alone, and can also be combined with other advanced oxidation processes or biological processes, which reduces the cost. In recent years, sulfate radical-based advanced oxidation processes have attracted lots of attention. The system of Co^{2+}/PMS has shown a great effect on phenol treatment [5 6], however, Izgorodin and his group already noted that the stability was one of the important indicators to identify the performance of catalysts. And Co^{2+} has toxicity itself that may bring about secondary metal pollution. Therefore, it was considered as an incongruous catalyst in practical application[7]. Manganese oxide was deemed to be a promising candidate for catalysis, which was valuable in various degradation systems with less harm[8-11].

It has been reported in journal articles, government reports, published conference proceedings and thesis that the maximum of the concentration of Mn ion in drinking water or potential drinking-water supplies was 400 μg/L[13]. There was a survey about Bangladesh stated that more than 60 million people were suffering from the overproof manganese [14], and in an

epidemiological study in Japan, some symptoms of poisoning such as lethargy, increased muscle tone, tremor, and mental disturbances were found near the dry-cell batteries buried area [15]. Therefore, a high performance manganese material was required, and with controlled leaching problem it would have less threat to human body and nature system [16]. In this chapter, a unique method was applied to synthesize manganese oxide catalysts with a high stability. The prepared catalysts showed high activity in the reaction of oxidizing phenol solutions.

4. 2. Experimental

4. 2.1 Chemicals

n-Butanol (99%), butyric acid (99%), potassium permanganate (99.9%), methanol (99%), phenol (99%) and Oxone ($2KHSO_5 \bullet 3KHSO_4 \bullet K_2SO_4$) were obtained from Sigma-Aldrich. All the chemicals were used as received without further purification.

4. 2.2. Material synthesis

The uniform-size porous manganese oxide spheres were synthesized via a one-step hydration method. 25 mL of 0.040 M $KMnO_4$ was added in a 25 mL aqueous mixture of 0.48 M butanol and 1.0 M butyric acid, then followed by 0.5 h stirring. The obtained black suspension was filtered and washed by deionized water and ethanol for three times. The obtained precipitate was dried overnight at 80 ℃, and the sample was labelled as M. The as-prepared M was calcined under air at different temperatures, and denoted as M-n (n = 0, 200, 400, 600, and 800℃).

4.2.3 Catalytic oxidation of phenol solutions

The phenol degradation tests were carried out at 25 °C in a 250 mL conical flask which contained 20 ppm phenol solution. The conical flask was kept in a water bath with a temperature controller. Firstly, 0.03 g catalyst was put into the phenol solution at constant stirring of 400 rpm for few minutes until it was dispersed well. The second step was to start the oxidation reaction with adding 0.3 g Oxone into the reactor, and the reaction was then kept running for 150 min. During the reaction, 1 mL of the solution sample was taken out from the reaction solution at set intervals using a syringe with a filter of 0.45 μm and filtered into a high performance liquid chromatography (HPLC) vial. Then, quenching the reaction was conducted by adding 0.5 mL methanol into the vial. The HPLC analysis and stability tests were the same as that in Chapter 3.

4.3 Results and discussion

4. 3.1 Characterization of the materials

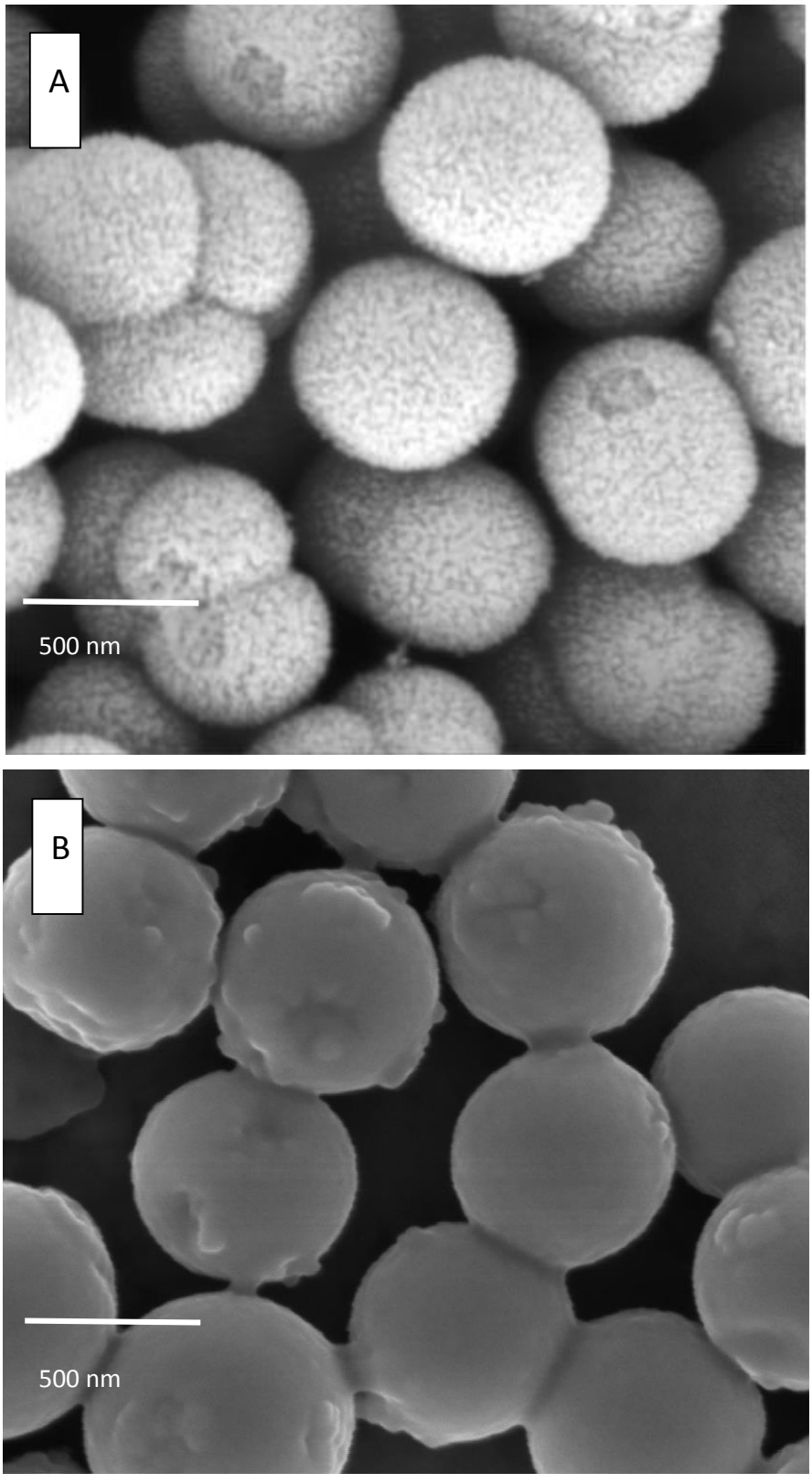

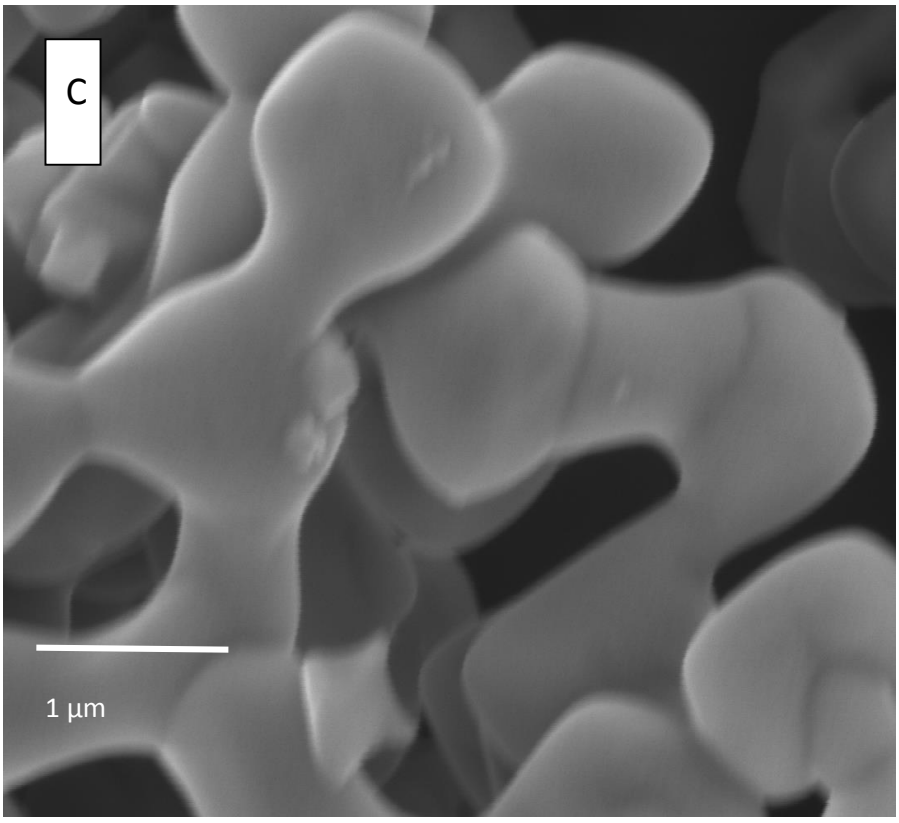
C
1 µm

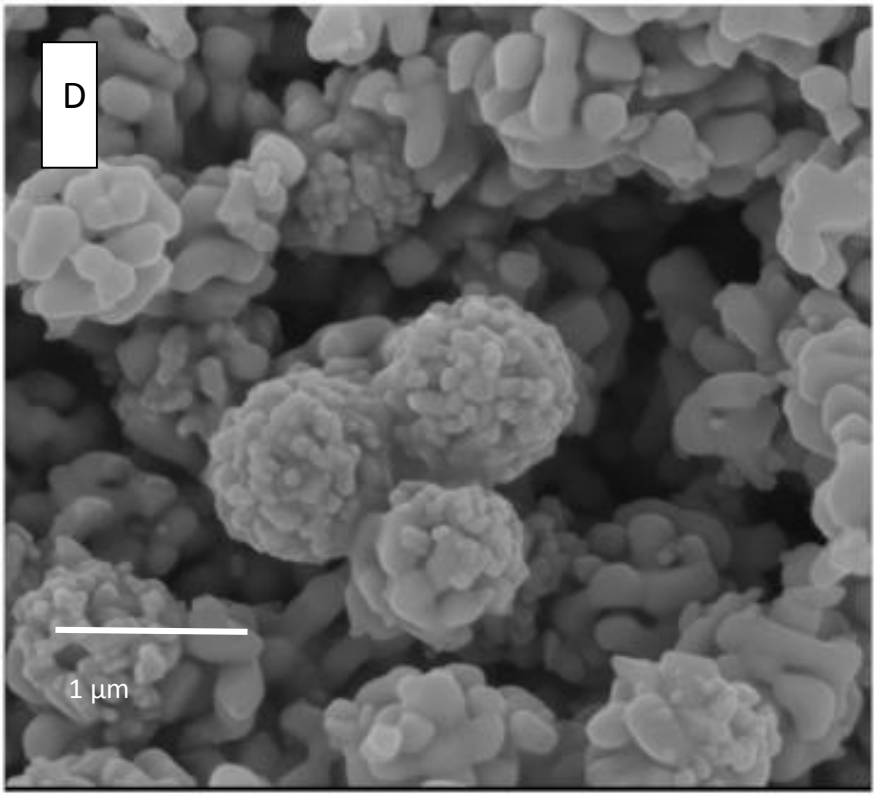
D
1 µm

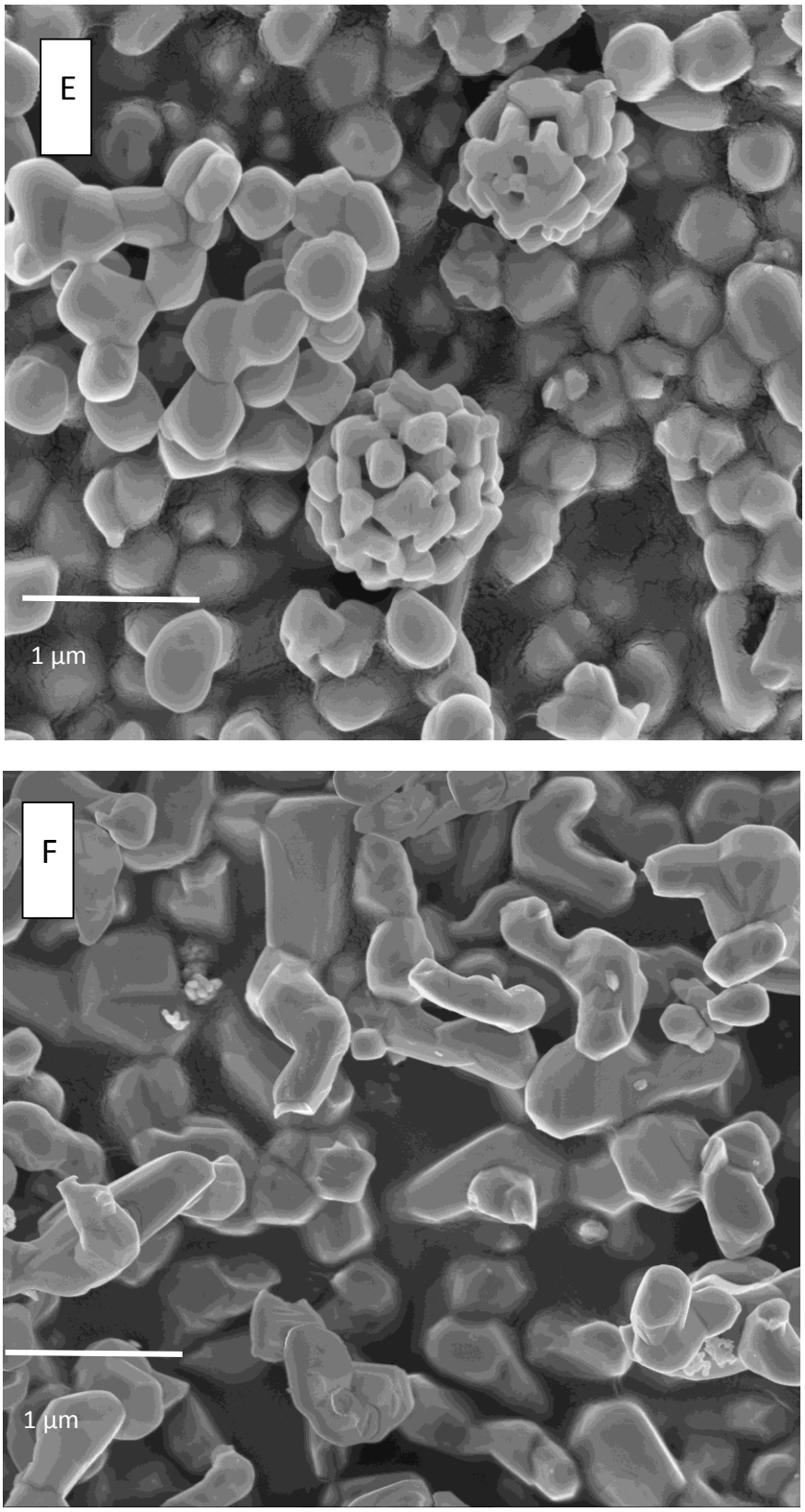

Fig. 4. 1. SEM images of (A) M-0, (B) M-200, (C) M-400, (D) M-600, (E) M-800 and (F) M-1000.

Morphologies and sizes of the catalysts are shown in SEM images of Fig. 4.1. M-0 (Fig.1.A) exhibited a mainly spherical shape with high monodispersion, and the average size of the spheres was about 400 nm. The calcination to 200 ºC, would make water and organic additives be burned out [17]. Some variations appeared on the original porous surface to produce a less smooth surface. It could be observed in Fig. 4.1C that aggregation occurred during heating to 400 ºC, and there might be some chemical state changes along with the annealing process [18]. At 600 ºC, the manganese oxides continued to aggregate and form porous spheres, with an average size of 500 nm. The construction might be due to the growing of the granules which acted as constitutional unit of the spheres. In Fig. 1D (M-800), the granules separated from the initial spheres, and kept growing of the size to the average diameter of 200 nm. When the calcination temperature reached 1000 ºC, the secondary sintering appeared, and several granules gathered and agglomerated.

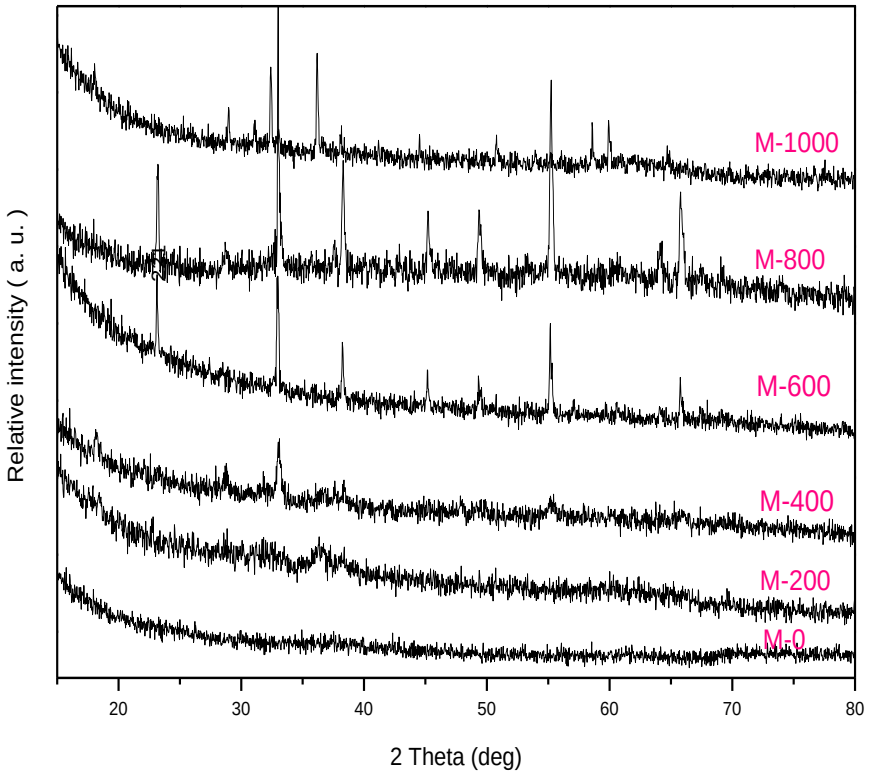

Fig. 4. 2. XRD patterns of M-n catalysts.

Figure 4.2 displays XRD patterns of the as-prepared M-0, M-200, M-400. M-600, M-800 and M-1000. It can be seen that M-0 and M-200 did not show any characteristic peaks for phase determination, revealing that no calcination or below 200 ^{o}C would result in poor crystallinity. As seen, the peaks began to appear with heating to 400 ^{o}C. M-600 and M-800 showed strong diffraction peaks at 23.08, 37.84, 45.06, 49.23, 55.05 and 65.17 ^{o}, which confirmed that M-400 was not fully crystallized with a large extent of amorphous phase. Meanwhile M-600 and M-800 had developed the formation of Mn_2O_3 single-phase cubic system, with no other impurity diffraction peak according to JCPDF card (No. 89-4836, a = 9.406 Å) [9]. The M-800 shows sharper peaks, indicating that the higher calcination

temperature, the better crystallinity. The diffraction peaks of M-1000 were at 28.92, 30.98, 36.08, 38.11, 44.41, 50.84, 53.88 and 59.95°, corresponding to Mn_3O_4 according to the JCPDF card (No. 80-0382, a = 5.749 Å) [18]. The above results of XRD patterns illustrated that with the annealing temperature growing, the valence state transformed from +3 to +4.

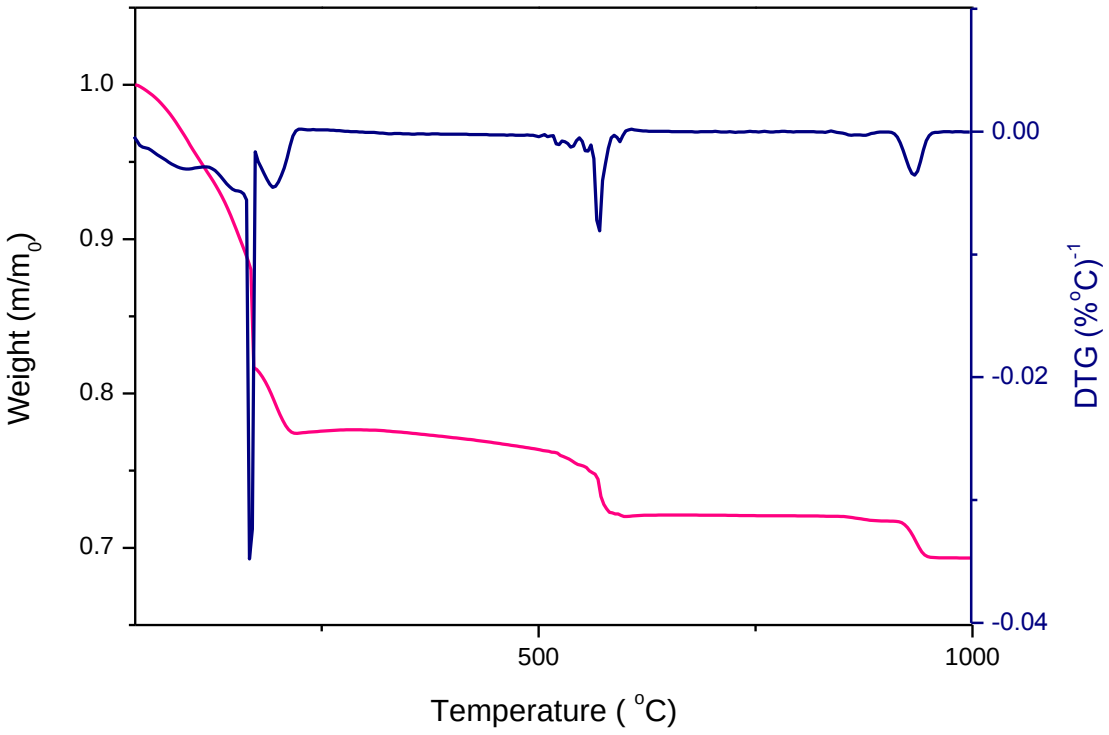

Fig. 4. 3. TG-DSC profiles of M-n under air.

DTA-TGA results are presented in Fig.4.3. The sample was heated in air with a rising rate of 10 ℃/min. The TG curve showed three significant processes of weight loss and three stable zones. The first step showed a loss of 22% of the weight, from 30 to 200 ℃. It might be on account of the removal of moisture adsorbed on the surface of catalyst [19]. After 200 ℃, the curve tended to stabilize, which could be assigned to forming crystalline state. There was an imperceptible weight loss occurred at 550 ℃, and followed with a slight reduction of weight at 900 ℃. There was no more weight loss after 900 ℃. Together with the XRD results, the TGA

and DTG curves suggested that the weight loss might be due to crystal phase changes. The crystal transform temperature was 550 ^{o}C for Mn_2O_3 and 900 ^{o}C for Mn_3O_4, respectively.

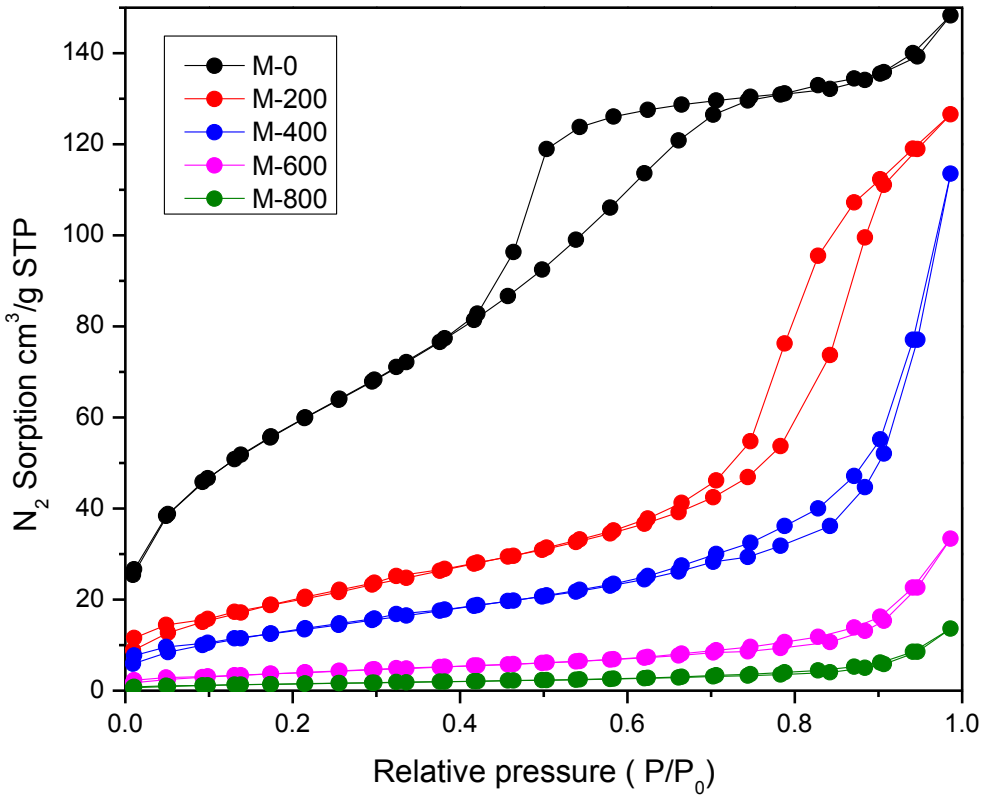

Fig. 4. 4. N_2 sorption isotherms of M-0, M-200, M-400, M-600 and M-800.

Fig.4.4 shows N_2 adsorption-desorption isotherms and Table 4.1 lists the pore volume and pore size of M-0, M-200, M-400, M-600 and M-800. The hysteresis loops were started at 0.4, 0.55, 0.5, 0.7 and 0.8, respectively, and all of them were ended at 0.99 of the relative pressure (P/P0), which indicated the mesoporous structure of the samples. Furthermore, the appearances of the H_2-type hysteresis loop suggested they were porous materials with relatively high uniform channel-like pores. The specific surface areas were 115, 65.1, 41.8, 15.5 and 6.1 m^2/g, respectively. In terms of pore size distribution, as seen, all of the samples displayed a single

mode of pore size at 3.9, 10.1, 11.2 and 9.6 of M-0, M-200, M-400, M-600 and M-800, respectively. According to the BET analysis, with growing heating temperature, the surface area tended to be smaller that might result in less active sites on the surface, which could reduce the catalytic activity of the samples.

Table 4.1. Textural properties of M-n samples.

Catalyst	Surface area (S_{BET}, m^2g^{-1})	Pore volume ($cm^3\ g^{-1}$)	Average pore radius (Å)
M-0	115.5	0.520	3.9
M-200	65.1	0.293	10.1
M-400	41.8	0.188	11.2
M-600	15.5	0.069	9.6
M-800	6.1	0.027	11.6

4.3.2 Catalytic oxidation of phenol solutions

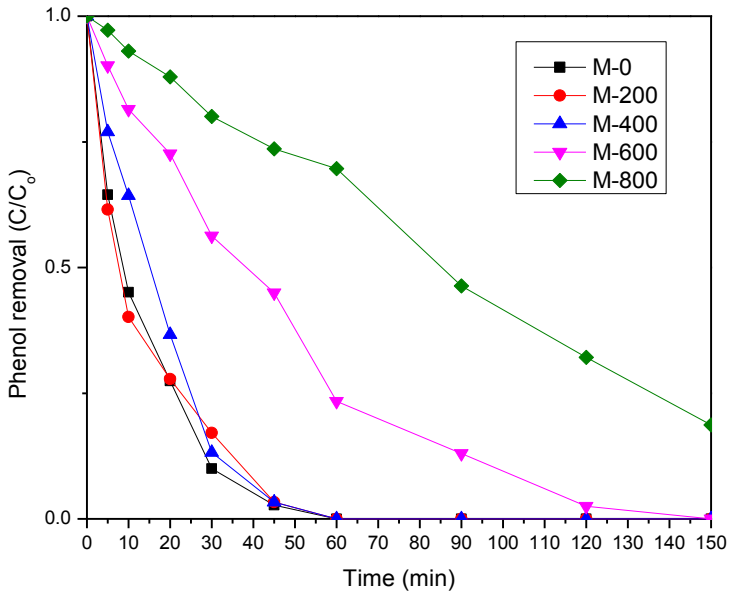

Fig. 4. 5. Phenol removal using M-n (n=0,200, 400, 600, 800) as the catalysts.

The adsorption and catalytic oxidation of phenol solutions are shown in Fig.4.6. For the reaction without a catalyst, and adsorption of M-0, M-200, and M-400, the final phenol removal rates were all about 10% in 150 min. This suggested that PMS in homogeneous solution could not induce phenol oxidation, and the phenol adsorption on catalysts themselves were negligible. Compared with the catalytic oxidation reactions, all of the final phenol removal rates could reach 100% in 60 min.

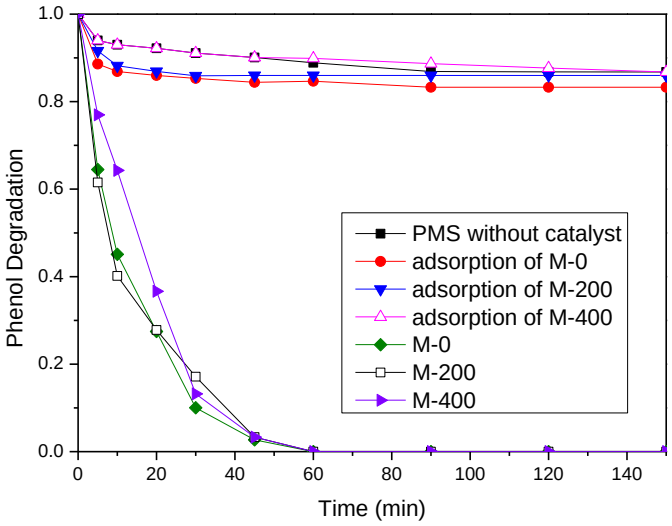

Fig. 4. 6. Phenol removal in various reaction conditions

The adsorption and catalytic oxidation of phenol solutions are shown in Fig.4.6. For the reaction without a catalyst, and adsorption M-0 only, M-200 only, M-400 only and PMS, the final phenol removal rates were all about 10% in 150 min. This suggested that PMS in homogeneous solution could not induce phenol oxidation, and the phenol adsorption on catalysts themselves were negligible. Compared with the catalytic oxidation reactions, all of the final phenol removal rates could reach 100% in 60 min.

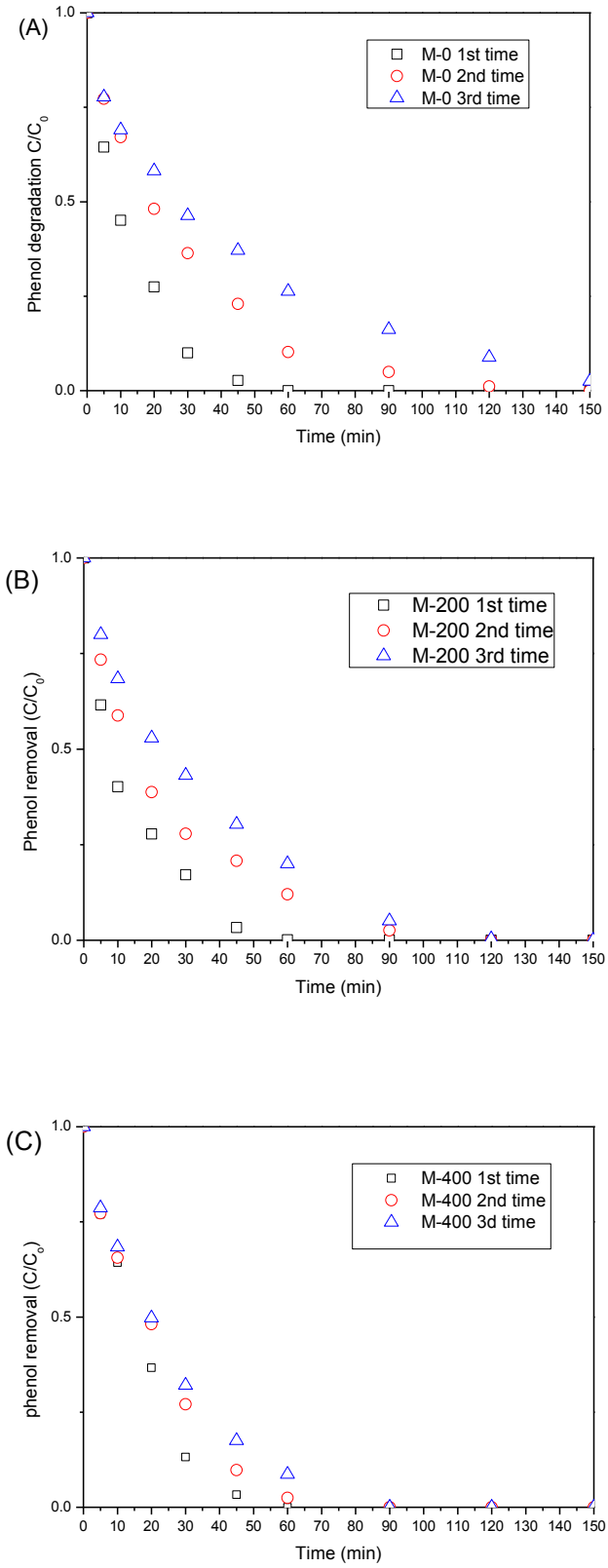

Fig. 4. 7. A comparison of phenol degradation at different runs on M-0, M-200 and M-400.

Reusability tests gave for the stabilities of M-0, M-200 and M-400 (Fig.4.7). For the reaction

using M-0, a significant decrease of degradation rate was shown in three runs (finished in 60, 120, and 150 min). The trend of M-200 was the same as that of M-0. Phenol was totally removed in 60, 120 and 150 min, respectively, for the three runs. However, in the second and third runs, phenol removal by M-400 were observed to be finished in 70 and 80 min, which were slightly longer than the first run. It suggested that M-400 had a much better stability and could be recycled for application.

Table 4.2. ICP analysis of the Mn leaching.

	M-0	M-200	M-400
C (mg/L)	5.3	2.5	0.13

In order to confirm the leaching of manganese ions, the filtered reaction solutions of M-0, M-200 and M-400 were collected and examined by inductively coupled plasma (ICP, Optima 5300DV, Perkin Elmer). Results in Table 4.2 illustrated that the manganese ions remaining in M-0 and M-200 solution (5.3 and 2.5 ppm) were more than that of M-400, with dissolved Mn ions of 0.13 ppm. This confirms that there was less serious leaching problem in M-400 catalytic system.

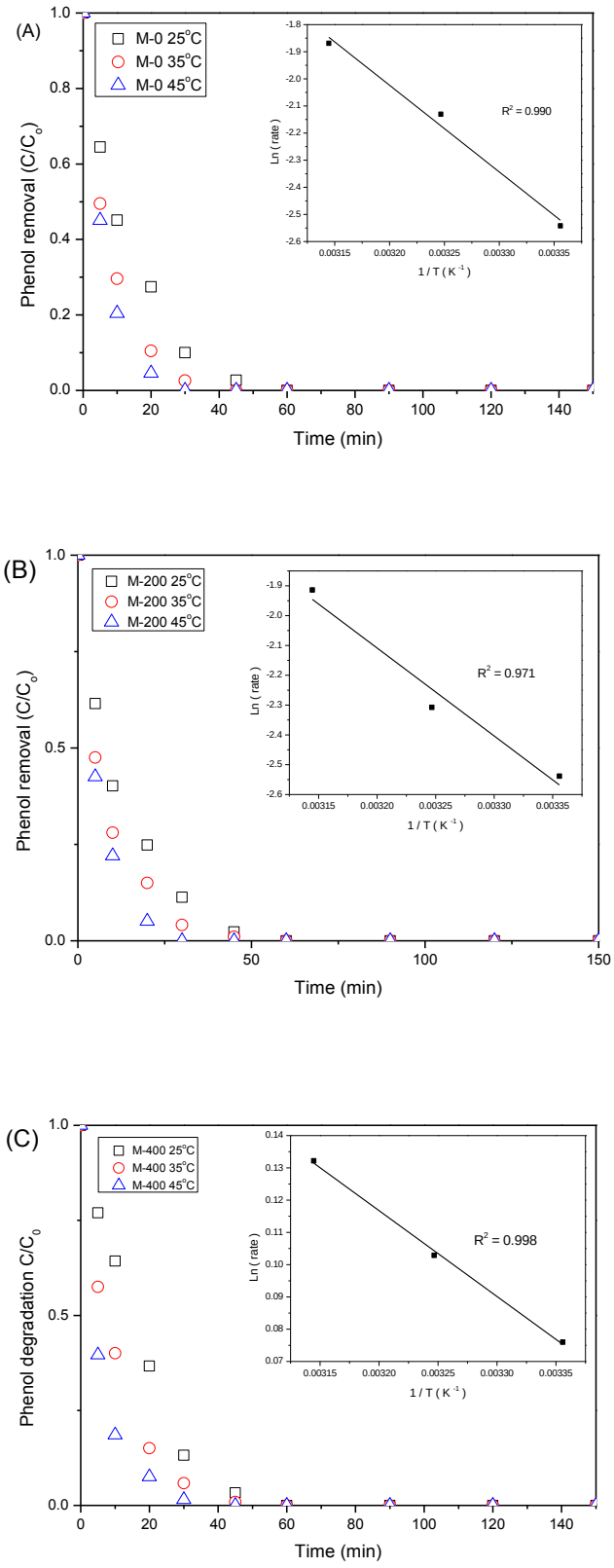

Fig. 4. 8. Effect of reaction temperature on phenol degradation and evaluation of activation energy.

Table. 4.3 Activation energy of heterogeneous catalysts with PMS for phenol removal.

Catalyst	Activation Energy (kJ/mol)	References
a-MnO_2 nanowire	39.3	8
Mn_2O_3 cube	61.2	21
$ZnFe_2O_4/MnO_2$	49.4	22
M-0	28.1	This work
M-200	25.5	This work
M-400	19.7	This work

Fig.4.8. shows the effect of reaction temperature on heterogeneous oxidation of phenol using M-0, M-200 and M-400 catalysts. For M-0, the reaction took place at 25, 35 and 45 °C, phenol removal rate reached to 100% in 60, 43 and 25 min, respectively. For M-200, the degradation took 60, 45 and 25 min to finish, and that of M-400 took 60, 47 and 30 min, respectively. The present results illustrated that a higher reaction temperature could enhance the reaction rate. According to the first order kinetics, the reaction rate constant were used to evaluate the activation energy. The activation energies of M-0, M-200 and M-400 were then calculated as 28.1, 25.5 and 19.7 kJ/mol, respectively.

4.4 Conclusions

In conclusion, the one-step method was successfully applied to prepare uniform-size porous manganese oxide spheres. It was found that calcination at 400 ºC can synthesize the material with a great efficiency and stability as a catalyst for activation of PMS in phenol degradation.

4.5 References

1. Duan X.; Sun H.; Wang Y.; Kang J.; Wang S. N-Doping Induced Non-Radical Reaction on Single-Walled Carbon Nanotubes for Catalytic Phenol Oxidation, ACS Catalysis,. 5 (2014) pp. 553-559.

2. Shukla P.; Sun H.; Wang S.; Ang H.; Tadé M. Nanosized Co_3O_4/SiO_2 for heterogeneous oxidation of phenolic contaminants in waste water Sep. Purif. Technol., 77 (2011), pp. 230–236

3. Sandau Court. Environmental forensics for persistent organic. Amsterdam: Elsevier 2014

4. Tuty Emilia. Comparison of various advanced oxidation processes for the treatment of winery wastewater / Tuty Emilia Agustina. Curtin University of Technology. Dept. of Chemical Engineering. Thesis (Ph. D.)--Curtin University of Technology. 2007

5. Hazar E.; Houssam E. Al-Ghoul, Mazen Cosynthesis, Coexistence, and Self-Organization of α- and β-Cobalt Hydroxide Based on Diffusion and Reaction in Organic Gels. The Journal of Physical Chemistry A, 112 (2008), pp.7755-7757

6. Saputra E.; Muhammad S.; Sun H.; Ang H.; Tade M.; Wang S. A comparative study of spinel structured Mn3O4, Co3O4 and Fe3O4 nanoparticles in catalytic oxidation of phenolic contaminants in aqueous solutions. Journal of Colloid and Interface Science, 407 (2013) 467-473.

7. Izgorodin A.; Hocking R.; Orawan W.; Matthias H.; Bjorn W.; Douglas R. Phosphorylated manganese oxide electrodeposited from ionic liquid as a stable, high efficiency water oxidation catalyst. Catalysis Today, 200 (2013), Pages 36–40

8. Y. Wang, S. Indrawirawan, X. Duan, H. Sun, , H. Ang, M. O. Tadé, S. WangNew insights into heterogeneous generation and evolution processes of sulfate radicals for phenol degradation over one-dimensional α-MnO_2 nanostructures. Chemical Engineering Journal, 15 April 2015, Vol.266, pp.12-20.

9. Saputra E.; Muhammad S.; Sun H.; Ang H. Manganese oxides at different oxidation states for heterogeneous activation of peroxymonosulfate for phenol degradation in aqueous solutions. Applied Catalysis B: Environmental 142-143 (2013) 729-735.

10. Saputra E.; Muhammad S.; Sun H.; Ang H.; Tade M.; Wang S. Different Crytallographic One-dimensional MnO2 Nanomaterials and their Superior Performance in Catalytic Phenol Degradation. Environmental Science & Technology 47 (2013) 5822-5887.

11. Wang Y.; Sun H.; Ang H.; Tade O.; Wang S. Synthesis of magnetic core/shell carbon nanophere supported manganese catalysts for oxidation of organics in water by peroxymonosulfate. Journal of Colloid and Interface Science 433 (2024) 68-75.

12. Intellectual impairment in school-age children exposed to manganese from drinking water. Bouchard MF, Sauvé S, Barbeau B, Legrand M, Brodeur MÈ, Bouffard T, Limoges E, Bellinger DC, Mergler D Environ Health Perspect. 2011 Jan; 119(1):138-43.

13. W H O (World Health Organization) Histories of Guideline Development for the Fourth Edition: Chemical Fact Sheets. Chemical Contaminants in Drinking-Water. Manganese: History of Guideline Development. 2011a.

14. Hasan S, Ali MA. Occurrence of manganese in groundwater of Bangladesh and its implications on safe water supply. J Civil Eng.2010; 38(2):121–128. .

15. Seth H. Frisbie, Erika J. Mitchell, Hannah Dustin, Donald M. Maynard, and Bibudhendra Sarkar. World Health Organization Discontinues Its Drinking-Water Guideline for Manganese. Environ Health Perspect. 120 (2012) pp. 775–778.

16. Ecology. Waste Management Research; Studies from Zhejiang Normal University Yield New Information about Waste Management Research (controlled leaching with prolonged activity for Co-LDH supported catalyst during treatment of organic dyes using bicarbonate activation of hydrogen), Environment & Conservation, May 22, 2015, p.1182

17. WangY.; SunH.; Ang H.; TadeM.; Wang S. Synthesis of magnetic core/shell carbon nanosphere supported manganese catalysts for oxidation of organics in water by peroxymonosulfate. Journal of Colloid and Interface Science 2014, 433, 68-75.

18. Augustin M.; Fenske D.; Bardenhagen I.; Westphal A.; M. Knipper; Plaggenborg T.; Kolny-Olesiak J.; Parisi J. Manganese oxide phases and morphologies: A study on calcination temperature and atmospheric dependence. Beilstein journal of nanotechnology, 6(2015) pp.47-59

19. Chu, Hsin, Characterization of gamma-alumina-supported manganese oxide as an incineration catalyst for trichloroethylene, Environmental Science & Technology, Jan 1, 2003, Vol.37(1), pp.171-176

20. Saputra, E.; Muhammad, S.; Sun, H.; Patel A.; Zhu Z.; Wang, S. α-MnO2 acivation of peroxymonosulfate for catalytic phenol degradation in aqueous solutions. Catalysis Communications 26 (2012) 144-148.

21. Saputra, E.; Muhammad, S.; Sun, H.; Ang, H.; Tadé, M.; Wang, S. Shape-controlled activation of peroxymonosulfate by single crystal α-Mn_2O_3 for catalytic phenol degradation in

aqueous solution, Applied Catalysis B: Environmental, 2014. 154-155, pp.246-251.

22. Wang, Y.; Sun, H., Ang, H.; Tade, M.; Wang, S. Facile Synthesis of Hierarchically Structured Magnetic MnO2/ZnFe2O4 Hybrid Materials and Their Performance in Heterogeneous Activation of Peroxymonosulfate, ACS. Mater. Interfaces 6 (2014) pp. 19914-19923.

Saputra, E.; Muhammad, S.; Sun, H.; Ang, H.; Tade, M.; Wang, S. Different Crystallographic One-dimensional MnO2 Nanomaterials and Their Superior Performance in Catalytic Phenol Degradation.Environ. Sci. Technol. 2013. 47, 5882-5887.

5

Chapter 5: Synthesis of GO supported calcium-manganese oxide catalysts

A B S T R A C T

GO supported calcium-manganese oxide catalysts (GO/$CaMn_3O_6$, GO/$CaMn_4O_8$) were synthesized by a two-step method. The calcium-manganese oxide and graphene oxide were prepared separately, and then were hybridized together via a hydrothermal route. The samples were characterized by X-Ray diffraction (XRD), field emission scanning electron microscopy (FE-SEM), thermogravimetric analysis/differential temperature gradient (TGA/DTG) and Fourier transform infrared spectroscopy (FT-IR). The two catalysts were evaluated for phenol degradation, and achieved 96 and 67% phenol removal in 180 min, respectively, higher than single compound without hybridization.

5.1 Introduction

In recent years, mixed valent manganites have attracted more attention than conventional manganese oxide because of their potential application in various fields[12 13]. In a recent study, a new kind of spinel $LiMn_2O_4$ was applied as a promising electrode material due to its high thermal stability, low cost, abundance, and environmental affinity[14]. To our best knowledge, most of the investigations of mixed valent manganites were applied in energy generation and storage. However few studies were conducted for wastewater treatment, and no further investigation has been reported on the application of calcium-manganese oxide or calcium-manganese oxide based composite material as catalysts to active PMS for phenol removal. In this chapter, mixed valent manganites ($CaMn_3O_6$ and $CaMn_4O_8$) were synthesized and employed as catalysts for oxidative degradation of phenol in aqueous phase.

5.2 Experimental

5.2.1 Chemicals

Graphite powder (99.99%), sodium nitrate (99.9%), potassium permanganate ($KMnO_4$) (99.9%), sulfuric acid (99%), hydrogen (30%), calcium carbonate (99.5%), ammonium carbonate (99%), nitric acid (70%), manganese carbonate (99.8%), ammonium hydroxide (28%), methanol (99%), phenol (99%) and Oxone ($2KHSO_5 \cdot 3KHSO_4 \cdot K_2SO_4$) were obtained from Sigma-Aldrich. All of the chemicals were used as received without further purification.

5.2.2 Synthesis of graphene oxide

GO was prepared by the modified Hummers method [16]. In a typical process, 50 mL of sulfuric acid was added into the mixture of graphite and sodium nitrate with stirring, and the beaker

was kept in the ice bath to make sure it was maintained below 4 °C for 5 min. And then $KMnO_4$ (6 g) was added into the mixed solution, and kept the reaction mixture stirring at 20 °C for 4 h. DI water (100 mL) was slowing added into the reactor carefully, ensuring that the reaction mixture need to be kept below 95 °C. The mixture was then allowed to stir for another 30 min at 95 °C. To stop the oxidation reaction via adding 30% H_2O_2 (20 mL) and distilled water (100 mL), which were used to reduce the excess $KMnO_4$. The oxidized product, GO, was filtered, washed with 5% nitric acid aqueous solution and distilled water for three times until neutralization, and dried in a vacuum oven at 60 °C for 24 h.

5.2.3. Synthesis of calcium-manganese oxide microspheres ($CaMn_3O_6$ and $CaMn_4O_8$)

The calcium manganese oxides were synthesized using a modified co-precipitation method. For the synthesis of $CaMn_3O_6$, 10 mmol calcium carbonate and 30 mmol manganese carbonate were dissolved in 80 mL diluted nitric acid (1 M). With vigorous stirring, 200 mL of ammonium carbonate solution (2 M) was then added into the mixture to adjust the pH of solution (higher than 8). Filtered the product by vacuum filtration and followed with washing for three times, the brownish precipitate was obtained. Then the precipitate was dried at 60 ^oC in an oven for 24 h. After that, the dried precipitate was transferred into a crucible and heated in a muffle furnace at 800 ^oC for 18 h. The obtained black powder was named as $CaMn_3O_6$. The $CaMn_4O_8$ was synthesized via the similar method of $CaMn_3O_6$, with the dosage of $MnCO_3$ changing to 40 mmol only.

5.2.4. Synthesis of GO supported calcium-manganese oxide catalyst (GO/ $CaMn_3O_6$ and GO/ $CaMn_4O_8$)

The GO supported calcium manganite samples were then prepared by a one-pot hydrothermal

method. In a typical procedure, 1 g GO was dispersed in aqueous solution (0.0112 g/mL) with ultrasonication for 2 h, and then 1 g $CaMn_3O_6$ powders were added into GO suspension with stirring, and the pH of solution was adjusted to 10 using ammonium hydroxide. The solution was magnetically stirred for 1 h and transferred into a autoclave. The hydrothermal reaction was carried out at 185 °C for 18 h. Black sediment was then collected and washed with ethanol and distilled water several times. The obtained samples were referred as GO/$CaMn_3O_6$. GO/$CaMn_4O_8$ was synthesized using the same method as that of GO/$CaMn_3O_6$.

5.3. Results and discussion

Detailed characterization techniques can be referred to Chapters 3 and 4.

5. 3. 1 Characterization of the materials

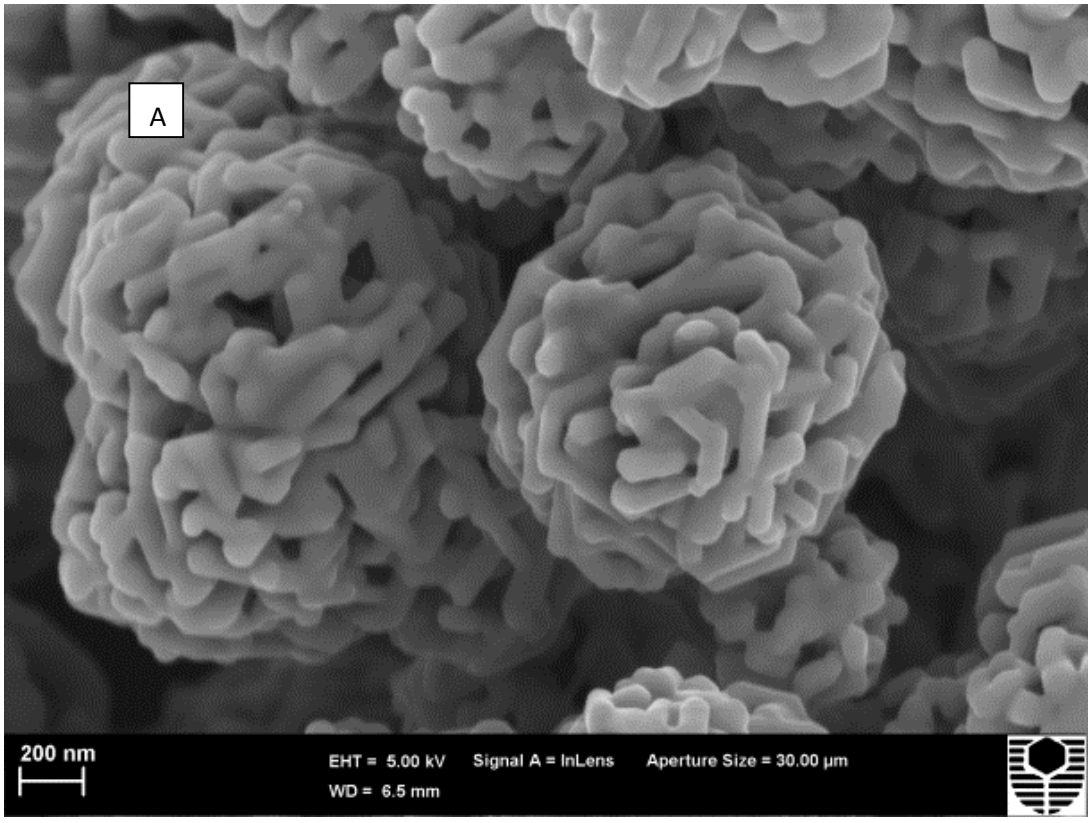

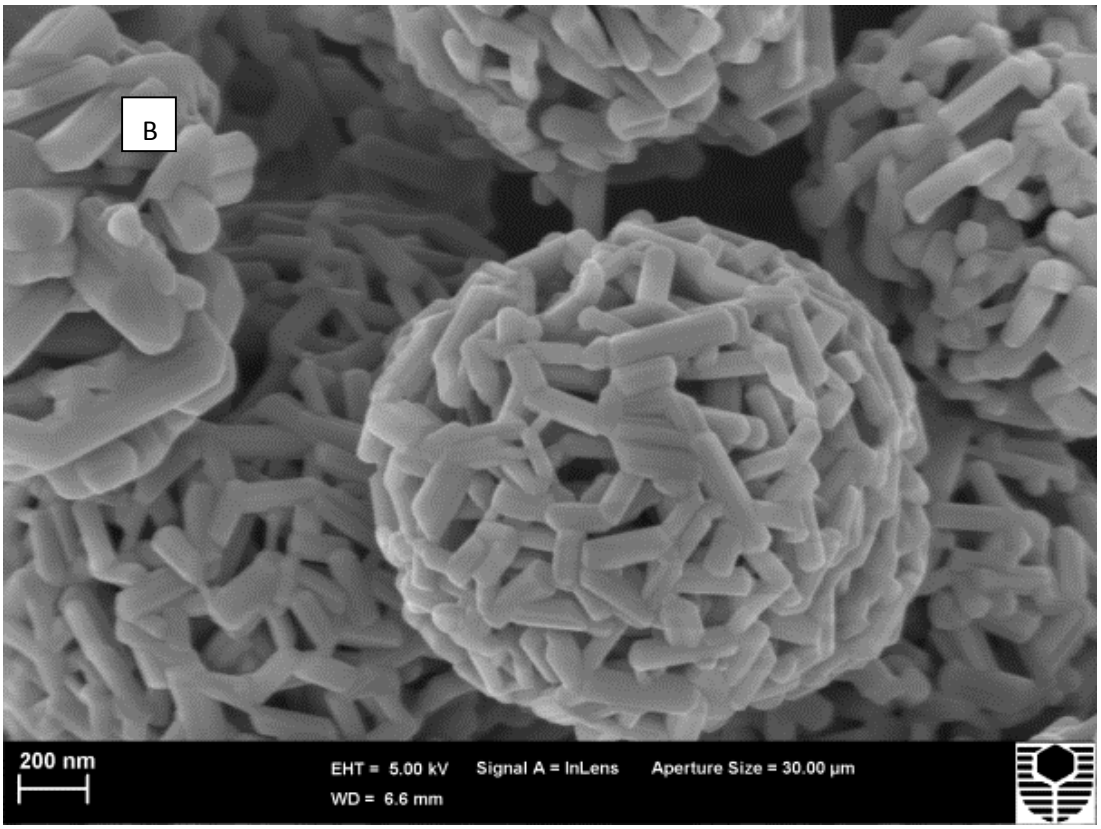
B
200 nm
EHT = 5.00 kV
Signal A = InLens
Aperture Size = 30.00 µm
WD = 6.6 mm

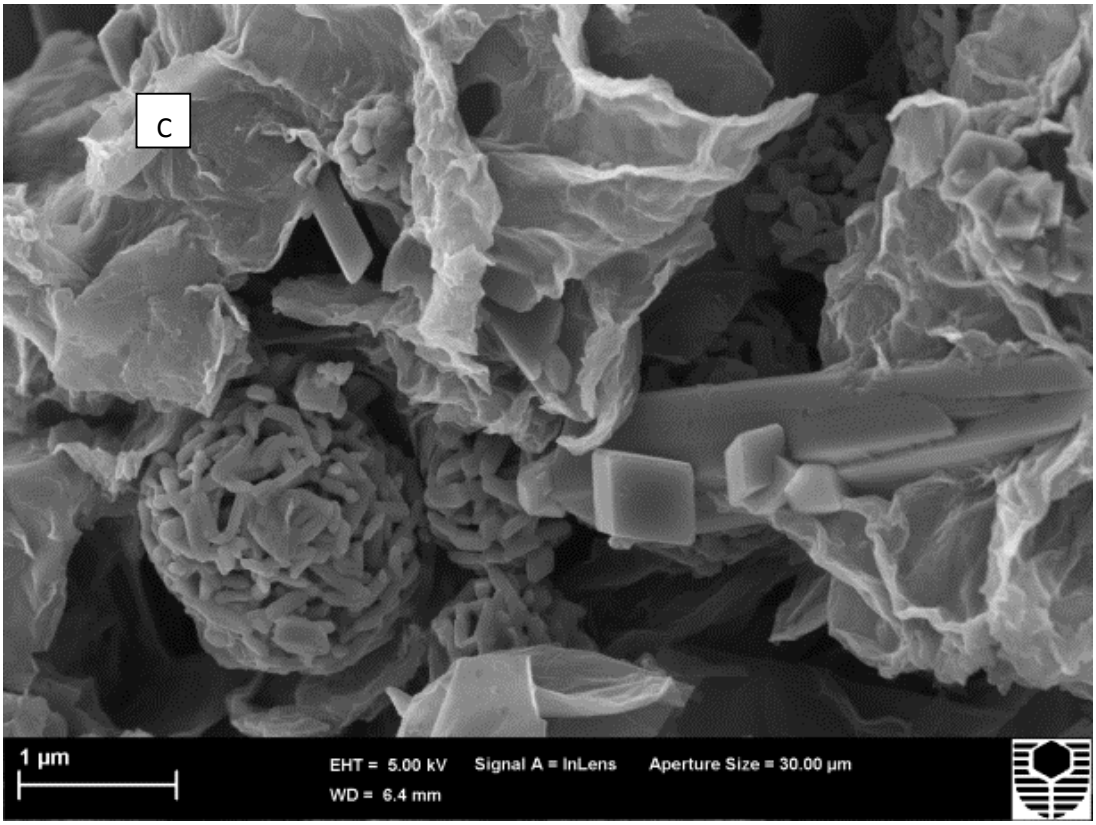
C
1 µm
EHT = 5.00 kV
Signal A = InLens
Aperture Size = 30.00 µm
WD = 6.4 mm


D
1 µm
EHT = 5.00 kV
WD = 6.4 mm
Signal A = InLens
Aperture Size = 30.00 µm

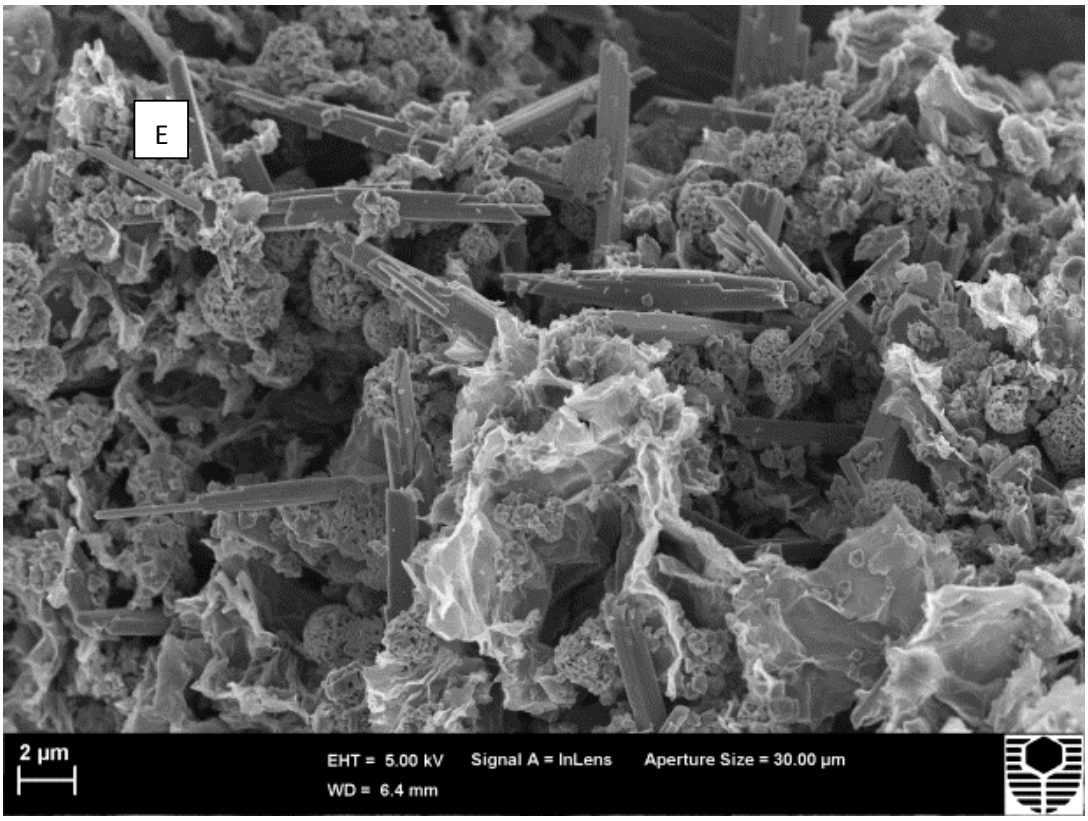
E
2 µm
EHT = 5.00 kV
WD = 6.4 mm
Signal A = InLens
Aperture Size = 30.00 µm

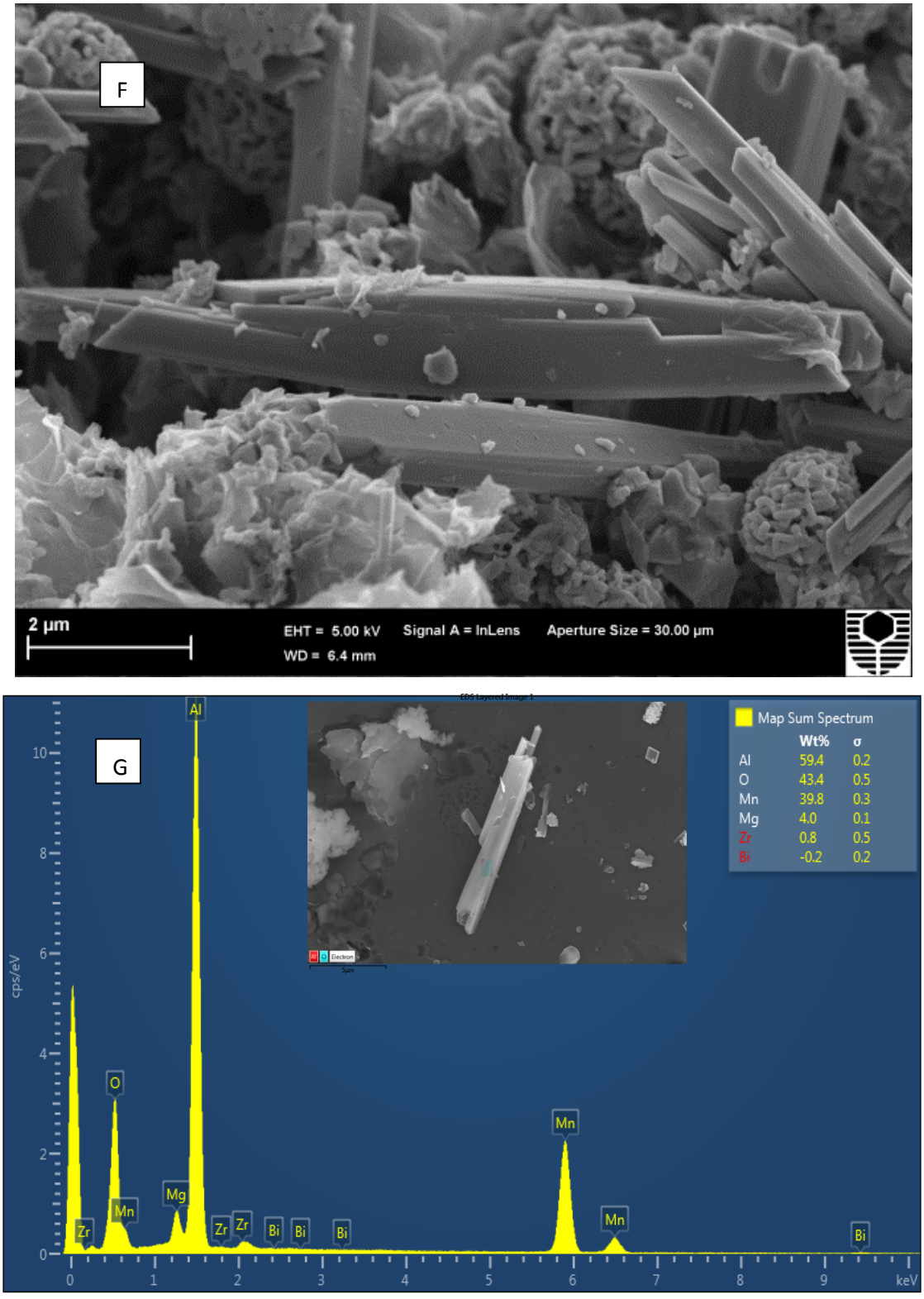

Fig. 5. 1. SEM images of $CaMn_3O_6$ (A), $CaMn_4O_8$ (B), GO/$CaMn_3O_6$ (C) and GO/$CaMn_4O_8$ (D, E, F), and EDS and elemental mapping of (G).

The morphology and structure of the catalysts were analyzed by FESEM imaging. Figs. 5.1 (A) and (B) show that $CaMn_3O_6$ and $CaMn_4O_8$ samples appeared in 3D microsphere structure, the diameters were 1 and 1.2 μm, respectively. It could be observed that the structures were constructed by nanorods (average length is 200 nm). According to the literature, $CaMn_3O_6$ and $CaMn_4O_8$ were constituted with the rutile-type chain of edge-sharing octahedral MnO_6 which are connected by double chains, and the Ca^{2+} ions present in the common corners of the chain [17 18]. The graphene oxide is clearly visible from the FESEM images shown in Figs. 5. 1(C)–(F), which presented a polylaminated structure, and distributed among the calcium manganese microspheres. As seen in Figs. 5. 1(E) and (F), there formed some new substances with rod-like structure, which were scatterly distributed among GO and calcium manganese oxides. The EDS and elemental mapping of new-formed material illustrated that it was manganese oxide.

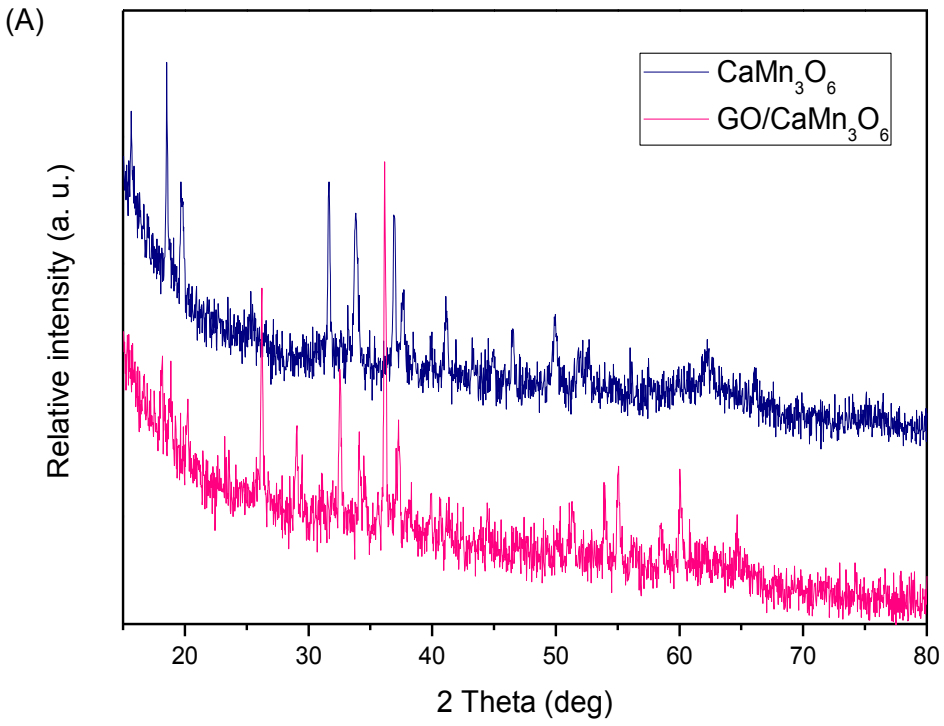

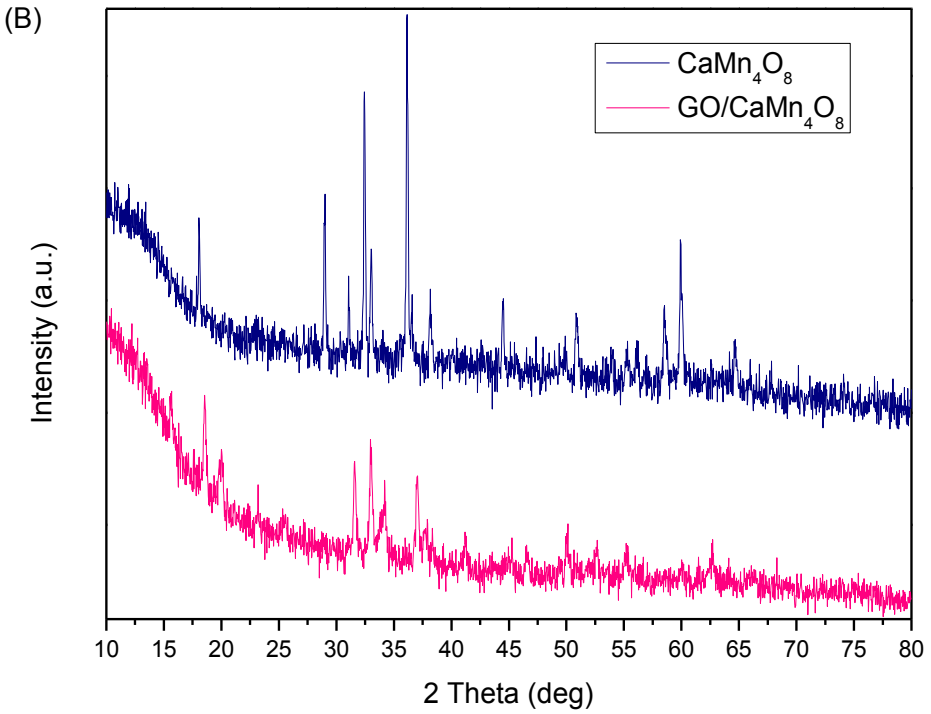

Fig.5.2. XRD patterns of GO/$CaMn_3O_6$ (A) and GO/$CaMn_4O_8$ (B).

Figure 5.2 displays XRD patterns of the as-prepared $CaMn_3O_6$, GO/$CaMn_3O_6$, $CaMn_4O_8$ and GO/$CaMn_4O_8$. The diffraction peaks of $CaMn_3O_6$ and $CaMn_4O_8$, which matched JCPDF card (No. 31-0285 and No. 31-0286) with no other impurity diffraction peak, indicating that the samples were confirmed to be highly purified [19 20]. For the two mixed valent calcium manganite samples, the peaks at 25.2° was observed, while no diffraction peak at 11°, which manifest that the GO was reduced to rGO after the compounding[21]. However, in GO/$CaMn_3O_6$ pattern, there were some new peaks occurred at 26.81, 28.88, 32.14, 38.13, 53.76, 55.05 and 59.91 °, corresponding to Mn_3O_4 and Mn_2O_3 (JCPDS No. 80-0382, a = 5.749 Å and No. 89-4836, a = 9.406 Å). While in GO/$CaMn_4O_8$ pattern, the new emerging diffraction peaks at 32.37, 38.09 and 50.84 ° could match JCPDF card (No. 80-0382 and No. 89-4836) to be Mn_3O_4 and Mn_2O_3

with some impure peaks. Those XRD results showed that the two mixed valent calcium manganites might have decomposed to manganese oxide and calcium oxide to a certain extent after the hydrothermal treatment.

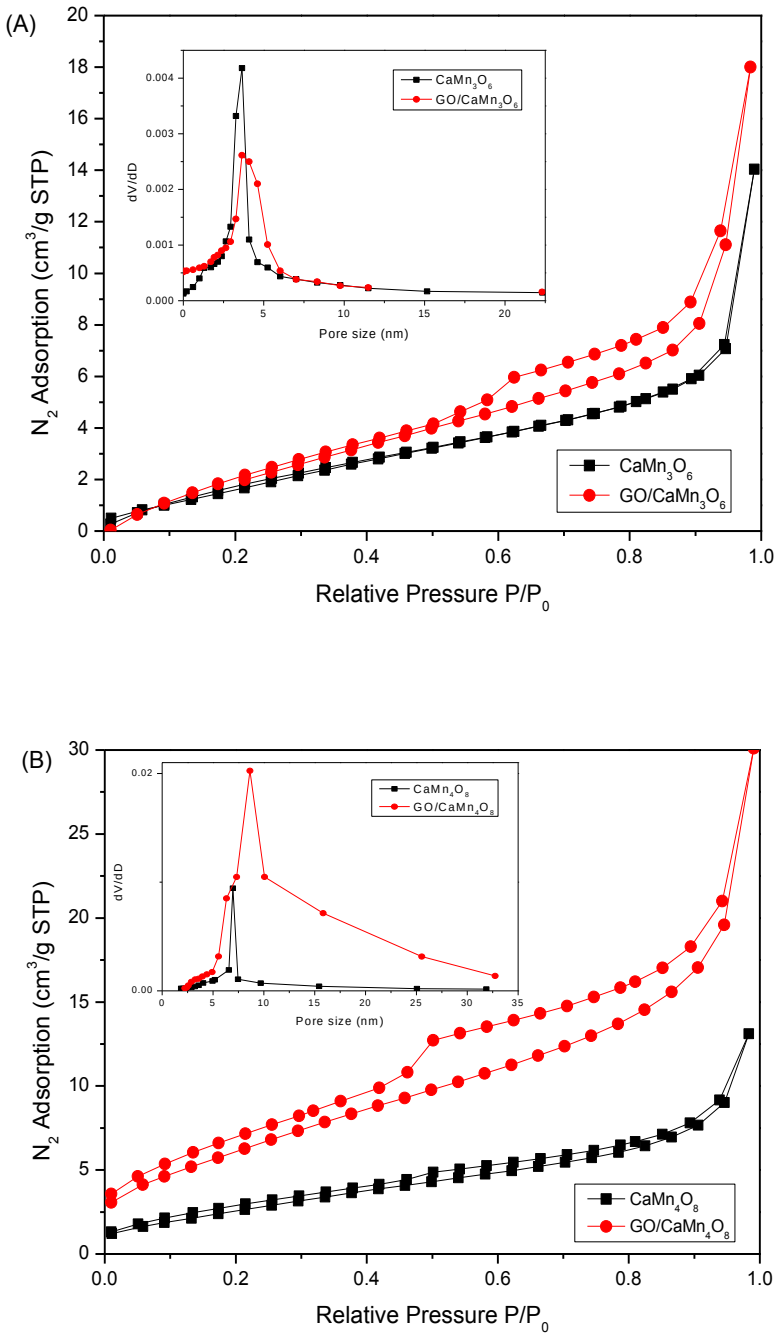

Fig.5.3. Nitrogen sorption isotherms and pore size distributions of (A) $GO/CaMn_3O_6$ and (B) $GO/CaMn_4O_8$.

Figs.5.3 (A) and (B) presents N_2 adsorption-desorption isotherms and the pore size distributions of the samples. The H_2-type hysteresis loop suggested these samples are mesoporous materials. The specific surface areas were 8.7, 6.9, 10.9 and 9.6 m^2/g, with the pore volume of 0.021, 0.020, 0.032 and 0.030 cm^3/g, respectively, and the pore size were 3.5, 3.7, 7.43 and 7.58 nm of $CaMn_3O_6$, $CaMn_4O_8$, GO/$CaMn_3O_6$ and GO/$CaMn_4O_8$.

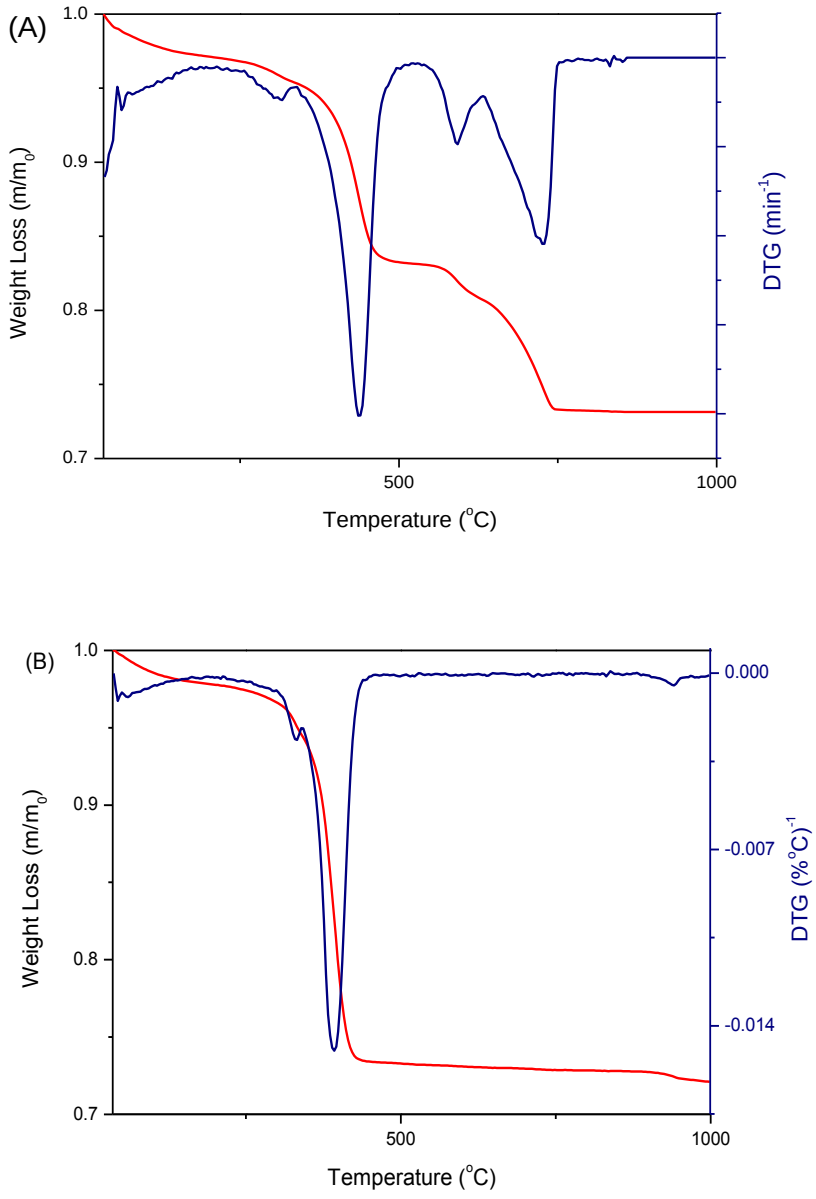

Fig. 5.4. TGA curves of (A) GO/$CaMn_3O_6$ and (B) GO/$CaMn_4O_8$.

Fig.5.4 shows TGA results. The test was carried out in air with a heating rate of 10 ℃/min.

There were two weight loss stages in the TGA curve of GO/$CaMn_3O_6$. It presented two obvious declines of weight in the range from 300 to 450 ℃ and from 600 to 750 ℃. The first decrease step could be assigned to the burning out of GO, and the second step could due to the further oxygenization of manganese oxide. While for GO/$CaMn_4O_8$, there was one conspicuous decrease occurred between 300 to 400 ℃, which could be assigned to the decomposition of graphene oxide.

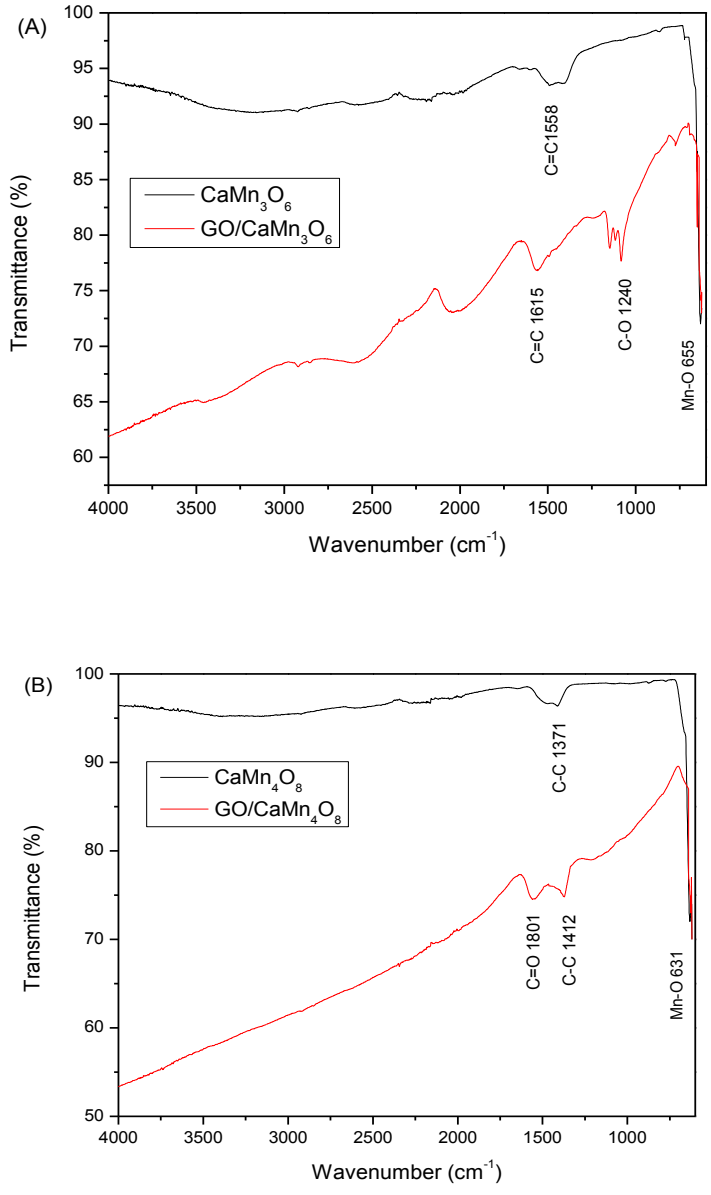

Fig. 5. 5. FT-IR spectra of $CaMn_3O_6$ and GO/$CaMn_3O_6$ (A), $CaMn_4O_8$ and GO/$CaMn_4O_8$ (B).

Fig.5.5 shows FT-IR results which were used to analyze the functional groups on the GO/$CaMn_3O_6$ and GO/$CaMn_4O_8$. According to Fig.5.5 (A), the bands at 1615, 1240 and 655 cm^{-1} were assigned to be C=C, C-O, Mn-O, respectively. While in the spectra of GO/$CaMn_4O_8$, the bands at 1801, 1412 and 631 cm^{-1} were assigned to be C=O, C-C and Mn-O, respectively.

5. 3. 2 Catalytic oxidation of phenol solutions

The study of phenol degradation tests was detailed in Chapters 3 and 4.

5. 3. 2. 1 Effects of reaction parameters on phenol degradation

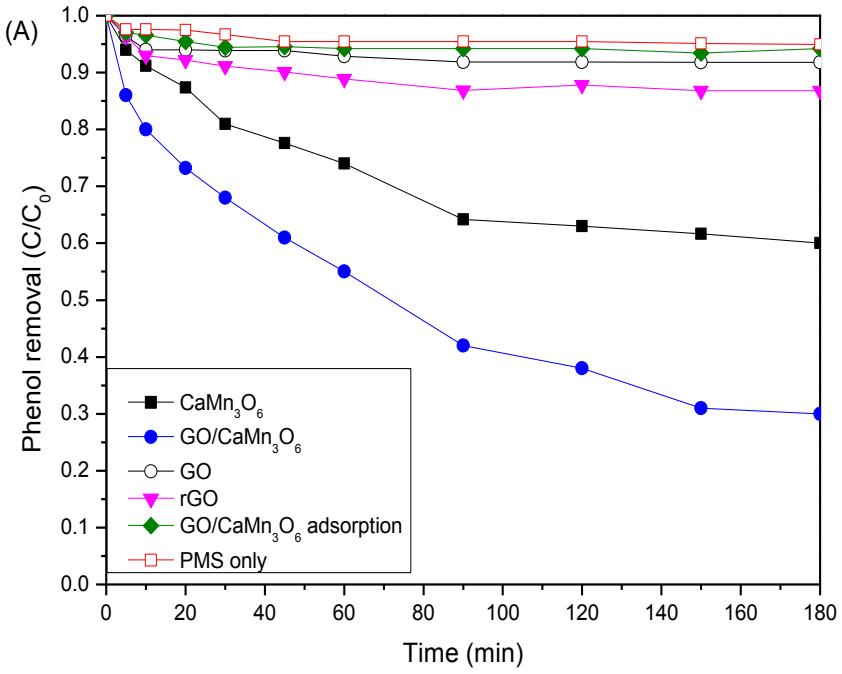

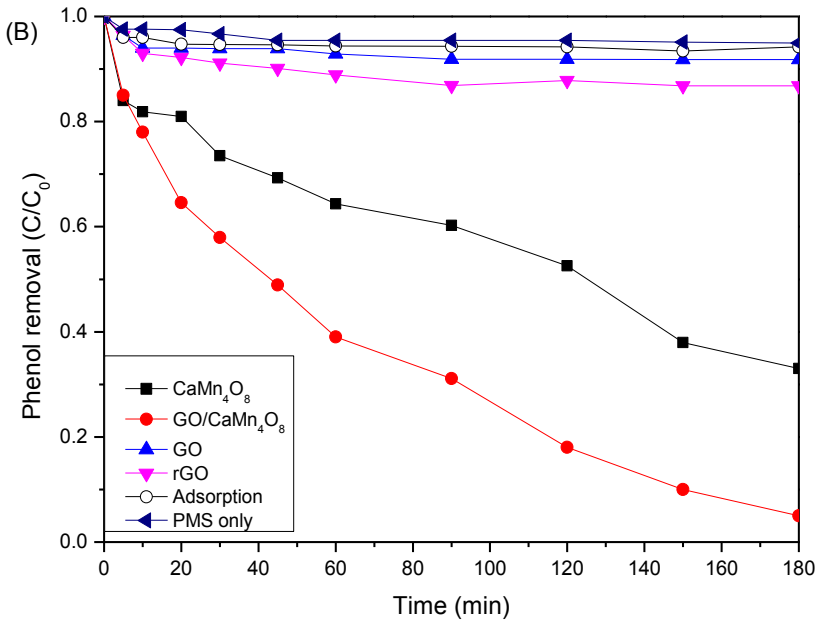

Fig.5.6. Phenol removal in different conditions.

The phenol decomposition in different conditions is demonstrated in Figs.5.6 (A) and (B). Comparing with all degradation, the one using GO/$CaMn_4O_8$ as a catalyst showed the best performance, and the degradation rate was higher than that of $CaMn_4O_8$, the rates were 96% and 63%, respectively in 180 min. While, compared with the GO/$CaMn_3O_6$ and $CaMn_3O_6$, they showed a similar trend. The final phenol removal rate of the composite was higher at about 67% and 38% for GO/$CaMn_3O_6$, and $CaMn_3O_6$. For the adsorption, the final phenol removal rates were 6% and 5.1% by GO/$CaMn_4O_8$ and GO/$CaMn_3O_6$, respectively. For the reaction using GO as the adsorbent, the removal was 7% in the end, while rGO brought final phenol removal of 10%. The comparison suggests that GO supported calcium manganese had higher catalytic activity than calcium manganese, GO or rGO in the system of phenol degradation. For the reaction without a catalyst and employed PMS only, the final phenol removal rate was about 5% in 180 min, which demonstrated that the PMS only and adsorption could not induce

phenol oxidation.

5. 3. 2. 2 Effects of reaction parameters on phenol degradation and the stability of the catalysts

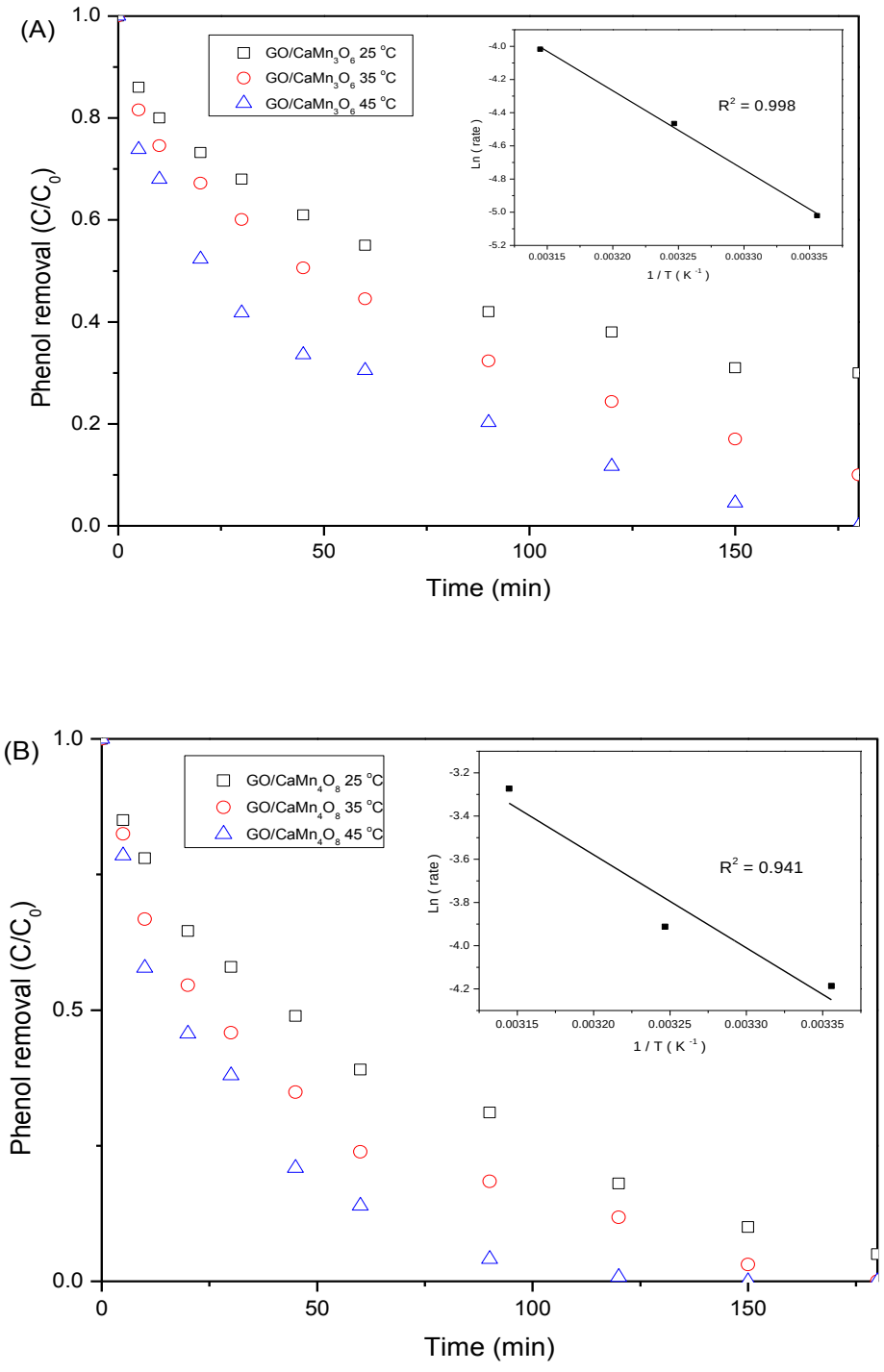

Fig.5.7. Phenol removal at different temperatures.

Table. 5. 1. Kinetic results of GO/$CaMn_3O_6$ and GO/$CaMn_4O_8$ catalysts in activation of PMS for phenol degradation at different temperatures.

catalysts	T (^oC)	K (min^{-1})	R^2 of k	Ea (kJ/mol)	R^2 of Ea
GO/$CaMn_3O_6$	25	0.0066	0.9623	39.6	0.998
	35	0.0115	0.9901		
	45	0.0180	0.9734		
GO/$CaMn_4O_8$	25	0.0152	0.9838	35.8	0.941
	35	0.0020	0.9628		
	45	0.0379	0.9854		

Lots of conditions can influence the final phenol degradation rate in heterogeneous catalytic oxidation of phenol. This section will show the effect of reaction temperature on phenol degradation. Fig.5.7 (A) shows the performance of GO/$CaMn_4O_8$ catalysts for heterogeneous oxidation of phenol at varying temperatures. It was seen that reaction temperature dramatically affected oxidation efficiency and degradation rate. At 25 ^oC the final degradation rate was 96% in 180 min. When the reaction took place at 35 and 45 ^oC, phenol removal rates reached to 100% in 170 and 120 min, respectively. The same trend to GO/$CaMn_3O_6$ (Fig.5.7 (B)), with increasing rates of 69, 83 and 100% at temperatures of 25, 35 and 45 ^oC, respectively, suggesting that a higher temperature could make a significant contribution to rapid phenol degradation. Based on reaction rate at different temperatures, the apparent activation energy of GO/$CaMn_3O_6$ was calculated as 39.6 kJ/mol, while that of GO/$CaMn_4O_8$ was 35.8 kJ/mol.

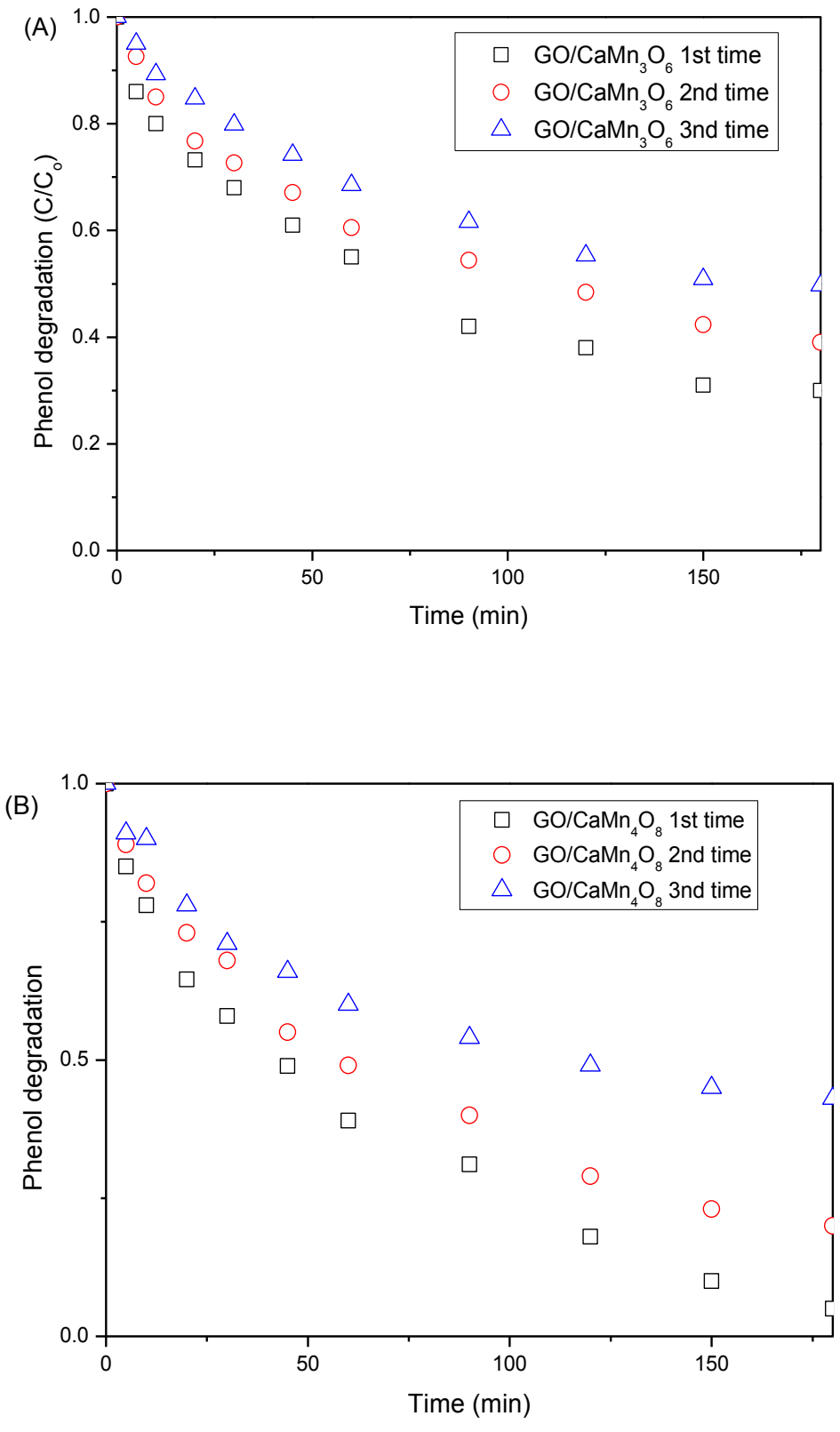

Fig.5.8. Reusability tests of (A) GO/ $CaMn_3O_6$ and (B) GO/$CaMn_4O_8$ catalysts.

The reuse performance of GO/$CaMn_3O_6$ and GO/$CaMn_4O_8$ were demonstrated by three-time running stability tests (Fig. 5.8). After the first run, catalysts were washed with water and dried at 80 ^oC overnight, without any further regeneration. In the second time, the phenol removal rates were 59 and 80% in 180 min, respectively, for GO/$CaMn_3O_6$ and GO/$CaMn_4O_8$. For the third time, the degradation rates were 45% in GO/$CaMn_3O_6$ system, and 52% in GO/$CaMn_4O_8$ system. It suggested that the catalytic activities decreased in the recycled tests for both catalyst systems. The decline of catalytic activity might be due to the attachment of reaction intermediate on the surface of the catalyst, which make the correspondent active sites disabled. And it was hard to remove all of the intermediates by simply washed with water, because the van de Waals force were strong.

5. 4 Conclusions

In conclusion, the catalytic activities were examined by activating PMS for phenol degradation. It was found that the composite materials presented higher BET surface area and higher activity than GO and calcium-manganese oxide themselves. GO supported calcium-manganese oxide catalysts were synthesized via two-step methods. The catalytic properties of the calcium-manganese oxide materials were improved by compositing with GO. 96% and 67% of phenol could be decomposed within 180 min with catalysts of GO/$CaMn_3O_6$ and GO/$CaMn_4O_8$. The first order kinetic model was used to evaluate the kinetics, and the activation energies for GO/$CaMn_3O_6$ and GO/$CaMn_4O_8$ were calculated to be 39.6 kJ/mol and 35.8 kJ/mol, respectively.

5.5 References

1. Duan X.; Sun H.; Wang Y.; Kang J.; Wang S. N-Doping Induced Non-Radical Reaction on Single-Walled Carbon Nanotubes for Catalytic Phenol Oxidation, ACS Catalysis, 2014. 5 (2): pp. 553-559.

2. Shukla P.; Sun H.; Wang S.; Ang H.; Tadé M. Nanosized Co_3O_4/SiO_2 for heterogeneous oxidation of phenolic contaminants in waste water Sep. Purif. Technol., 77 (2011), pp. 230–236

3. Court. S, Environmental forensics for persistent organic pollutants. Amsterdam: Elsevier 2014

4. Tuty Emilia. Comparison of various advanced oxidation processes for the treatment of winery wastewater. Curtin University of Technology. Dept. of Chemical Engineering. Thesis (Ph. D.)--Curtin University of Technology. 2007

5. Luck, F. Wet air oxidation: past, present and future. Catalysis Today, 1999, Vol. 53(1), pp.81-91

6. Bhargava, S. Catalytic Wet Air Oxidation of Industrial Aqueous Streams. Catalysis Surveys from Asia, 2007. 11(1-2): pp. 70-86.

7. Wang, S. A comparative study of Fenton and Fenton-like reaction kinetics in decolourisation of wastewater. Dyes and Pigments. 76 (2008) pp. 714-720.

8. Ullah, R. Photocatalytic oxidation of air toxics via visible light irradiation and nano-photocatalysts, Curtin University, School of Chemical and Petroleum Engineering, Department of Chemical Engineering. Thesis (Ph.D.)--Curtin University. 2012

9. Zhao, J. ; Zhu, C. ; Lu, J. ; Hu, C. ; Peng, S. ; Chen, T. Electro-catalytic degradation of bisphenol A with modified Co3O4/β-PbO2/ Ti electrode, Electrochimica Acta, 2014, Vol.118, pp.169-175

10. Li D; Qu J; Environ J. The progress of catalytic technologies in water purification, Sci. 21 (2009), pp. 713–719.

11. Yang, Y. ; Pignatello, J. ; Ma, J. ; Mitch, W., Comparison of halide impacts on the efficiency of contaminant degradation by sulfate and hydroxyl radical-based advanced oxidation processes (AOPs), Environmental science & technology, 18 February 2014, Vol.48(4), pp.2344-51

12. Song M.; Cheng S.; Chen H.; Qin W.; Nam K.; Xu S.; Yang X., Bongiorno A.; Lee J.; Bai J.; Tyson T.; Cho J.; Liu M. Anomalous pseudocapacitive behavior of a nanostructured, mixed-valent manganese oxide film for electrical energy storage, Nano Lett., 12 (2012) 3483-3490.

13. Han X.; Zhang T.; Du J.; Cheng F.; Chen J.; Porous calcium-manganese oxide microspheres for electrocatalytic oxygen reduction with high activity, Chem. Sci., 4 (2013) 368-376.

14. Lee. M.; Lee S.; Oh P.; Kim Y.; Cho J. High performance $LiMn_2O_4$ cathode materials grown with epitaxial layered nanostructure for li-ion batteries, Nano Lett., 14 (2014) 993-999.

15. Wang T.; Qu G.; Li J.; Liang D.; Hu S. Depth dependence of p-nitrophenol removal in soil by pulsed discharge plasma, Chem. Eng. J., 239 (2014) 178-184.

16. Yao Y.; Cai Y.; Wei F.; Wang X.; Wang S. Magnetic recoverable $MnFe_2O_4$ and $MnFe_2O_4$-graphene hybrid as heterogeneous catalysts of peroxymonosulfate activation for efficient degradation of aqueous organic pollutants. Journal of Hazardous Materials, 270 (2014) pp.61-70.

17. Han X.; Zhang T.; J. Du, F.; Chen J. Porous calcium-manganese oxide microspheres for electrocatalytic oxygen reduction with high activity, Chem. Sci., 4 (2013) 368-376.

18. Hadermann J.; Abakumov A.; Gillie L.; Martin C.; Hervieu M. Coupled cation and charge ordering in the $CaMn_3O_6$ tunnel structure, Chem. Mater., 18 (2006) 5530-5536.

19. J. Hadermann, A.M. Abakumov, L.J. Gillie, C. Martin, M. Hervieu, Coupled cation and charge ordering in the $CaMn_3O_6$ tunnel structure, Chem. Mater., 18 (2006) 5530-5536.

20. N. Barrier, C. Michel, A. Maignan, M. Hervieu, B. Raveau, $CaMn_4O_8$, a mixed valence manganite with an original tunnel structure, J. Mater. Chem., 15 (2005) 386-393.

21. Fan, Z. ; Wang K.; Yan, J. ; Wei, T. ; Zhi, L. ; Feng, J. ; Ren, Y. ; Song, L. ; Wei, F.. Facile synthesis of graphene nanosheets via Fe reduction of exfoliated graphite oxide, ACS nano, 25 January 2011, Vol.5(1), pp.191-8.

6

Chapter 6: Effect of diluted acid treatment on catalysis over calcium-manganese oxide catalysts

A B S T R A C T

Calcium-manganese oxide catalysts were synthesized via a hydrothermal method followed by calcination. After treated with dilute acid, the catalysts ($H^+/CaMn_3O_6$, $H^+/CaMn_4O_8$) showed better performance in phenol degradation. The samples were characterized by X-ray diffraction (XRD), field emission scanning electron microscopy (SEM), thermogravimetric analysis/differential temperature gradient (TGA/DTG) and Fourier transform infrared spectroscopy (FT-IR) and inductively coupled plasma-atomic (optical) emission spectrometry (ICP). In the catalytic oxidation for 180 min, and the catalysts could remove 96 and 67% of phenol, respectively.

6.1 Introduction

In the 21st century, wastewater has become an important issue. Hazardous components from industrial processes were discharged into the environment arbitrarily, which brought great threats to the public health [1-4]. Phenol is one of the serious pollutants due to its toxicity and recalcitrance to natural degradation even at low concentration. Usually, the maximum permissions of phenol emission were prescribed less than 1 mg/L in many country, and 0.5 mg/L in Australian stipulation [56].

Advanced oxidation processes (AOPs) have been widely investigated as great methods to decompose macromolecular organic compounds into non-toxic compounds such as carbon dioxide and water. The operation of AOPs was based on the generation of reactive radicals, which had a high standard oxidation potential for non-selective reaction [7-10].

Recently, the applications of manganese oxide materials have attracted lots of research interests, due to the excellent efficiency in degradation and the low toxicity to the environment [11]. In the past few years, the mixed valent manganite materials have received increasing attention because of their unique physicochemical properties [12 13]. A number of methods have been employed to improve the performance of the mixed valent manganites catalysts. Si and his group found that the macroporous mixed valent manganites showed higher oxidation catalytic activity after treatment by diluted HNO_3, due to the removal of La cations, and the construction of the mixed valent manganites would not be destroyed via immersing in acid[14 15].

In this chapter, a unique treatment of calcium-manganese oxide ($CaMn_3O_6$, $CaMn_4O_8$)[16 17] catalysts is presented, and after diluted acid treatment, the prepared catalysts showed a higher

activity in the oxidation of phenol solutions.

6.2 Experimental

6.2.1 Chemicals

Calcium carbonate (99.5%), ammonium carbonate (99%), nitric acid (70%), manganese carbonate (99.8%), methanol (99%), phenol (99%) and Oxone ($2KHSO_5 \bullet 3KHSO_4 \bullet K_2SO_4$) were obtained from Sigma-Aldrich. All the chemicals were used as received without further purification.

6.2.2. Synthesis of calcium-manganese oxides ($CaMn_3O_6$, $CaMn_4O_8$)

The calcium manganese oxides were synthesized via a modified co-precipitation method. For the synthesis of $CaMn_3O_6$, 10 mmol calcium carbonate and 30 mmol manganese carbonate were dissolved in 80 mL diluted nitric acid (1 M). With vigorous stirring, 200 mL of ammonium carbonate solution (2 M) was then added into the mixture to adjust the pH of solution, which needed to be higher than 8. Filtered the product by vacuum filtration and followed with washing by ultrapure water and ethanol, the brownish precipitate was obtained. Then the precipitate was dried at 60 ^oC in an oven for 24 h. After that, the dried precipitate was transferred into a crucible and heated in a muffle furnace at 800 ^oC for 18 h. The obtained black powder was named as $CaMn_3O_6$. Synthesis of the $CaMn_4O_8$ used the similar process of $CaMn_3O_6$, with only change of the dosage of $MnCO_3$ to 40 mmol.

6.2.3. Acid treatment of calcium manganese oxide catalysts (H^+/ $CaMn_3O_6$, H^+/ $CaMn_4O_8$)

The samples were treated by diluted HNO_3, and in a typical treatment, 1 g $CaMn_3O_6$ and $CaMn_4O_8$ powders were added into 1 mM nitric acid solution with string. The solutions were magnetically stirred for 0.5 h and transferred into a filter, the catalysts were washed with

ethanol and distilled water for three times to collected the black precipitates, which were then dry in an oven at 60 ℃ for 12 h. The final samples were named as $H^+/CaMn_3O_6$ and $H^+/CaMn_4O_8$, respectively.

6. 3 Results and discussion

6.3.1 Characterization of samples

Detailed characterization methods were the same as those in Chapters 3, 4 and 5.

6.3.1.1 X-ray diffraction patterns

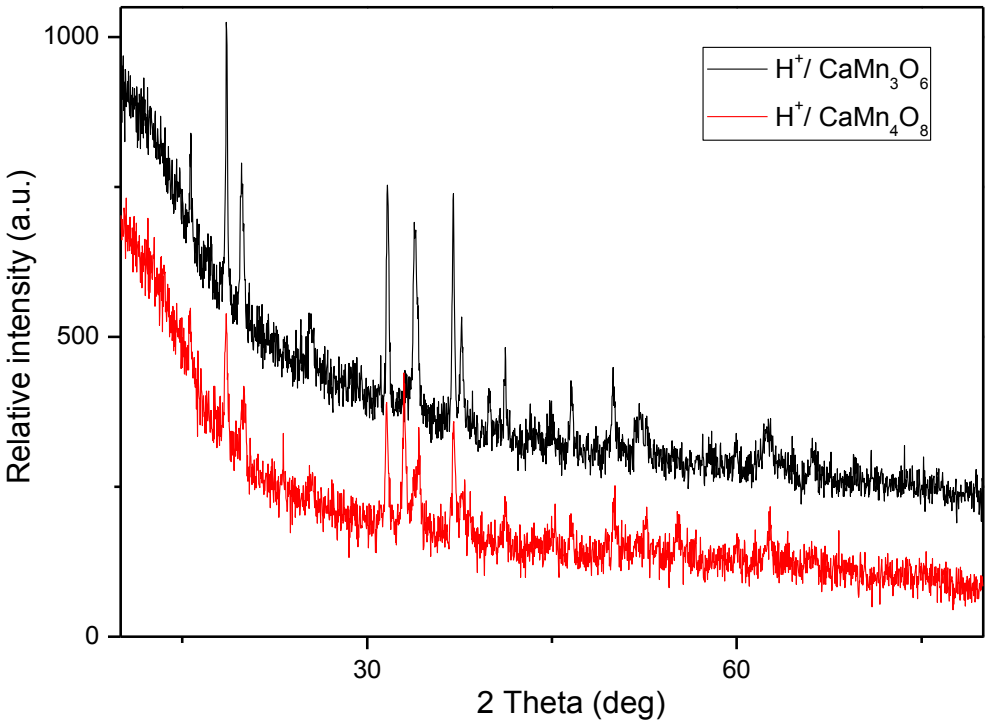

Fig. 6.1. XRD patterns of $H^+/CaMn_3O_6$ and $H^+/CaMn_4O_8$.

Fig. 6. 1 shows XRD patterns of $H^+/CaMn_3O_6$ and $H^+/CaMn_4O_8$. The diffraction peaks of $H^+/CaMn_3O_6$ were occurred at 18.01, 19.87, 32.01, 33.93, 37.52, 50.01 and 62.50°, which

matched with JCPDF card of $CaMn_3O_6$ (no. 31-0285). $H^+/CaMn_4O_8$ showed the peaks at 18.69, 19.95, 31.95, 33.34, 34.57, 37.60, 50.00 and 62.59°, corresponding to $CaMn_4O_8$ (JCPDS No. 31-0286), with no other impurity diffraction peak, indicating the samples were confirmed to be highly purified [18 19] and acid treatment would not change the crystal structure of the samples.

6.3.1.2 SEM and TEM images

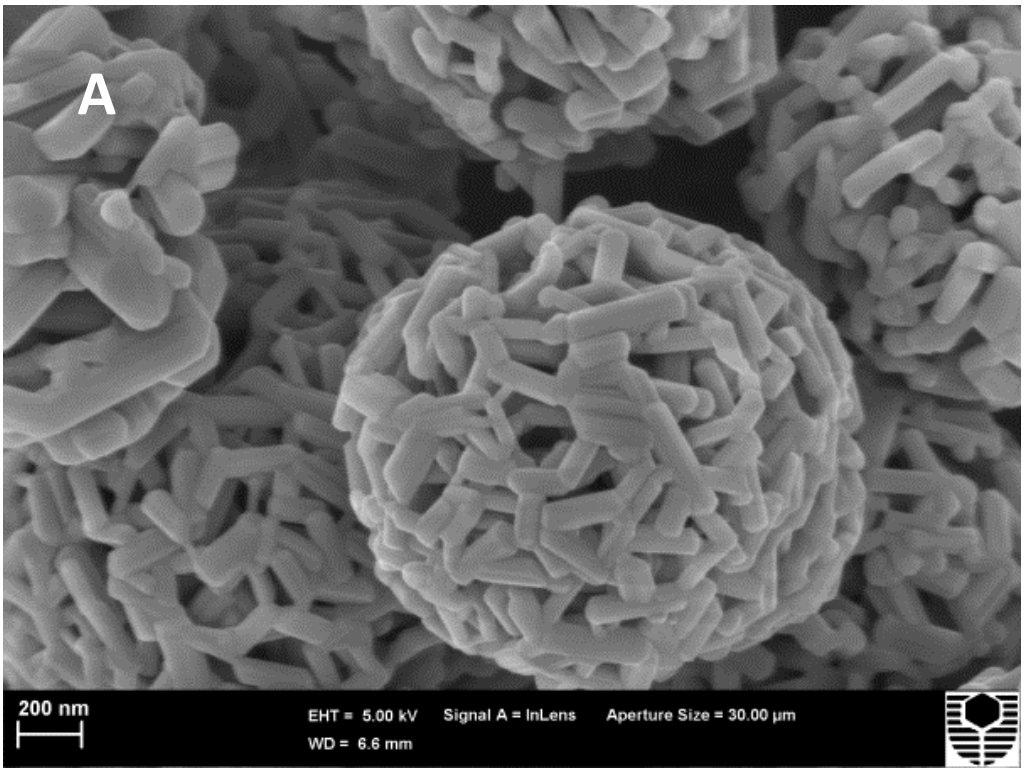

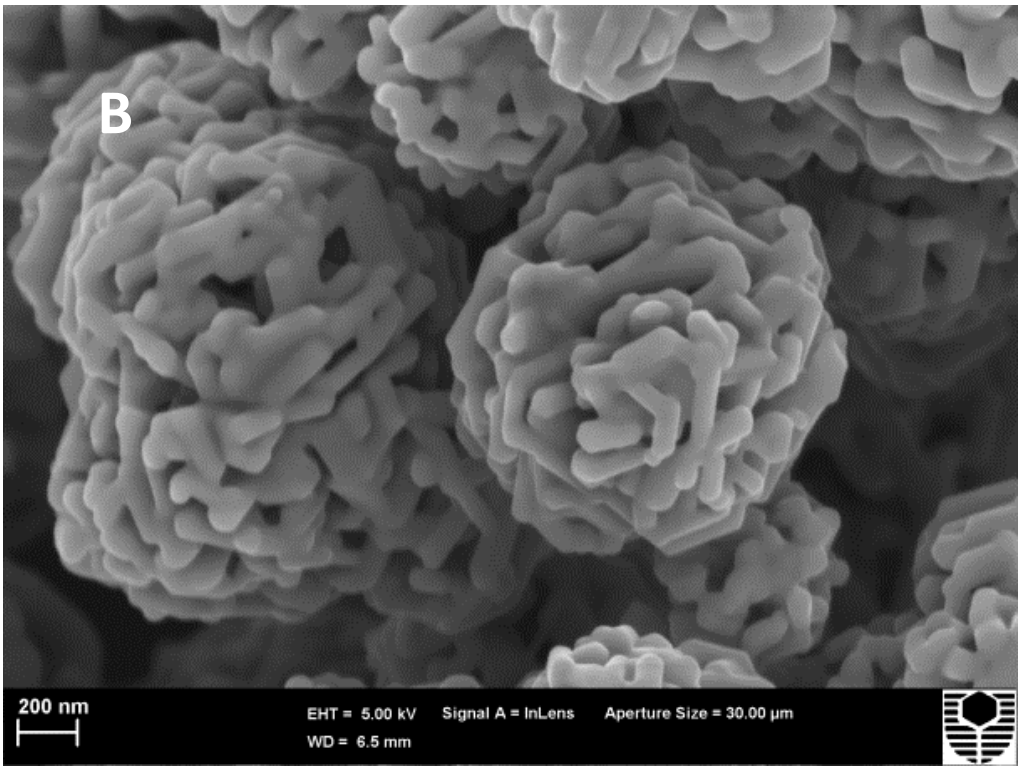
B
200 nm
EHT = 5.00 kV
WD = 6.5 mm
Signal A = InLens
Aperture Size = 30.00 µm

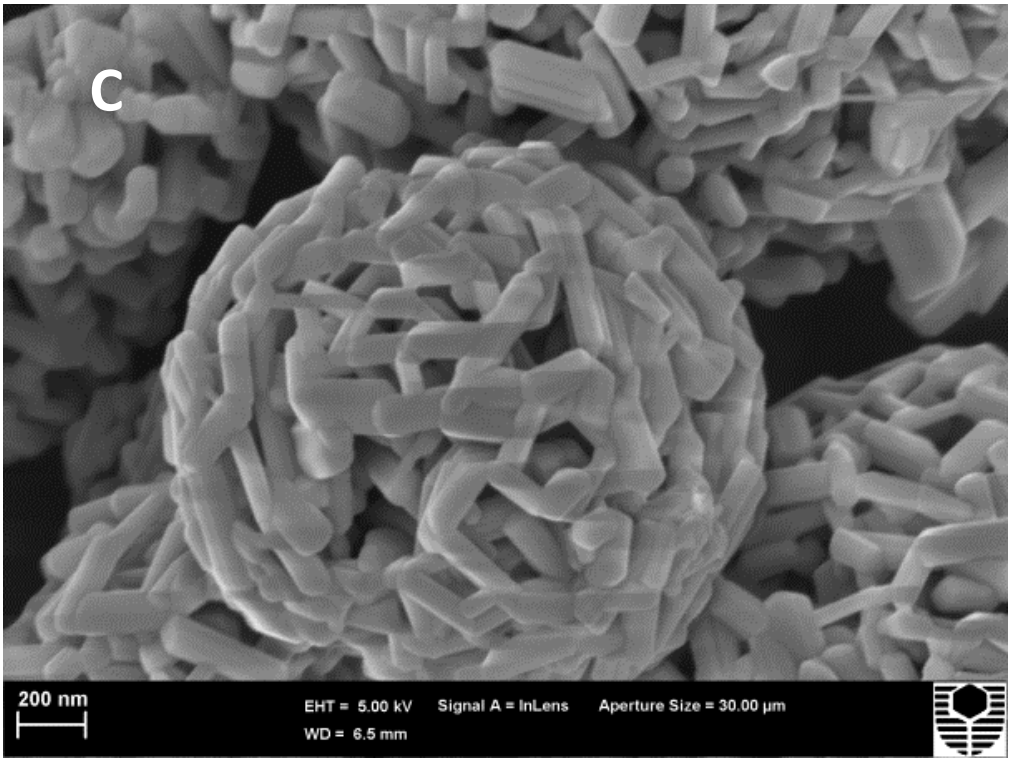
C
200 nm
EHT = 5.00 kV
WD = 6.5 mm
Signal A = InLens
Aperture Size = 30.00 µm

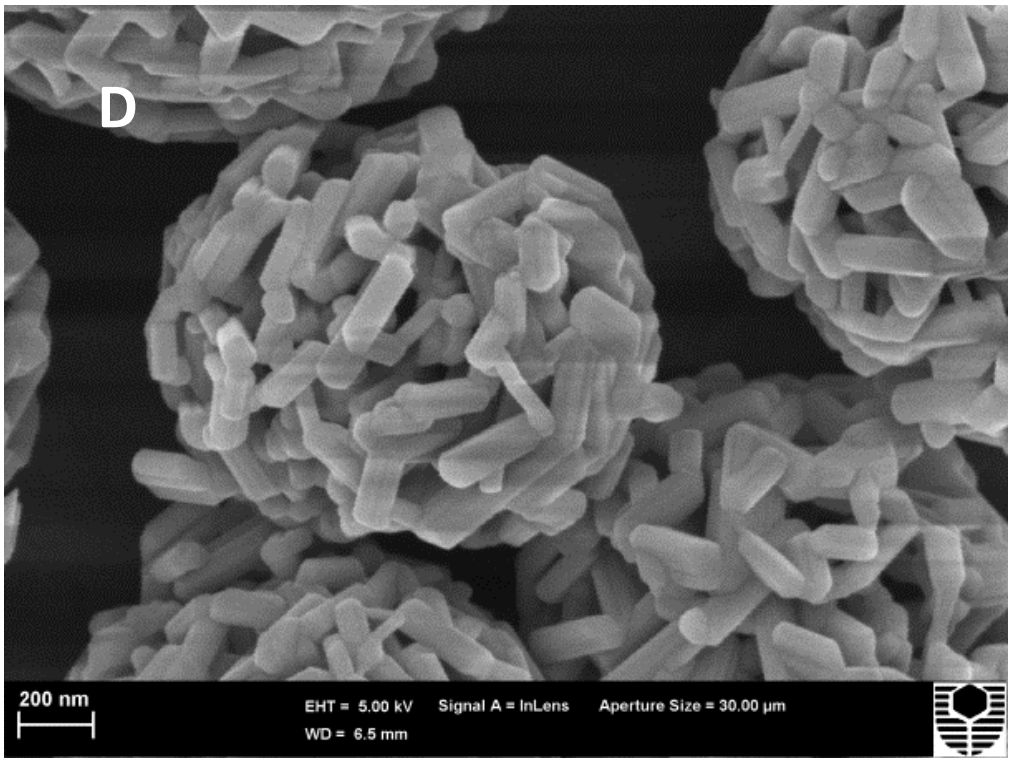

Fig. 6.2. SEM images of (A) $CaMn_3O_6$, (B) $CaMn_4O_8$, (C) $H^+/CaMn_3O_6$ and (D) $H^+/CaMn_4O_8$.

The morphology and structure of the catalysts were analyzed by FESEM. Fig.6.2 (A) and Fig.6.2 (B) showed that the $CaMn_3O_6$ and $CaMn_4O_8$ samples appeared in 3D microsphere structure, the diameters were 1 and 1.2 μm, respectively. The spherical structures were constructed by nanorods (average length is 200 nm). It could be seen in Fig. 3(C) and (D) that the changes of morphology were not very noticeable with the acid treatment, which presented porous structures.

6.3.1.3 Nitrogen sorption isotherms

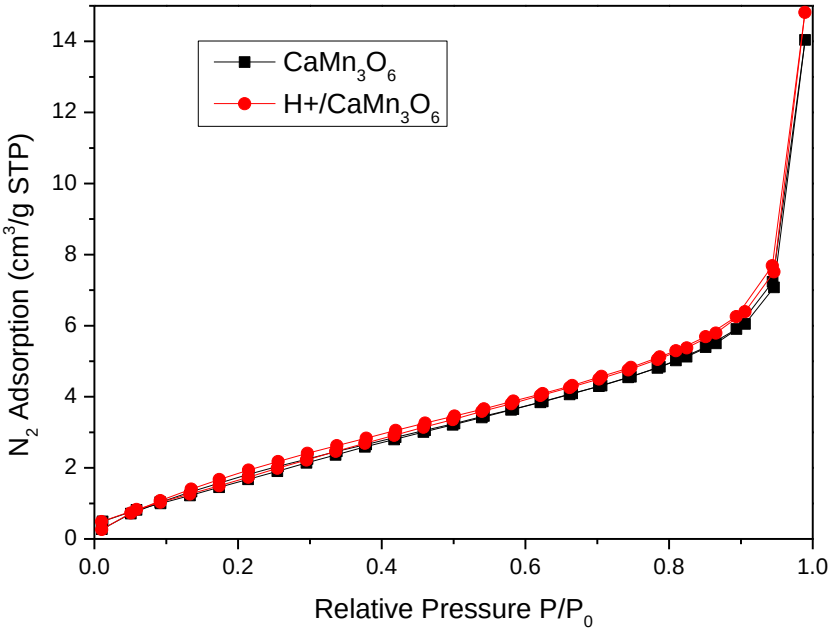

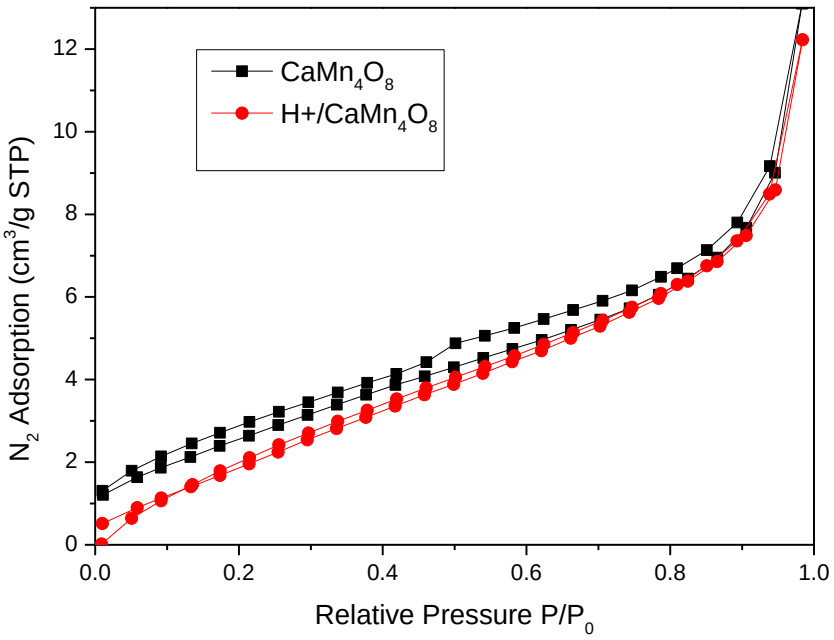

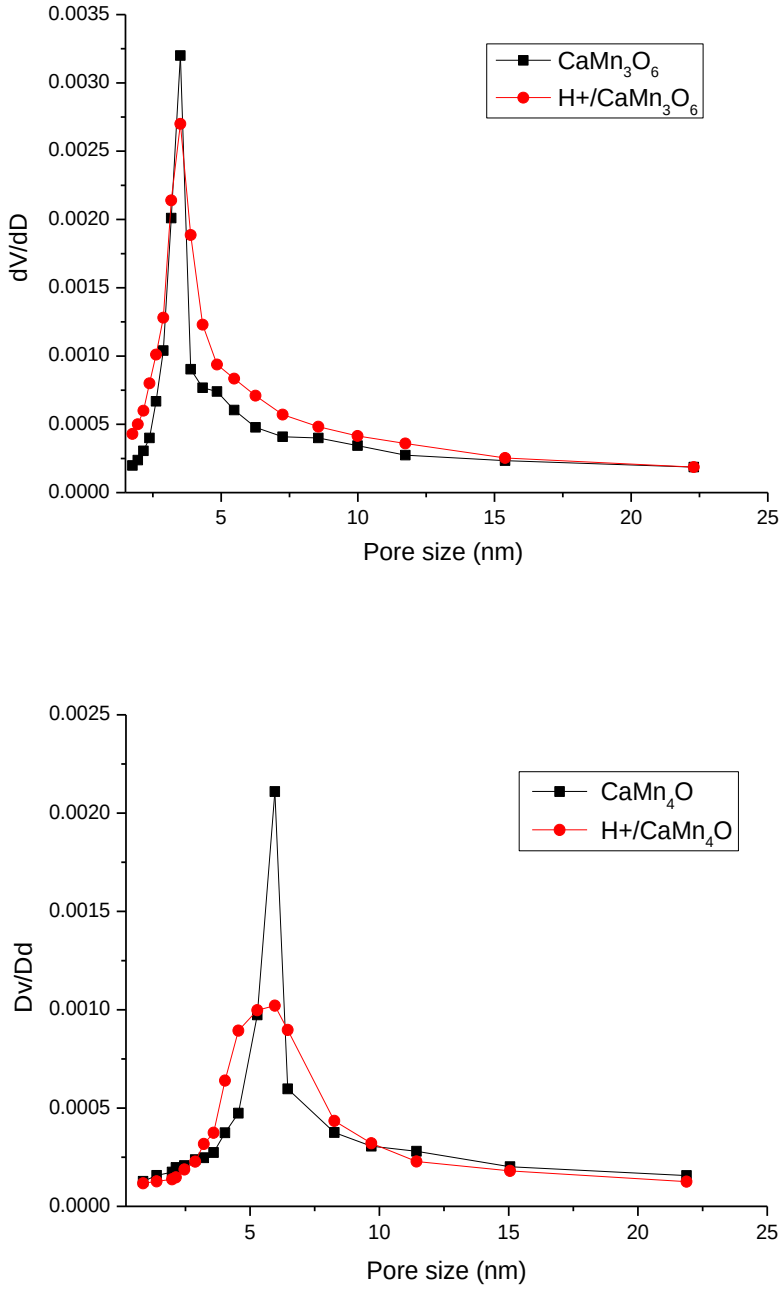

Fig. 6.3. Nitrogen sorption isotherms and pore size distribution for (A) $H^+/CaMn_3O_6$ and (B) $H^+/CaMn_4O_8$. Pore size distribution of (C) $H^+/CaMn_3O_6$ and (D) $H^+/CaMn_4O_8$.

Figs. 6.3(A) and (B) present N_2 adsorption-desorption isotherms and Figs.6.3 (C) and (D) show the pore size distributions of the samples. A type IV isotherm with a type of H_3 hysteresis loop

were observed for all samples, indicating the $CaMn_3O_6$, $CaMn_4O_8$, $H^+/CaMn_3O_6$ and $H^+/CaMn_4O_8$ were presented as mesoporous structures. The specific surface areas of them were 8.7, 6.9, 18.1 and 12.7 m^2/g, with the pore volume of 0.021, 0.032, 0.022 and 0.028 cm^3/g respectively, indicating that the acid treated samples presented a higher BET specific surface area. The pore sizes were 3.5, 3.7, 7.43 and 7.07 nm of $CaMn_3O_6$, $CaMn_4O_8$, $H^+/CaMn_3O_6$ and $H^+/CaMn_4O_8$.

6.3.1.4 TGA analysis

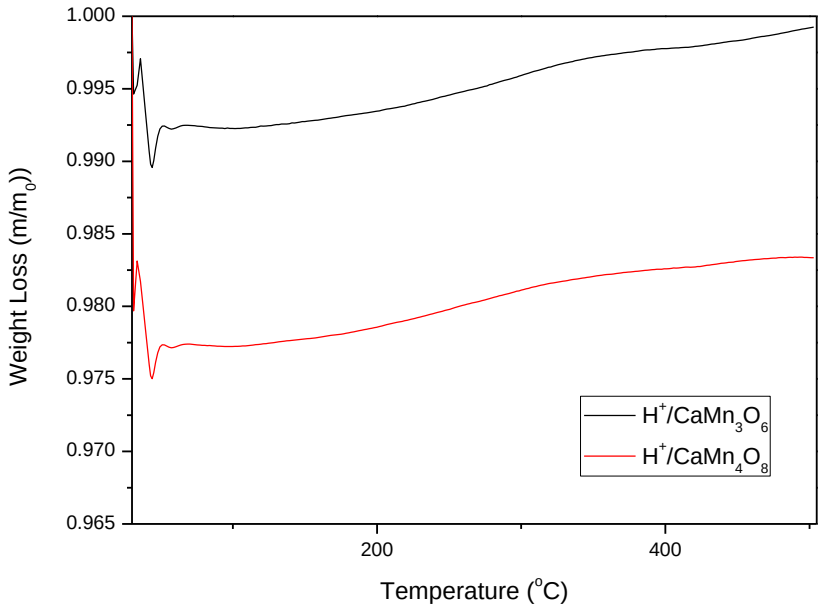

Fig.6.4. TGA curves of $H^+/CaMn_3O_6$ and $H^+/CaMn_4O_8$.

Fig.6.4 showed the TGA results, which determined the content of each element in the hybrids. The test was carried out in air with a heating rate of 10 ℃ per min. There were nearly no weight

loss procedures for both samples, which proved the samples of $H^+/CaMn_3O_6$ and $H^+/CaMn_4O_8$ had high thermostability.

6.3.1.5 FTIR analysis

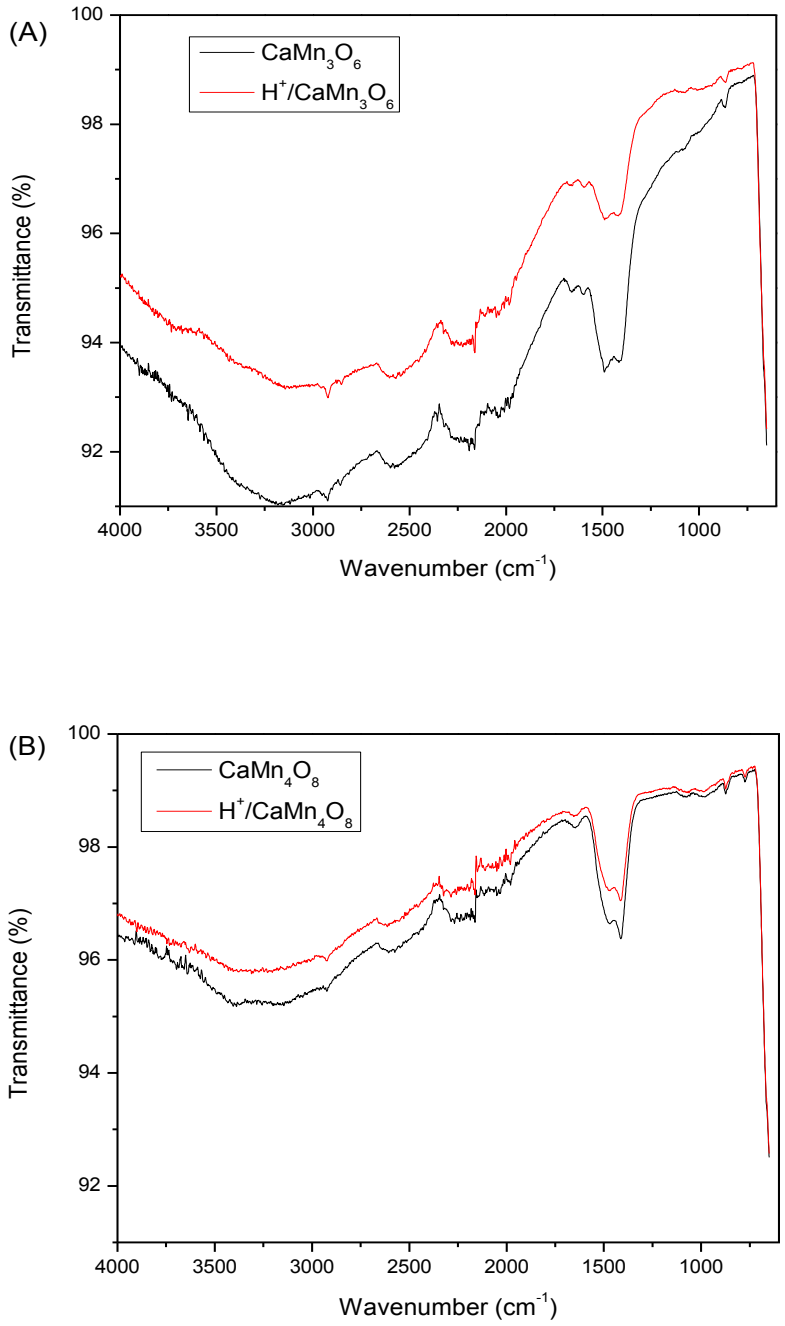

Fig.6.5. FT-IR spectra of $CaMn_3O_6$, $H^+/CaMn_3O_6$, $CaMn_4O_8$ and $H^+/CaMn_4O_8$.

Fig.6.5 shows FT-IR spectra which were used to analyze the functional groups on the $H^+/CaMn_3O_6$ and $H^+/CaMn_4O_8$. According the above two figures, the bands at 3449, 1679 and 1415 cm^{-1} were assigned to –OH, C=O and C-C, respectively. And the absorptions at 600 and 400 cm^{-1} were assigned to the Mn–O deformation modes of $CaMn_3O_6$ and $CaMn_4O_8$.

6. 3.1.6 ICP analysis

Table. 6.1. ICP analysis of the filtered solutions after the acid treatment.

C (mg/L)	$H^+/CaMn_3O_6$	$H^+/CaMn_4O_8$
Ca ions	17.03	11.16
Mn ions	1.15	1.25

In order to confirm the chemical modification of the dissolved materials via acid treatment, the filtered solution of $H^+/CaMn_3O_6$ and $H^+/CaMn_4O_8$ were collected and examined by inductively coupled plasma (ICP, Optima 5300DV, Perkin Elmer). Results illustrated that the solvency of Ca ions was stronger, and the leaching of Mn ions was insignificant with the concentration lower than 2 ppm (Table 6.1), indicating that the diluted HNO_3 had possibility of selectively dissolution on Ca-site cations from $CaMn_3O_6$ and $CaMn_4O_8$.

6.3.2 Catalytic oxidation of phenol solutions

Phenol oxidation tests were carried out following the procedure as described in previous chapters.

6. 3.2.1 Effects of reaction parameters on phenol degradation

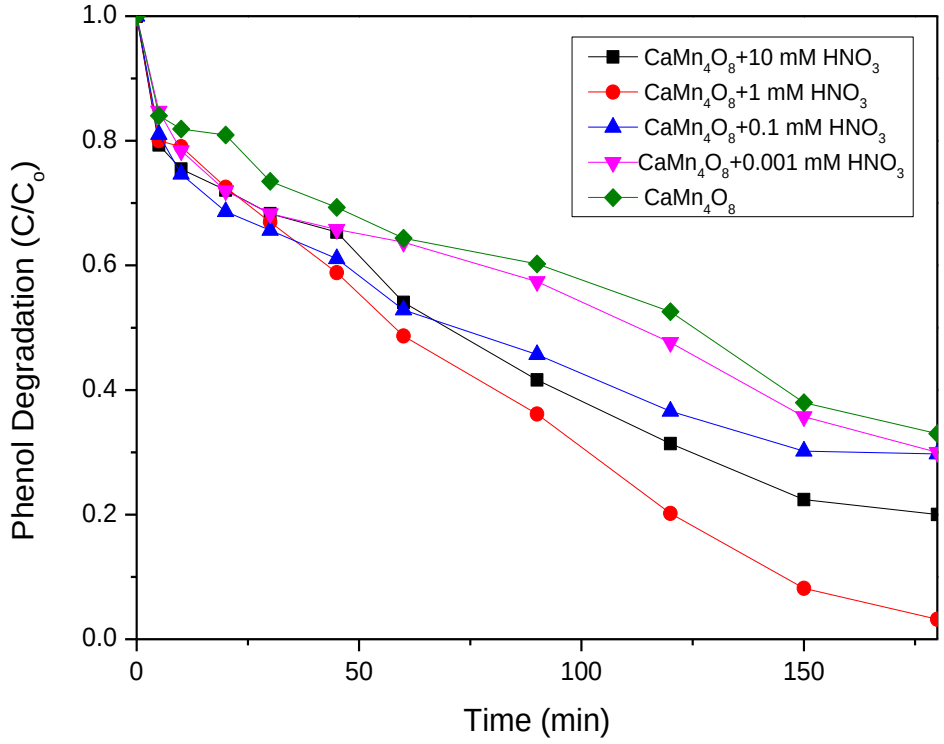

Fig.6.6. Phenol degradation by H^+/$CaMn_4O_8$ catalyst with different concentrations of acid.

The degradation results by the samples after treatment of diluted nitric acid in different concentrations are shown in Fig.6.6. The 1 mM one showed the fastest degradation, and the final phenol removal rate was about 97% in 180 min. Meanwhile for the catalysts with 10, 0.1 and 0.01 mM acid treatment, 80, 71 and 70% of phenol could be degraded in 180 min. It suggested that 1 mM was the most suitable concentration for the samples treatment.

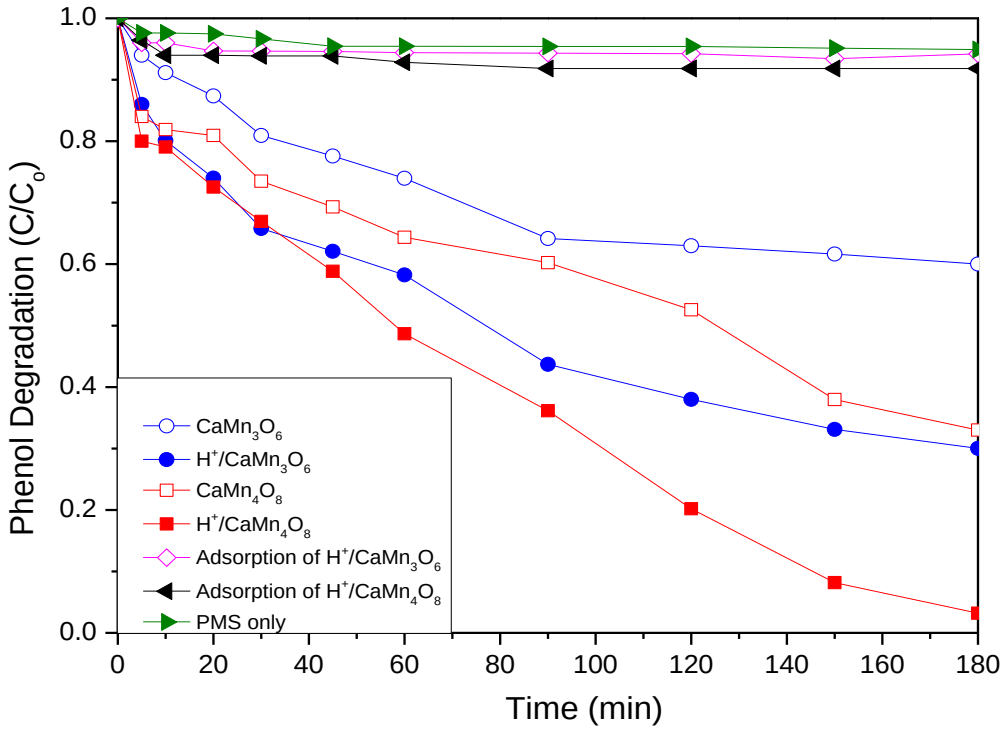

Fig. 6. 7. Phenol removal in different conditions.

The phenol decompositions in different conditions are demonstrated in Fig.6.7. The one using $H^+/CaMn_4O_8$ as the catalyst showed the best result, and the degradation rate was higher than that of $CaMn_4O_8$, showing 97 and 63% phenol degradation, respectively in 180 min. While, compared with the rates of GO/$CaMn_3O_6$ and $CaMn_3O_6$, they showed similar trends, and the final phenol removal rates were about 70 and 38% respectively. For the adsorption tests, the final phenol removal rates were 6 and 5.1% by $H^+/CaMn_4O_8$ and $H^+/CaMn_3O_6$, respectively. For the reaction without a catalyst, the final phenol removal rate was about 5% in the end, which demonstrates that the PMS and catalyst itself in homogeneous solution could not induce phenol oxidation.

6.3.2.2 Effects of reaction parameters on phenol degradation and the stability of the catalysts

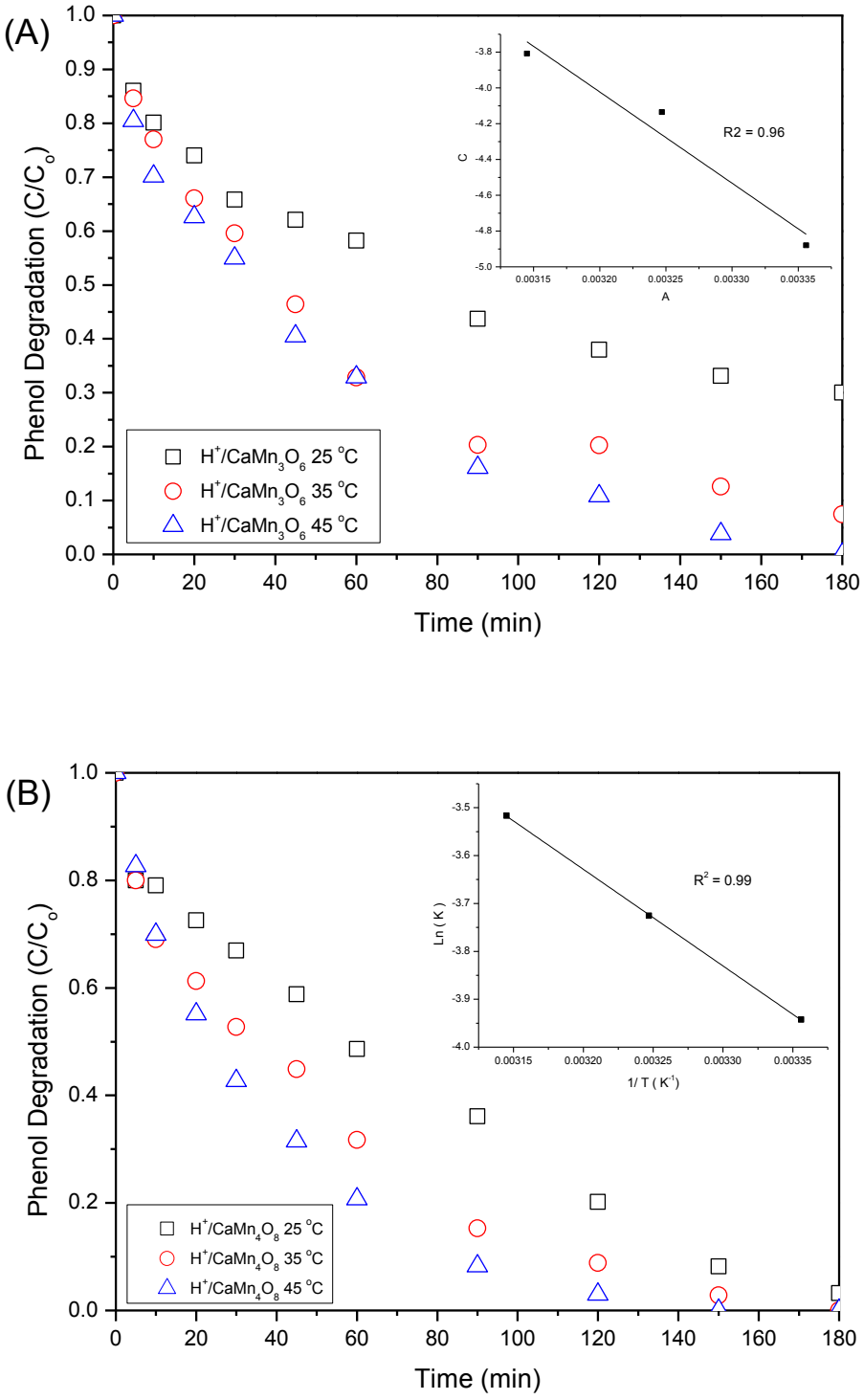

Fig. 6. 8. Phenol removal at different temperatures.

Table 6.2. Kinetic studies of $H^+/CaMn_3O_6$ and $H^+/CaMn_4O_8$ catalysts in activation of PMS for phenol degradation at different temperatures.

catalysts	T (°C)	K (min^{-1})	R^2 of k	Ea (kJ/mol)	R^2 of Ea
$H^+/CaMn_3O_6$	25	0.0076	0.9841	42.4	0.959
	35	0.0160	0.9706		
	45	0.0221	0.9481		
$H^+/CaMn_4O_8$	25	0.0194	0.8968	16.8	0.999
	35	0.0241	0.9567		
	45	0.0297	0.9848		

A lot of conditions can influence phenol degradation, and the effect of reaction temperature is one of the main factors in heterogeneous catalytic oxidation of phenol. Fig.6.8 (A) shows the performance of $H^+/CaMn_3O_6$ catalysts for phenol oxidation at varying temperatures. It was seen that the reaction temperature affected oxidation efficiency and degradation rate dramatically. At 25 ℃, the phenol removal rate was 68% in 180 min. When the reaction took place at 35 and 45 ℃, the final rates reached 83 and 100% in 180 min. In Fig.6.8 (B) the same trend could be observed for $H^+/CaMn_4O_8$, with the degradation rate of 98% in 180 min at 25 ℃, and removed all the organics in 150 and 120 min at 35 and 45 ℃, respectively. It suggested that higher temperature made more significant contribution to phenol degradation. Based on the reaction rates at different temperatures, the apparent activation energy of $H^+/CaMn_3O_6$ catalytic system was calculated as 42.4 kJ/mol, and 16.8 kJ/mol to $H^+/CaMn_4O_8$ catalytic system (Table 6.2).

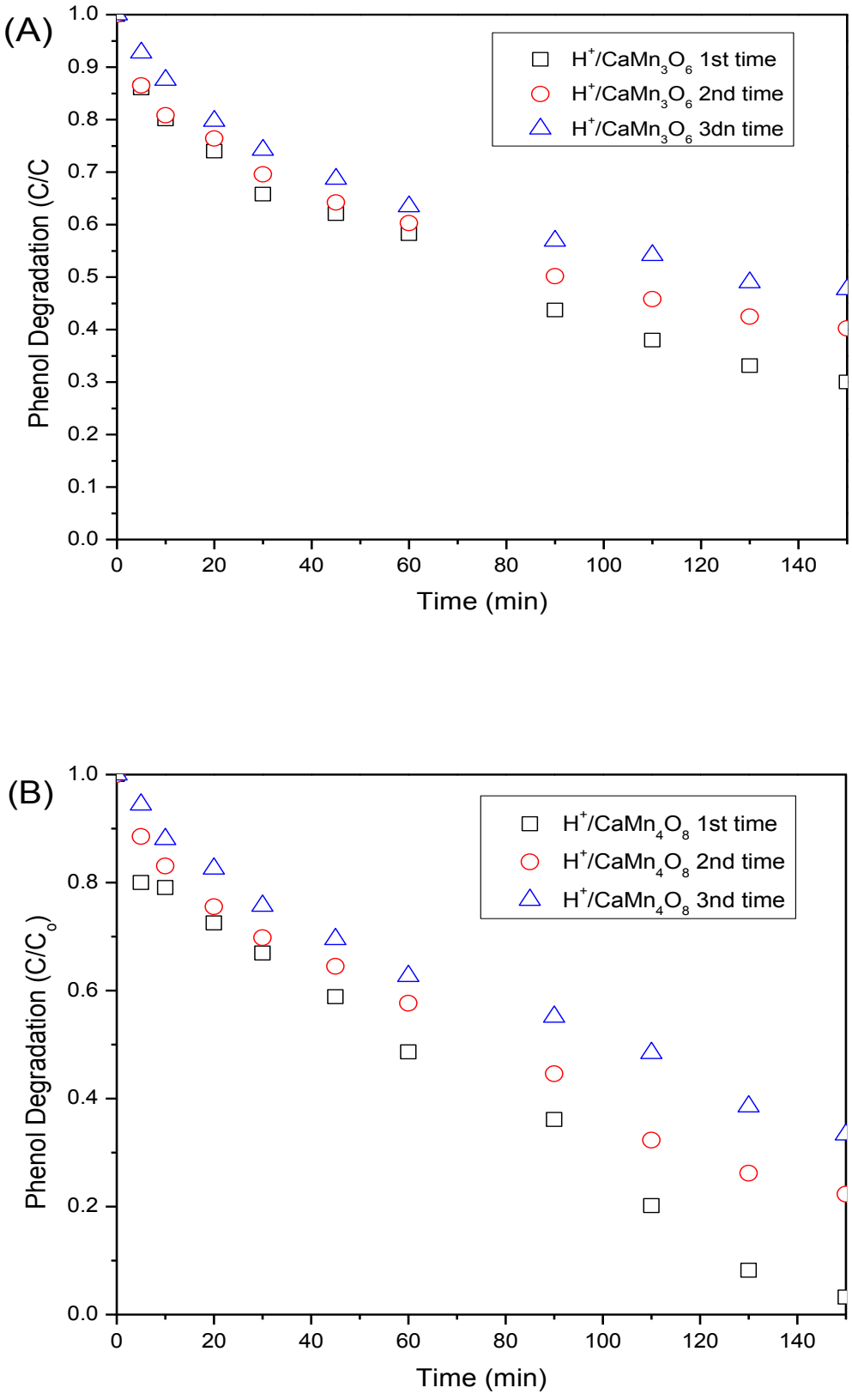

Fig. 6. 9. Reusability tests of (A) $H^+/CaMn_3O_6$ and (B) $H^+/CaMn_4O_8$ catalysts.

The stability performance of $H^+/CaMn_3O_6$ and $H^+/CaMn_4O_8$ were investigated by three-time running reusability tests. After the first run, catalysts were washed with water and dried at 80 ^oC overnight, without any further regeneration. According to Figs.6.9.(A) and (B), 70 and 97% of phenol were oxidized in $H^+/CaMn_3O_6$ and $H^+/CaMn_4O_8$ catalytic systems for the first runs. In the second times, the phenol removal rates reached 56 and 82% in 180 min, respectively. While for the third runs, the degradation rates were 49% in $H^+/CaMn_3O_6$ system, and 62% in $H^+/CaMn_4O_8$ system. It suggested that the catalytic activities decreased in recycled tests as the general trend for both catalyst systems. The decline of catalytic stability might be due to the attachment of reaction intermediates on the surface of the catalysts, which made the correspondent active sites disabled. Because of the van de Waals force, it was hard to remove all of the intermediates by simply washed with water, but could be removed by calcination in air[20].

6.4 Conclusions

In conclusion, it was found that, with diluted acid treatment, the calcium-manganese oxide materials presented a higher BET surface area and high catalytic activity. Acidic treatment can remove Ca-site cations, which increased the amount of surface oxygen species, and the active Mn-site cations were remained. In the catalytic performance examination, 97 and 63% of phenol were decomposed within 180 min with catalytic activation of $H^+/CaMn_3O_6$ and $H^+/CaMn_4O_8$. A first order kinetic model was used to evaluate the kinetic parameters, and the activation energies for $H^+/CaMn_3O_6$ and $H^+/CaMn_4O_8$ were calculated to be 42.4 and 16.8 kJ/mol, respectively.

References

1. Shukla, P., et al., Co-SBA-15 for heterogeneous oxidation of phenol with sulfate radical for wastewater treatment. Catalysis Today, 2011. 175(1): p. 380-385.

2. Gupta, V.K., et al., Chemical treatment technologies for waste-water recycling-an overview. RSC Advances, 2012. 2(16): p. 6380-6388.

3. Christoskova, S.G., M. Stoyanova, and M. Georgieva, Low-temperature iron-modified cobalt oxide system: Part 2. Catalytic oxidation of phenol in aqueous phase. Applied Catalysis A: General, 2001. 208(1–2): p. 243-249.

4. Fortuny, A., et al., Bimetallic catalysts for continuous catalytic wet air oxidation of phenol. Journal of Hazardous Materials, 1999. 64(2): p. 181-193.

5. M. Matheswaran, I.S. Moon, J. Ind. Eng. Chem. 15 (2009) 287-292.

6. M.Bosnic, J. Buljan, R.P. Daniels, United Nation Industrial Development Organization, 2000, pp. 1-26.

7. Calleja, G., et al., Activity and resistance of iron-containing amorphous, zeolitic and mesostructured materials for wet peroxide oxidation of phenol. Water Research, 2005. 39(9): p. 1741-1750.

8. Indrawirawan S.; Sun H.; Duan X.; Wang S. Lowtemperature combustion synthesis of nitrogen-doped graphene for metal-free catalytic oxidation. Journal of Material Chemistry A 3 (2015) pp.3432-3440.

9. Wang Y.; Xie Y.; Sun H.; Xiao J.; Cao H.; Wang S. 2D/2D nano-hybrids of γ-MnO2 on reduced graohene oxide for catalytic ozonation and coupling peroxymonosulfate activation.

Journal of Hazardous Materials 301 (2016) pp.56-64.

10. Saputra E.; Muhammad S.; Sun H.; Ang H. Shape-controlled activation of peroxymonosulfate by single crystal α-Mn2O3 for catalytic phenol degradation in aqueous solution. Applied Catalysis B: Environmental 154-155 (2014) pp.245-251.

11. Saputra E.; Muhammad S.; Sun H.; Ang H. Shape-controlled activation of peroxymonosulfate by single crystal α-Mn2O3 for catalytic phenol degradation in aqueous solution. Applied Catalysis B: Environmental 154-155 (2014) pp.245-251.

12. Song M., Cheng S., Chen H., Qin W., Nam K., Xu S., Yang X., Bongiorno A., Lee J., Bai J., Tyson T., Cho J., Liu M., Anomalous pseudocapacitive behavior of a nanostructured, mixed-valent manganese oxide film for electrical energy storage, Nano Lett., 12 (2012) 3483-3490.

13. Han X., Zhang T., Du J., Cheng F., Chen J., Porous calcium-manganese oxide microspheres for electrocatalytic oxygen reduction with high activity, Chem. Sci., 4 (2013) 368-376.

14. Si, W. ; Wang, Y. ; Peng, Y. ; Li, J. Selective Dissolution of A-Site Cations in ABO_3 Perovskites: A New Path to High-Performance Catalysts . Angewandte Chemie (International ed. in English), 54 (2015), pp.7954-7

15. Zhang C.; Hua W.; Wang C.; Guo Y.; Guo Y.; Lu G.; Baylet A.; Giroir-Fendler A. The effect of A-site substitution by Sr, Mg and Ce on the catalytic performance of $LaMnO_3$ catalysts for the oxidation of vinyl chloride emission. Applied Catalysis B: Environmental, 2013

16. Mohammad M.; Nayeri S.; Pashaei B. Nano-size amorphous calciummanganese oxide as an efficient and biomimetic water oxidizing catalyst for artificial photosynthesis: back to manganese Najafpour, Dalton Transactions, Dalton Transactions, 40 (2011), pp.9374-9378.

17. Wang Y.; Xie Y.; Sun H.; Xiao J.; Cao H.; Wang S., Hierarchical shape-controlled mixed-

valence calcium manganites for catalytic ozonation of aqueous phenolic compounds. Catalysis Science & Technology, 2016

18. J. Hadermann, A.M. Abakumov, L.J. Gillie, C. Martin, M. Hervieu, Coupled cation and charge ordering in the $CaMn_3O_6$ tunnel structure, Chem. Mater., 18 (2006) 5530-5536.

19. N. Barrier, C. Michel, A. Maignan, M. Hervieu, B. Raveau, $CaMn_4O_8$, a mixed valence manganite with an original tunnel structure, J. Mater. Chem., 15 (2005) 386-393.

20. Sun H.; Liang H.; Zhou G.; Wang S. Supported cobalt catalysts by one-pot aqueous combustion synthesis for catalytic phenol degradation. Journal of Colloid and Interface Science. 394 (2013) 394-400

7

Chapter 7: Conclusions and future work

7.1 Concluding comments

The main objective of this research is to synthesize inorganic nanocatalysts for chemical decomposition of organic pollutants in contaminated water. The porous manganese oxide catalysts were synthesized via one-step or two-step hydrothermal methods, and the size was controlled by varying the synthesis conditions. The obtained catalysts were used for degradation of phenol in aqueous phase.

The GO supported calcium-manganese oxide catalysts and acid treated calcium-manganese oxide catalysts were obtained by two-step processes which involve synthesis of calcium-manganese oxide ($CaMn_3O_6$, $CaMn_4O_8$) firstly, and then followed with further treatment. All of these synthesized catalysts were examined for peroxymonosulfate (PMS, Oxone) activation in the decomposition of phenol. The major outcomes of this research thesis are outlined as below.

7.2 The effect of particle size of the porous manganese oxide catalysts on phenol degradation

A series of manganese oxide catalysts with different particle sizes were successfully prepared by the one-step method. Varying size can affect the physical properties, and it was found that the smaller one has a larger specific surface area and highly porous structure for the enhanced phenol decomposition process.

7.3 The highly- stable manganese oxide catalysts

Manganese oxide catalysts were successfully synthesized by calcination of amorphous MnOx in air. The structures and catalytic properties were improved. M-400 (calcining in 400 ^oC) exhibited excellent efficiency in degradation of phenol, and also showed a high stability.

7.4 Catalytic activation by GO supported calcium-manganese oxides

GO supported calcium-manganese oxides were synthesized using a two-step method. The GO/$CaMn_3O_6$ and GO/$CaMn_4O_8$ composites showed better catalytic activities in decomposition of phenol than GO and calcium-manganese oxides, respectively.

7.5 Effect of diluted acid treatment on catalysis over calcium-manganese oxide catalysts

The catalytic activities of calcium-manganese oxide would be improved after diluted acid treatment.

7.6 Recommendation for future work

This research focused on inorganic nanocatalysts for chemical decomposition of organic pollutants in contaminated water. The results demonstrated that phenol can be decomposed into non-toxic matters using peroxymonosulfate (PMS) as an oxidant. However, the catalysts need to be examined for other organic pollutants.

In this thesis, the focus was to explore the activity and stability of the catalysts for phenol oxidation reaction. However, further study of the mechanism needs to be done to investigate the intermediate products which might cause the secondary pollution in water treatment processes.